Benign and Malignant Tumors: General Issues and Growth Patterns and Treatment Related Changes

BENIGN AND MALIGNANT TUMORS: GENERAL ISSUES, GROWTH PATTERNS, AND TREATMENT-RELATED CHANGES

ANTHONY A. MANCUSO

KEY POINTS

- Growth patterns of benign and malignant neoplasms
- Perineural spread of malignancies
- Computed tomography, magnetic resonance imaging, and ultrasound appearance of benign and malignant neoplasms
- General patterns of postradiotherapy and postsurgical changes following treatment for malignancies
- Principles of posttreatment surveillance including fluorine-18 2-fluoro-2-deoxy-D-glucose positron emission tomography

The classification used here is intended to aid the reader in forming a general understanding of the benign and malignant neoplasms that affect the extracranial head and neck. Some neoplasms occur exclusively in the head and neck region, such as juvenile angiofibroma, but most others are seen elsewhere in the body. In some neoplastic processes, such as lymphoma, the head and neck involvement may represent only a small component of the disease. This chapter and those that follow in this section (Chapters 22–43) take a pathoanatomic and pathologic point of view. Each tumor type is considered in terms of its occurrence at various head and neck sites and in particular the effect of a neoplasm's spread pattern, natural history, and cellular structure on its computed tomography (CT), magnetic resonance (MR), and ultrasound (US) appearance and its physiology as reflected on metabolic imaging studies such as fluorine-18 2-fluoro-2-deoxy-D-glucose positron emission tomography (FDG-PET). Other sections and chapters emphasize the clinical and imaging implications of a particular type of tumor at a specific anatomic location.

GENERAL ISSUES

CT and MR and, to a lesser extent, US and radionuclide studies currently play a central role for any multidisciplinary team that is called upon to manage head and neck neoplasms. The value of an imaging study in helping to care for the patients of surgeons, radiation oncologists, medical oncologists, and others on the health care team is directly proportional to the skill and interest of the diagnostic imager. If the decision making is a shared responsibility performed in an open forum, such as a Head and Neck Tumor Board, patients can be fully informed of their treatment options and prognosis before a perhaps less optimal path is chosen. This ability to adequately inform is, in large part, due to the extraordinary amount of information concerning the extent of disease available with current medical imaging technology and the exceptional accuracy of pathologic diagnosis compared to that available just three decades ago.

Knowledge continues to evolve about the specific value and limitations of imaging studies in head and neck neoplasms. It is the task of the interdisciplinary team and especially diagnostic radiologists to refine their use in the safest and most efficient manner. However, newer imaging approaches must respect the more than 50 to 60 years of clinical experience in treating these disorders and augment those lessons learned rather than ignore or, worse, undo them.

The most basic contribution of imaging is its ability to find disease spreading beyond the limits of the physical examination of the head and neck, including more advanced endoscopic and physiologic testing procedures. This manifests itself in several ways. Spread beneath intact mucosa is not visible to the endoscopist, and imaging can lead to the initial diagnosis of a mucosally not apparent primary cancer (Figs. 21.1–21.4).[1,2] Deep spread in a mucosally apparent tumor is often palpable but still usually difficult to assess objectively even with good bimanual palpation combined with inspection and history; however, experienced examiners can often anticipate involvement of many of the areas that are subsequently proven to be abnormal on imaging studies, principally CT and magnetic resonance imaging (MRI) (Figs. 21.5 and 21.6). Some locales are simply inaccessible for palpation, such as the skull base, pterygopalatine fossa, infratemporal fossa, orbits, and brain (Fig. 21.7). Critical management decisions frequently hinge on imaging findings alone (Fig. 21.7) and/or confirmation by imaging-guided biopsy (Fig. 21.8).

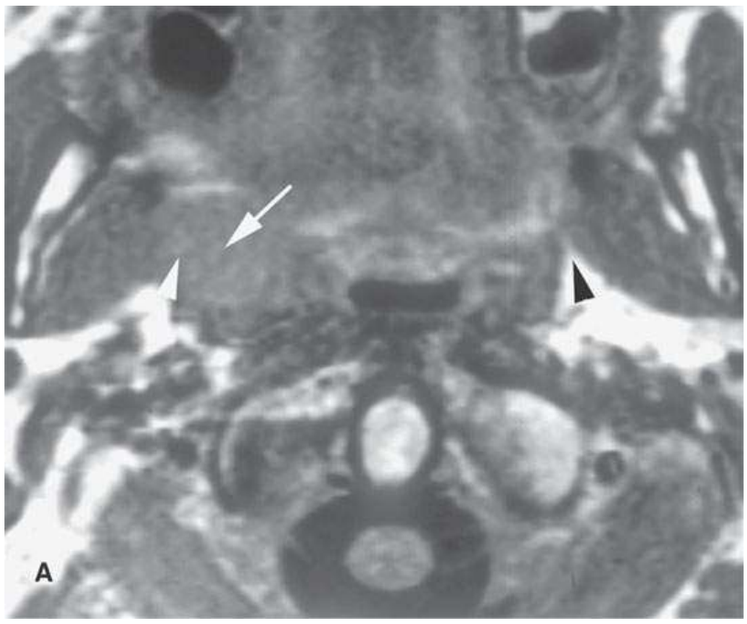
A

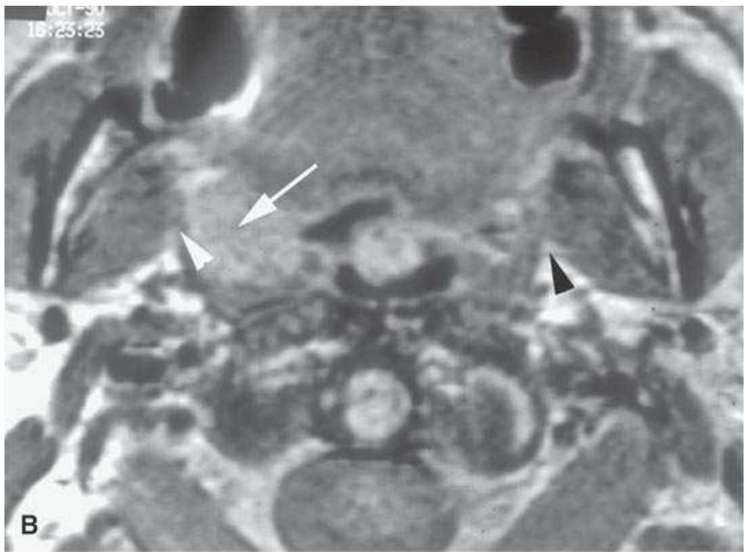
B

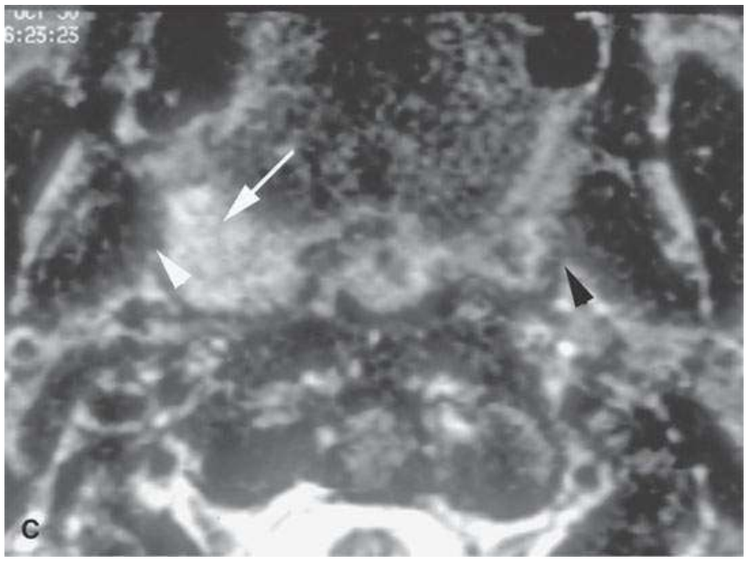
C

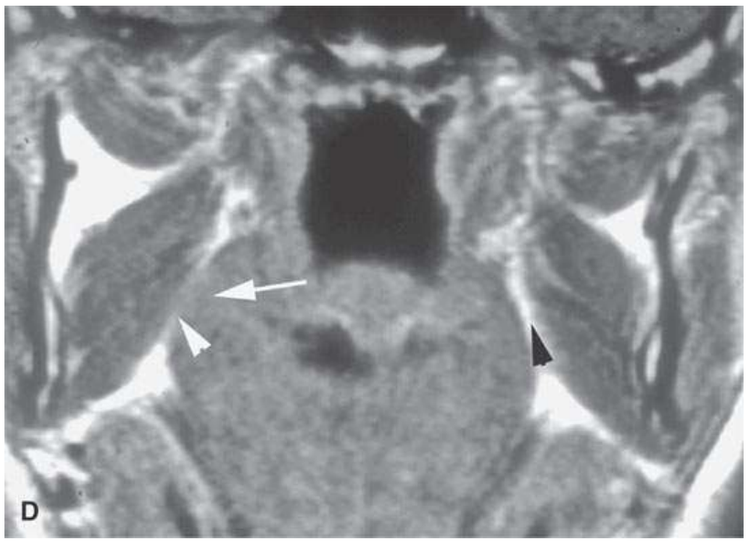

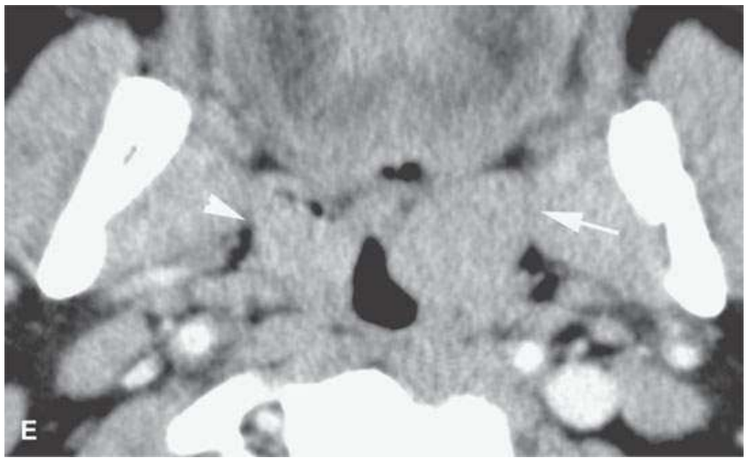

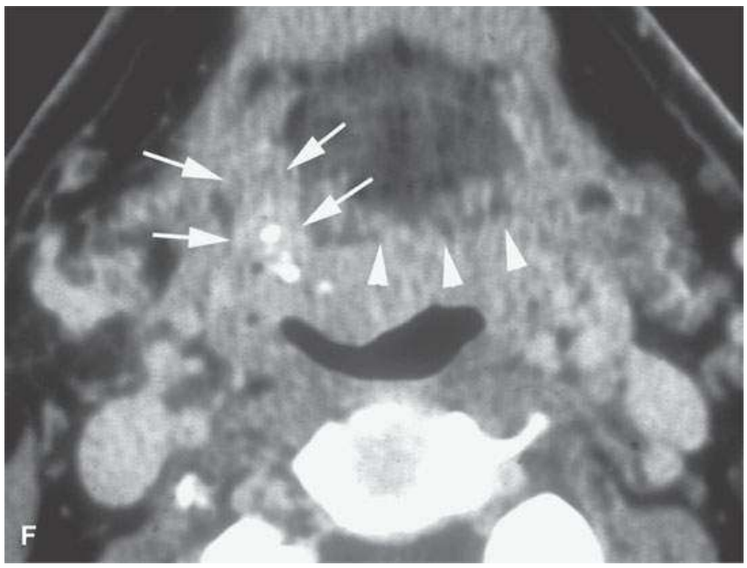

FIGURE 21.1. Three patients with submucosal cancers not visible to the endoscopist**. A–D**: Magnetic resonance imaging of a patient presenting with right-sided otalgia and no visible mucosal lesion—all pulse sequences show the enlarged right palatine tonsil *(arrows)* with obliteration of parapharyngeal fat on the right *(white arrowheads)* compared to the left *(black arrowheads)***. E**: Contrast-enhanced computed tomography (CT) of a patient with left level 2 neck node needle biopsy showing squamous cell carcinoma (SCCA)**.** The CT shows a prominent left tonsil with subtle encroachment on the parapharyngeal fat *(arrow*) compared to the normal side *(arrowhead)***. F**: Contrast-enhanced CT of a patient with right-sided otalgia and a right level 2 neck node needle biopsy showing SCCA**.** The submucosal tongue base cancer penetrates *(arrows)* the tongue base to a far greater degree than the normal carpet of lingual tonsillar and other glandular tissue *(arrowheads)***.**

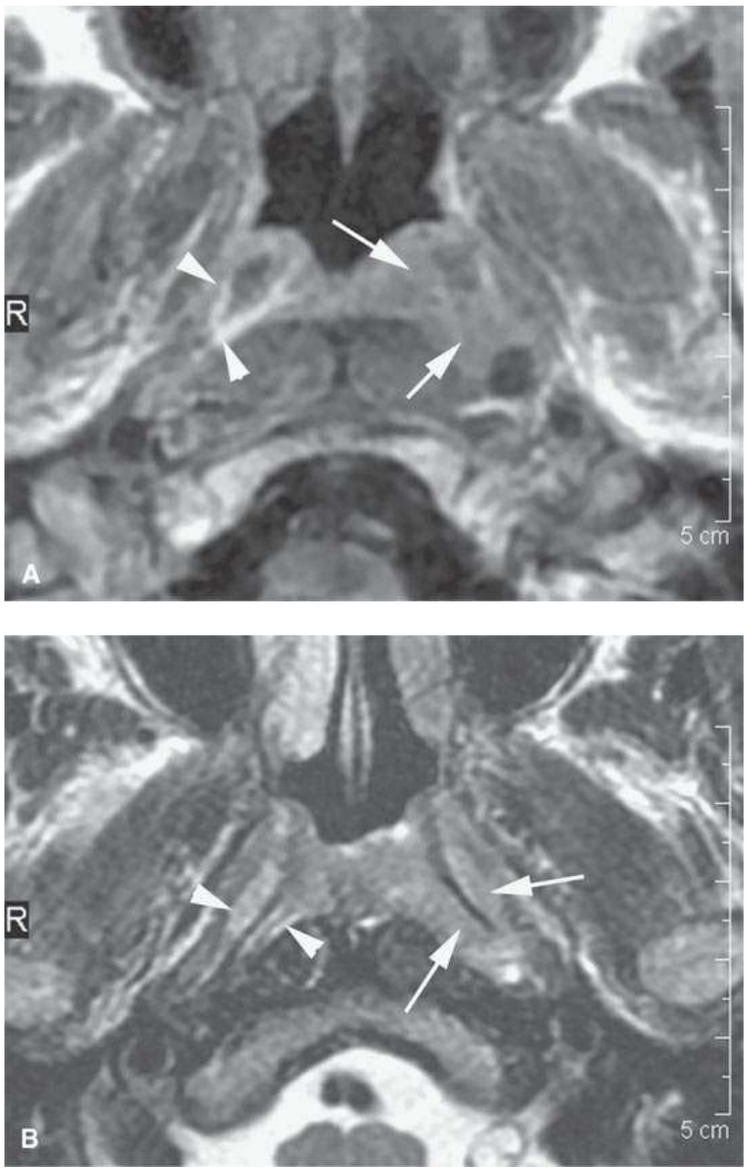

FIGURE 21.2. A patient with submucosal nasopharyngeal cancer not visible to the endoscopist, the patient presenting with chronic middle ear disease. The entirely submucosal squamous cell carcinoma invades the deep tissue planes *(arrows)* on the left compared to the normal side *(arrowheads)* on the right on both the contrast-enhanced T1-weighted image (aA) and the T2-weighted image (bB).

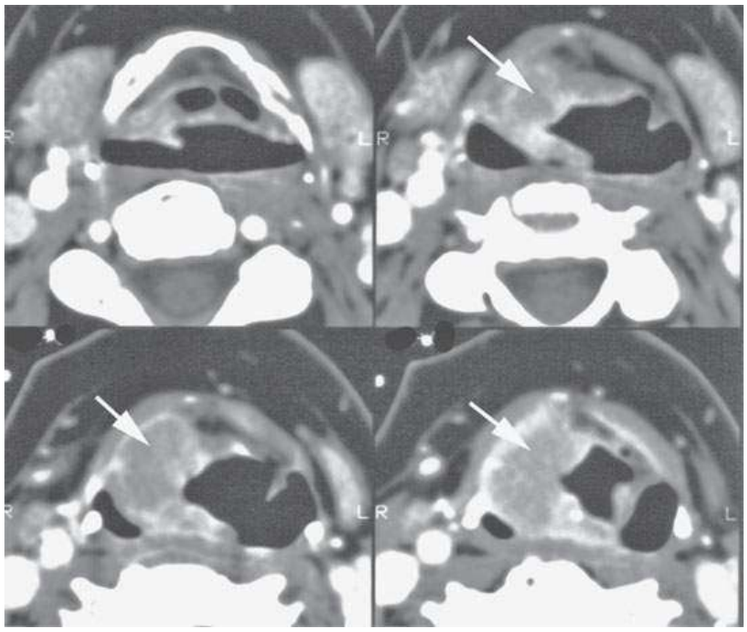

FIGURE 21.3. Contrast-enhanced computed tomography (CT) of the larynx in a patient with submucosal supraglottic cancer not visible to the endoscopist, the patient presenting with hoarseness and right-sided otalgia. This mass *(arrows)* was likely present for 2 years before a percutaneous CT-guided biopsy, following three negative endoscopic biopsy attempts, confirmed squamous cell carcinoma.

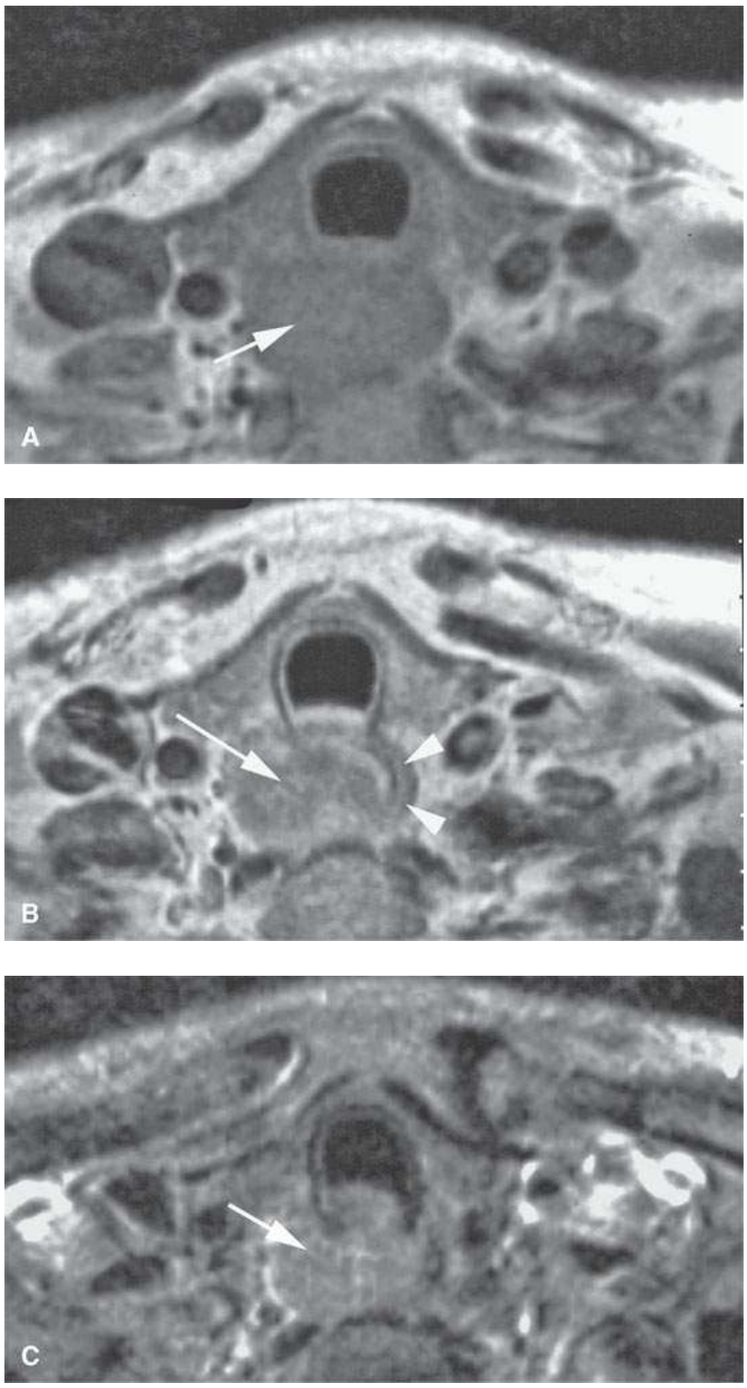

FIGURE 21.4. Contrast-enhanced magnetic resonance of the cervical esophagus in a patient with submucosal esophageal cancer not visible to the endoscopist presenting with chronic dysphagia**.** All sequences (A–, B and C) show the submucosal esophageal mass *(arrows)* and very little remaining muscle tissue (*arrowheads* in **B**)[SF1]**.** This mass was likely present for many months before a percutaneous computed tomography–guided biopsy, following two negative endoscopic biopsy attempts, confirmed squamous cell carcinoma**.**

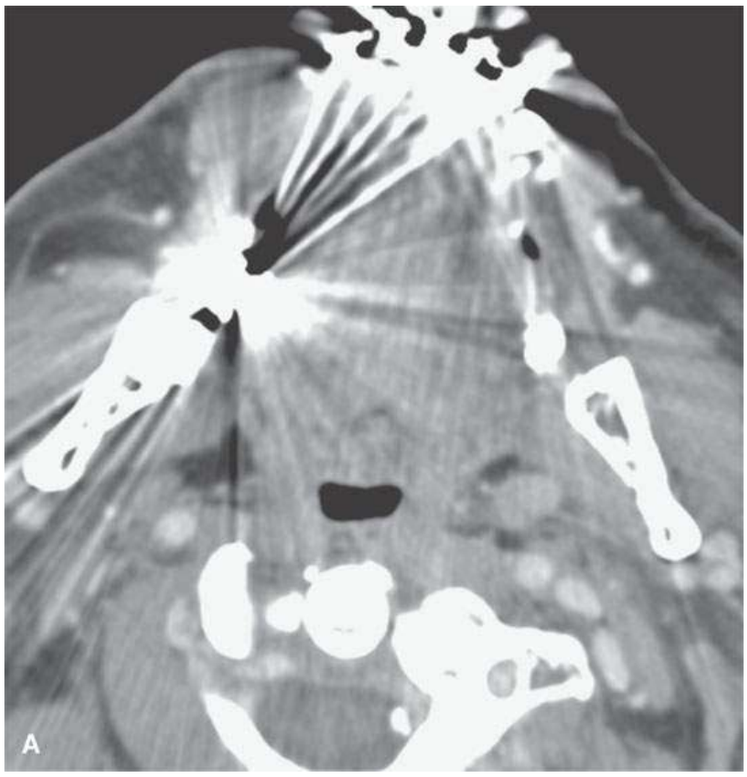
A

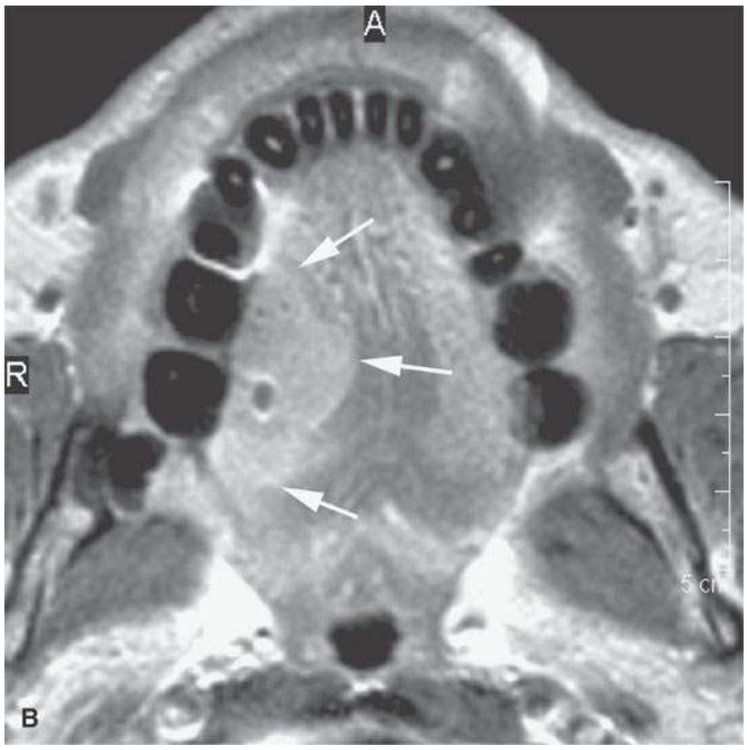
A
R
5 cm
B

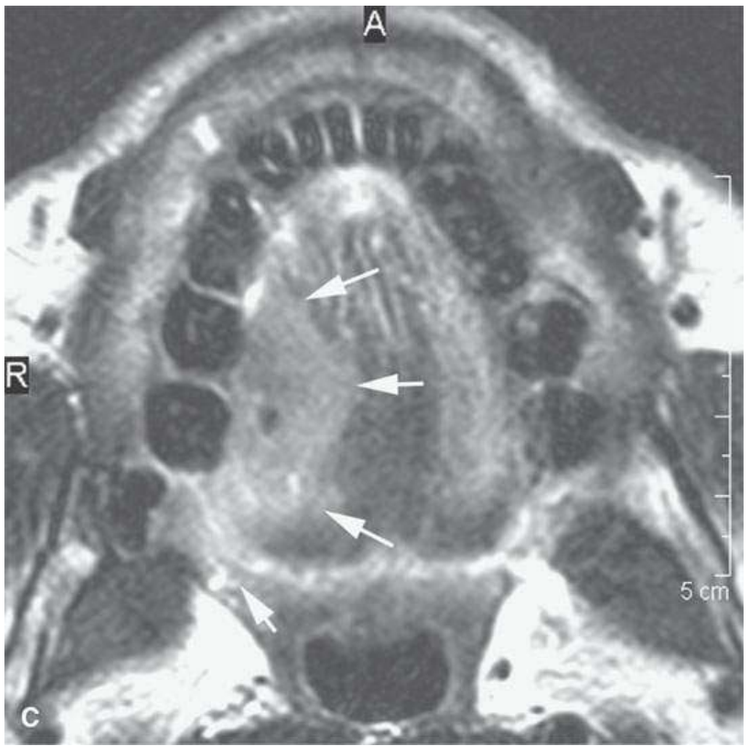

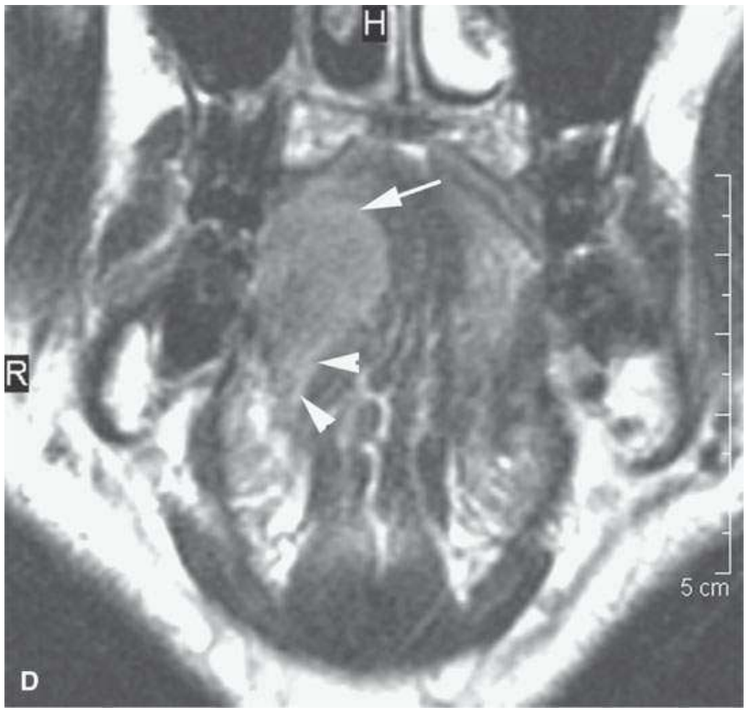

FIGURE 21.5. A patient with oral tongue cancer. The computed tomography (aA) was degraded by unavoidable artifacts. The magnetic resonance images (B–, C,D) mapped the lesion well *(arrows)*, including showing the minor invasion of the floor of the mouth (*arrowheads* in **D**). The signal intensity seen on the T2-weighted images (b and dCB, D) and the degree of enhancement as seen on the contrast-enhanced T1-weighted image **(A)** is fairly typical of squamous cell carcinoma. The margins as seen on these images are typical of a "pushing" as opposed to "infiltrating" margin. Compare this with the margins seen in Figure 21.6.

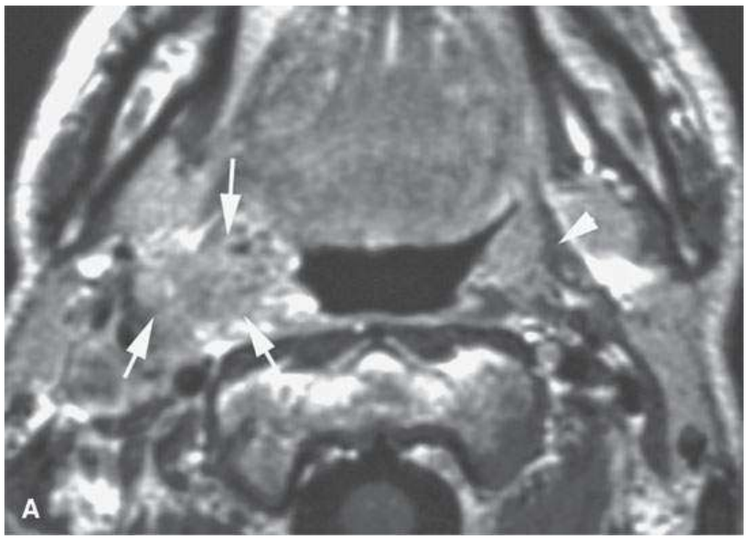

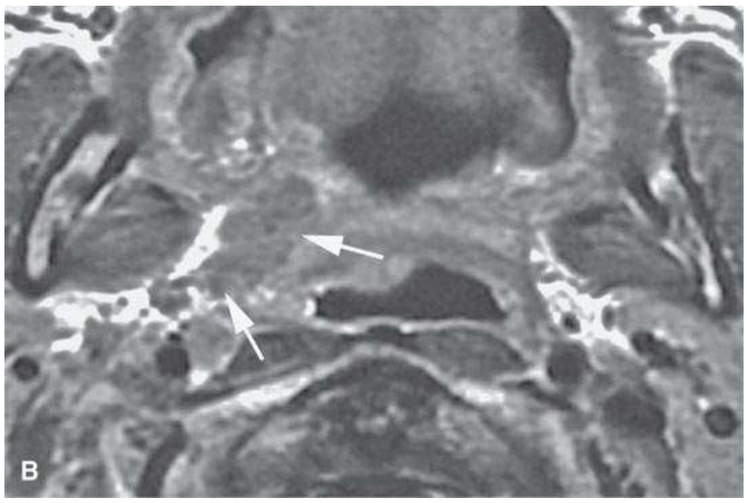

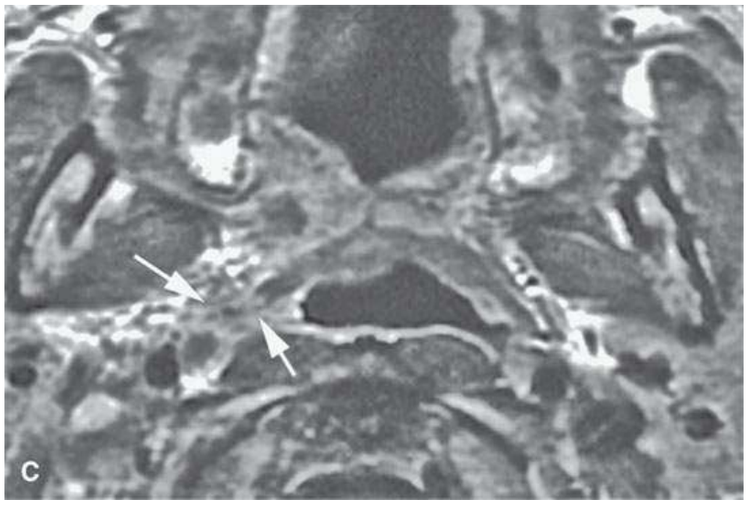

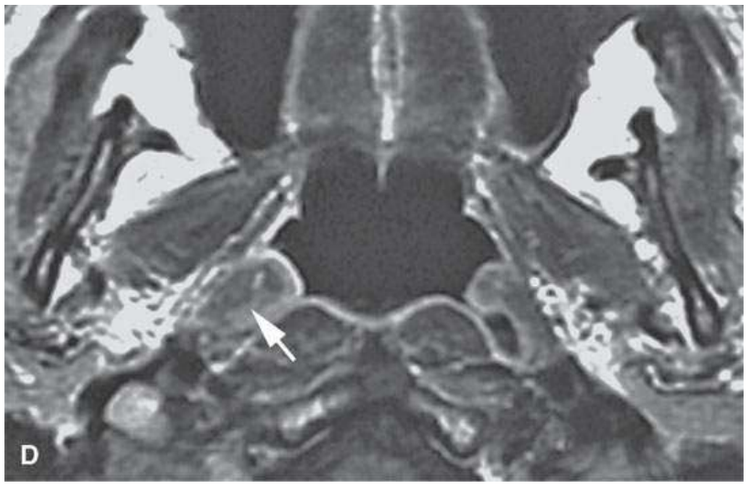

FIGURE 21.6. Contrast-enhanced magnetic resonance in a patient with tonsillar squamous cell carcinoma that was believed clinically to be confined to the tonsillar fossa. The magnetic resonance (MR) images show the lesion to have highly infiltrating rather that "pushing" margins (compare with MR images in Figure 21.5). **A:** Contrast-enhanced T1-weighted image showing a highly infiltrative mass invading the styloglossus muscle and parapharyngeal fat *(arrows)*. Compare with normal styloglossus muscle *(arrowhead)* and surrounding anatomy on the left. B–D: Contrast-enhanced T1-weighted images show the continued very aggressive infiltrating margins *(arrows)* of the lesion extending all the way to the eustachian tube in (dD). Note that while the margins are more aggressive, the signal intensity relative to normal tissues and the degree of enhancement is about the same as seen in the less aggressive lesion in Figure 21.5.

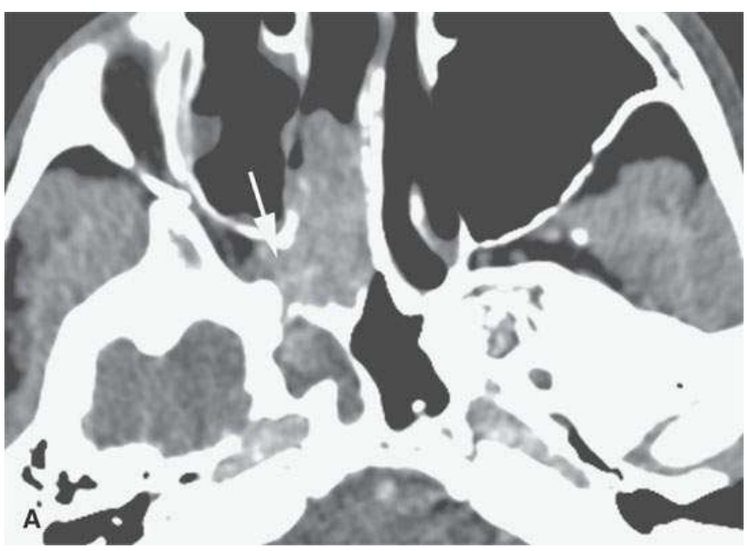

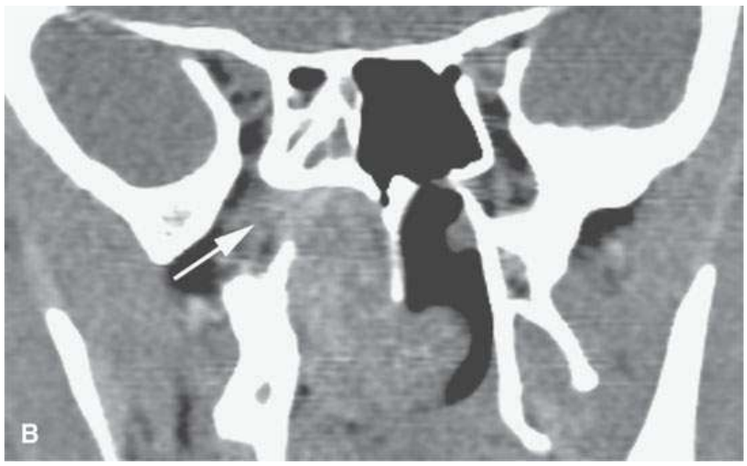

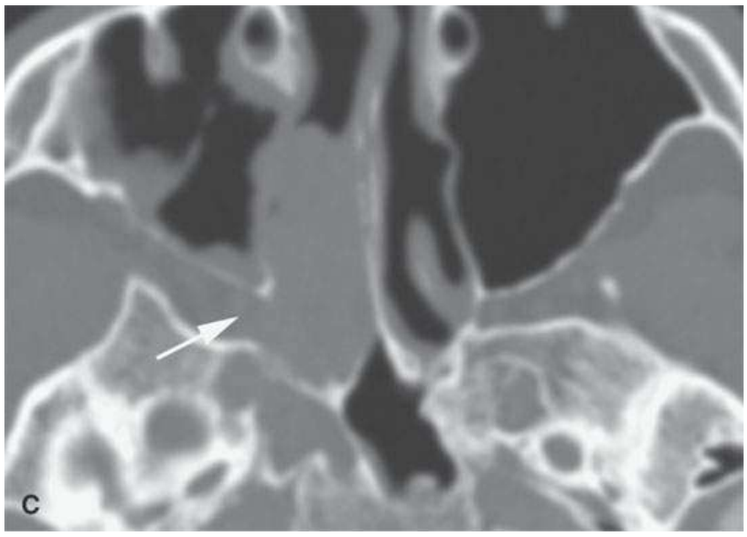

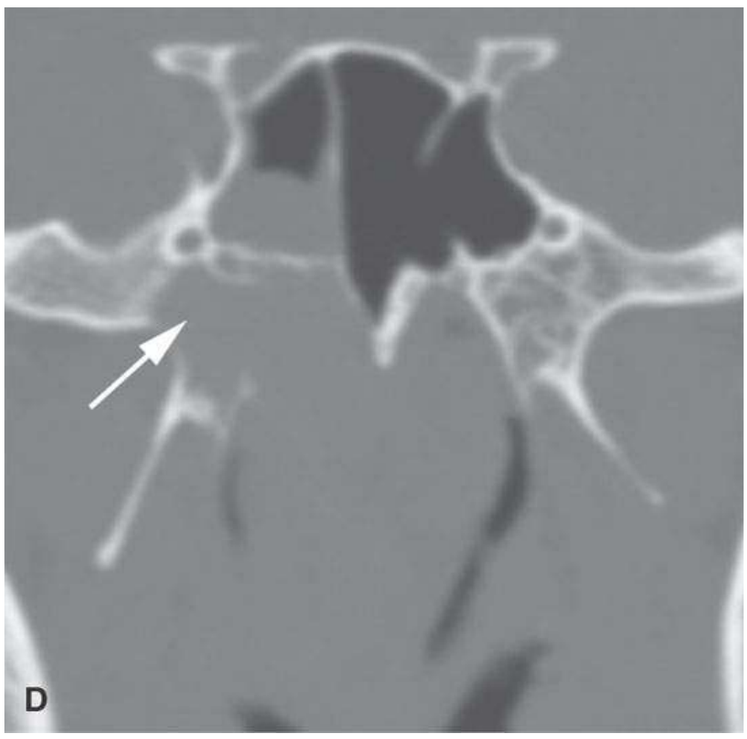

FIGURE 21.7. Non–contrast-enhanced computed tomography of a teenaged male presenting with nosebleeds and a right nasal cavity mass**.** The mass grows into the pterygopalatine fossa (*arrows* in **A** and **B**) and causes chronic remodeling of the bordering bone (*arrows* in **C** and **D**)**.** Given the clinical situation, the lesion morphology is essentially diagnostic of juvenile angiofibroma and needs only to be confirmed by angiography to decide on how it will be managed**.**

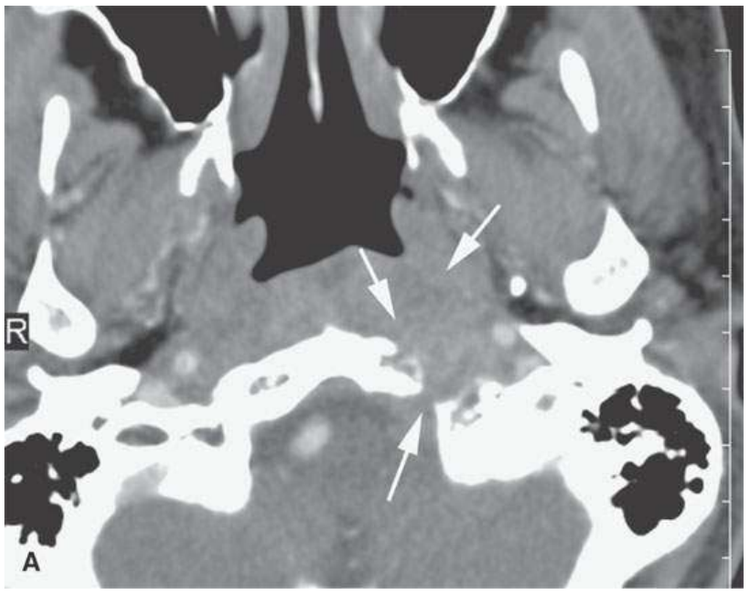
R
A

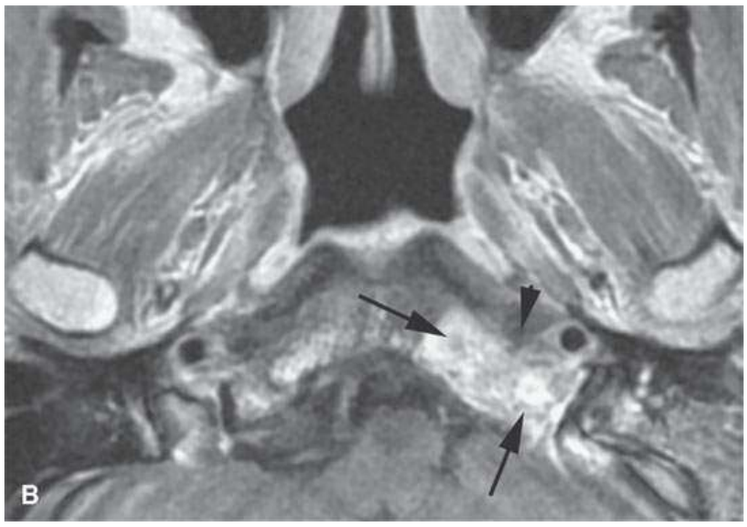
B

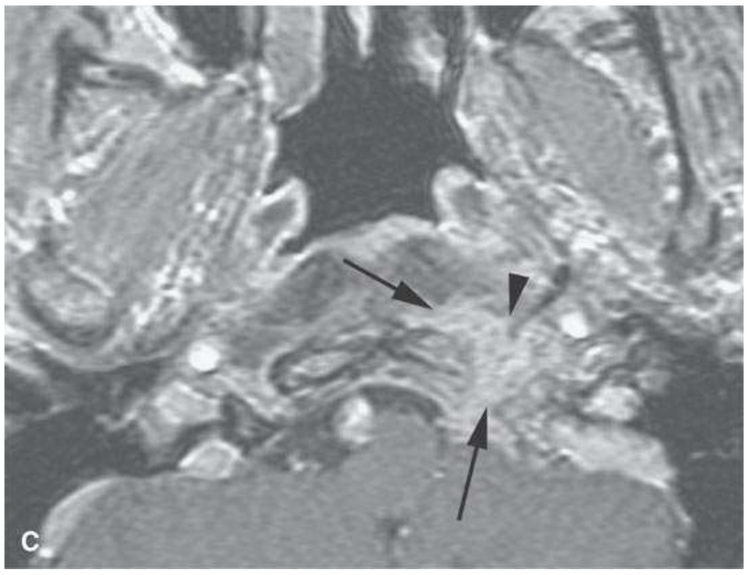
C

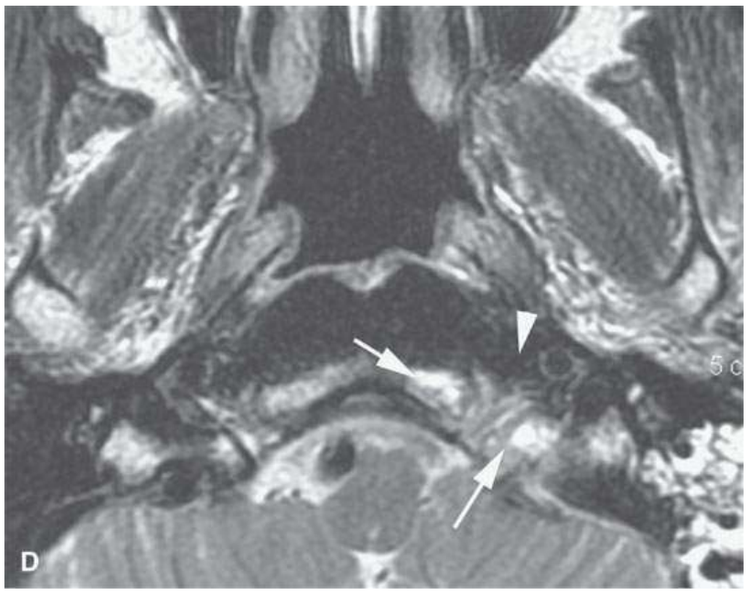

FIGURE 21.8. A patient presenting with unilateral serous otitis media and left Xth and XIIth cranial nerve deficits. **A:** Contrast-enhanced computed tomography (CT) shows a mass of the left retrostyloid parapharyngeal space invading the skull base *(arrows)*. **B:** Contrast-enhanced T1-weighted (T1W) image shows the enhancing mass mainly in the skull base *(arrow)* with a less intense and possibly fibrous component *(arrowhead)*. **C:** Contrast-enhanced T1W gradient echo image from a three-dimensional Fourier transform acquisition shows the soft tissue component to be more extensive. **D:** T2-weighted image shows the brighter component *(arrows)* in the skull base and the darker component *(arrowhead)* in the retrostyloid parapharyngeal space soft tissues. Based on the imaging, it was elected to do a percutaneous CT-guided biopsy of the component in the clivus. It returned squamous cell carcinoma, and the diagnosis of nasopharyngeal carcinoma with skull base invasion was made. This case illustrates the tendency for enhancing cancers to become isointense with fat within or outside the skull base.

Perineural spread can also take malignancies far from the site of tumor origin and well beyond the limits of even the most skilled clinician's physical examination (Figs. 21.9–21.11).[3]

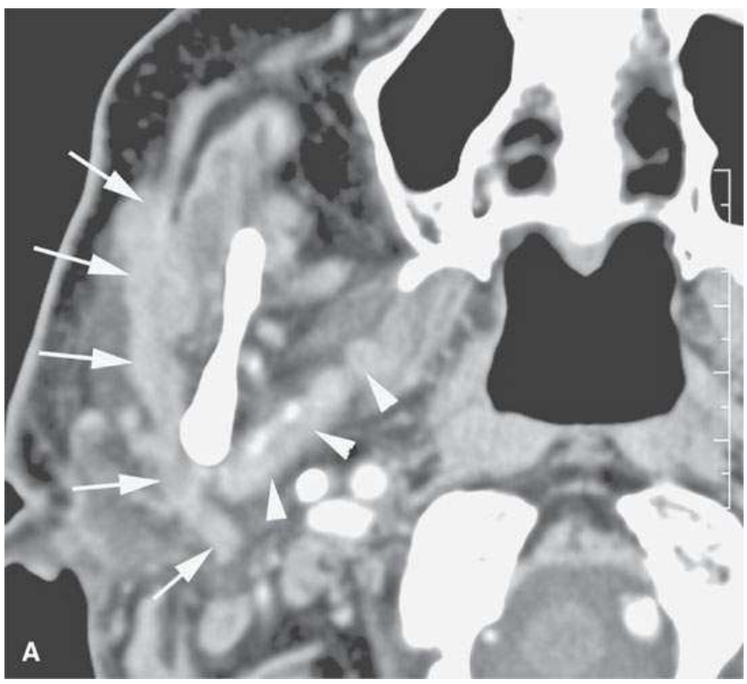

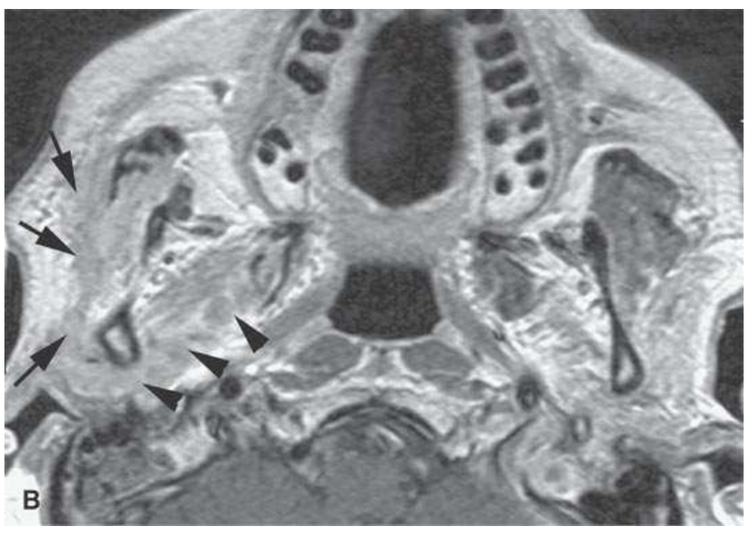

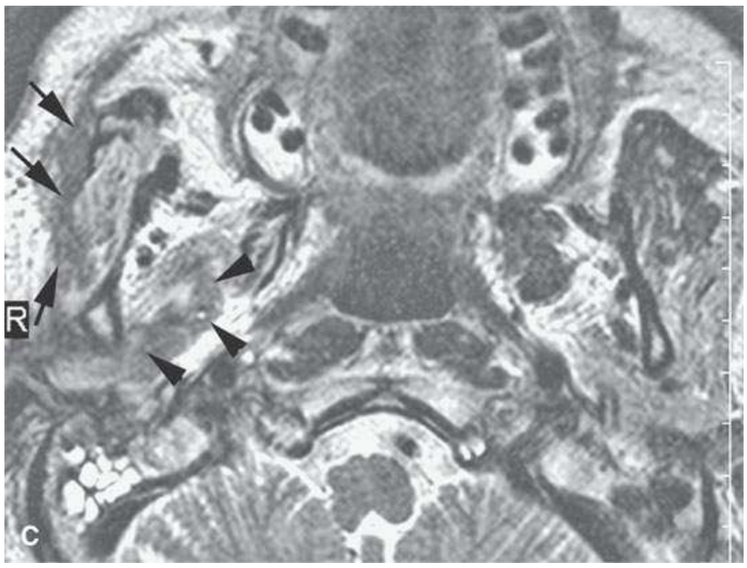

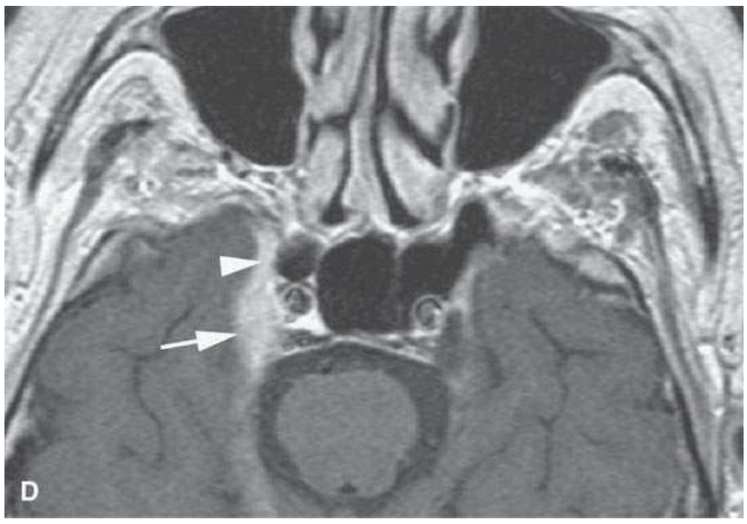

FIGURE 21.9. A patient with peripheral fifth and seventh cranial nerve weakness for over 1 year with two prior magnetic resonance imaging (MRI) studies interpreted as showing only a cavernous sinus mass; the patient was scheduled for a craniotomy. These following computed tomography (CT) and MRI studies done within a month of the latest prior study showed perineural spread of a neurofibrosarcoma along the fifth and seventh cranial nerves. The confirmatory procedure was changed to a percutaneous CT-guided biopsy, but open biopsy of the facial nerve was necessary for a complete final pathologic diagnosis. **A**: Contrast-enhanced CT shows tumor spreading along the facial nerve *(arrows)* to its junction with the auriculotemporal nerve and then along the mandibular division of the trigeminal nerve *(arrowheads)*. **B**: Contrast-enhanced T1-weighted (T1W) image shows tumor spreading along the facial nerve *(arrows)* to its junction with the auriculotemporal nerve and then along the mandibular division of the trigeminal nerve *(arrowheads)*. **C**: T2-weighted image shows tumor spreading along the facial nerve *(arrows)* to its junction with the auriculotemporal nerve and then along the mandibular division of the trigeminal nerve *(arrowheads)*. Note that the tumor is about muscle equivalent in signal intensity—a finding unusual in epithelial perineural spread and related to the fibrous component in this neurogenic sarcoma. **D**: Contrast-enhanced T1W image shows the tumor to have spread to the trigeminal ganglion *(arrow)* and then anterograde along V2 to the foramen rotundum *(arrowhead)*.

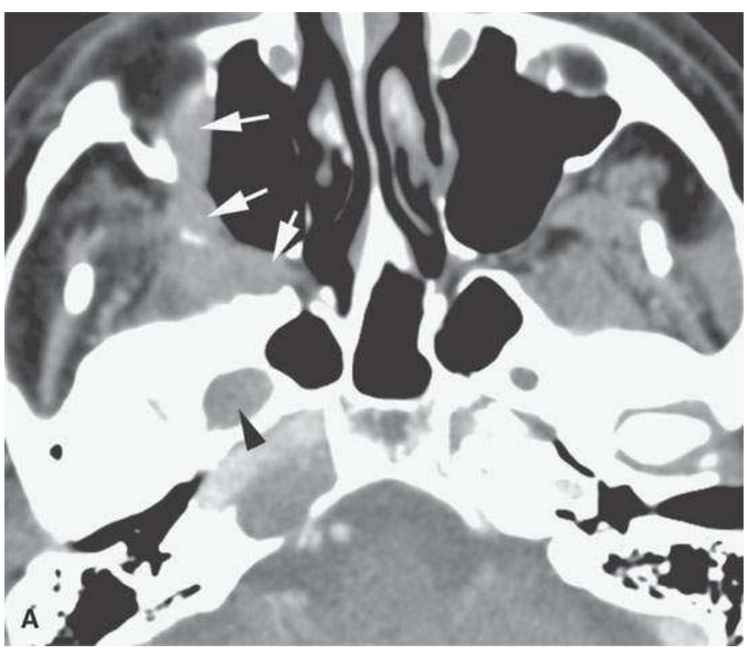

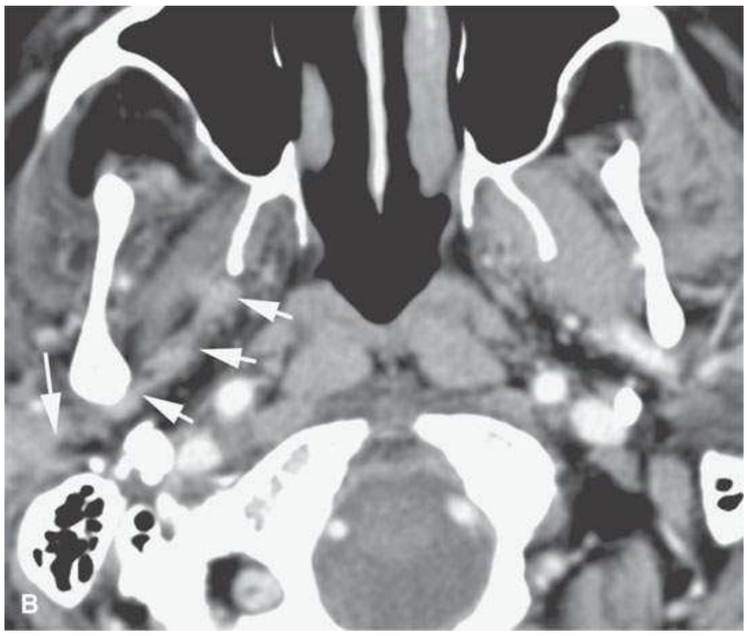

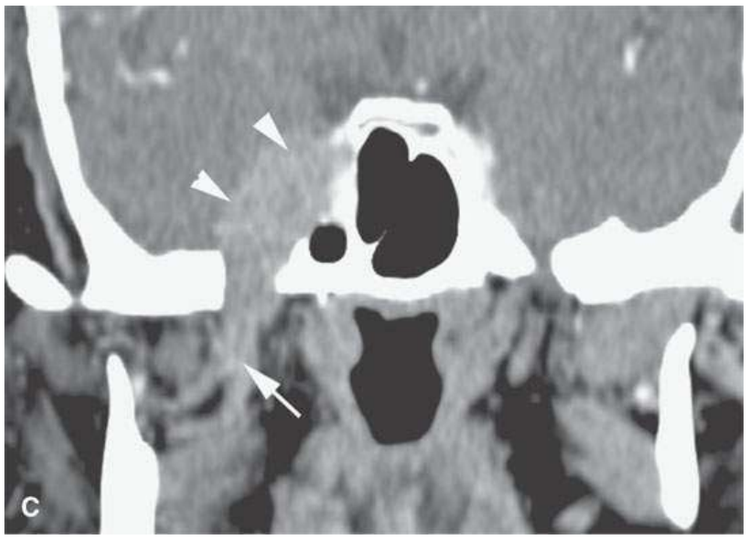

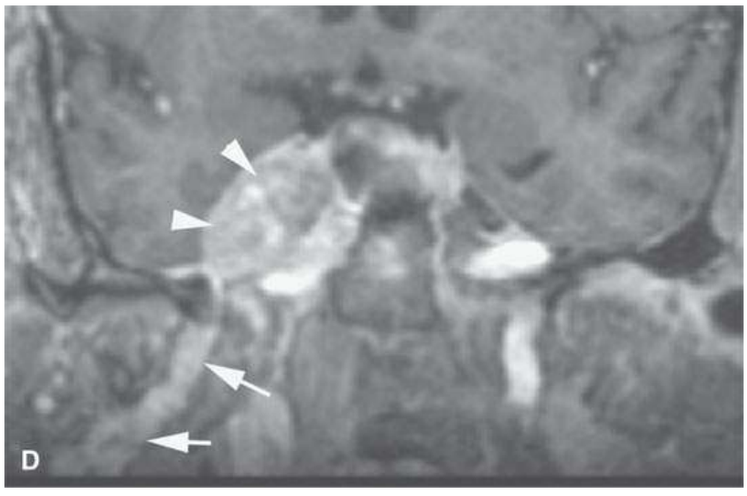

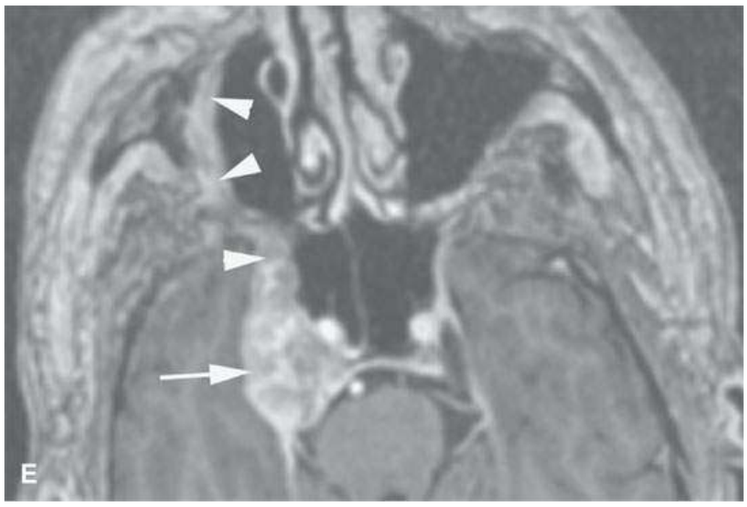

FIGURE 21.10. Imaging studies in a patient with facial pain and a history of remote removal of a skin lesion in the periauricular region of uncertain histology. Prior outside imaging was interpreted as a cavernous sinus meningioma. This study shows an obvious perineural spread pattern. Percutaneous computed

tomography (CT)-guided biopsy of the tumor in the pterygopalatine fossa showed perineural malignant melanoma. **A:** Contrast-enhanced CT shows tumor spreading along the infraorbital nerve *(arrows)* to the pterygopalatine fossa *(arrow)* and enlargement of the foramen ovale *(arrowhead)* **B:** Contrast-enhanced CT shows tumor spreading along the auriculotemporal nerve and then along the mandibular division of the trigeminal nerve *(arrowheads)* and toward the foramen ovale. **C:** Coronal reformations of the CT images show the spread along V3 *(arrows)* to "blossom" in the cavernous sinus *(arrowheads)*. **D:** Contrast-enhanced T1W gradient echo coronal image from a 3DFT acquisition shows the tumor to have spread to the trigeminal ganglion *arrowheads)* along V3 *(arrow)* **E:** Contrast-enhanced T1-weighted (T1W) gradient echo axial image from a three-dimensional Fourier transform (3DFT) acquisition shows the tumor to have spread to the trigeminal ganglion *(arrow)* and then anterograde along V2 through the foramen rotundum and to the peripheral aspect of the infraorbital nerve *(arrowheads)*.

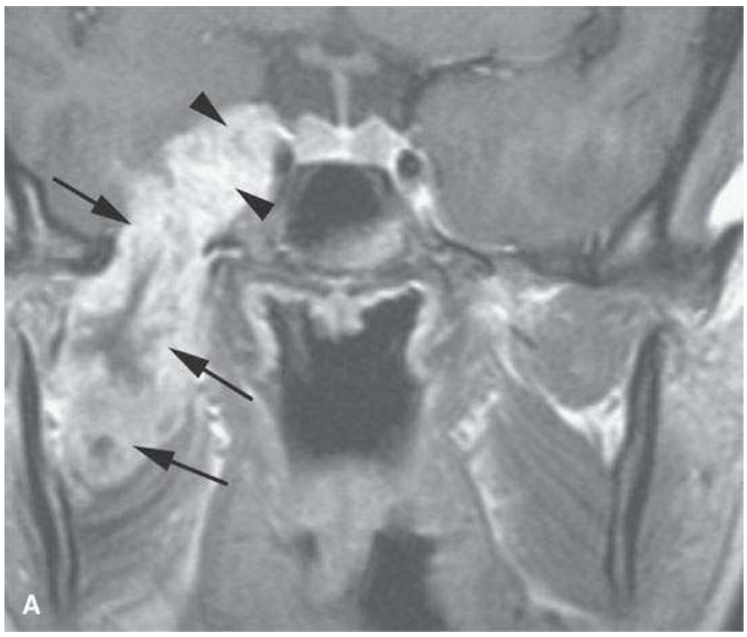

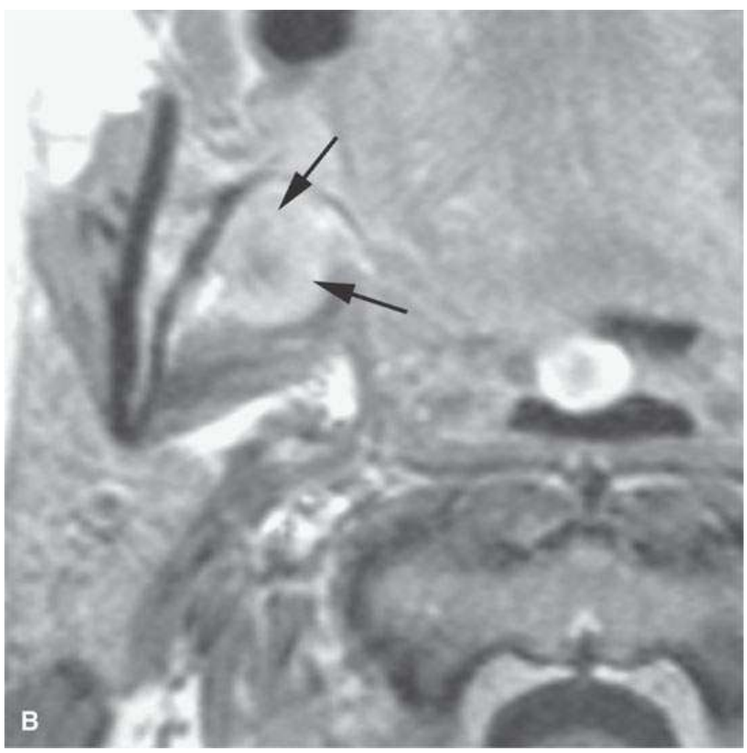

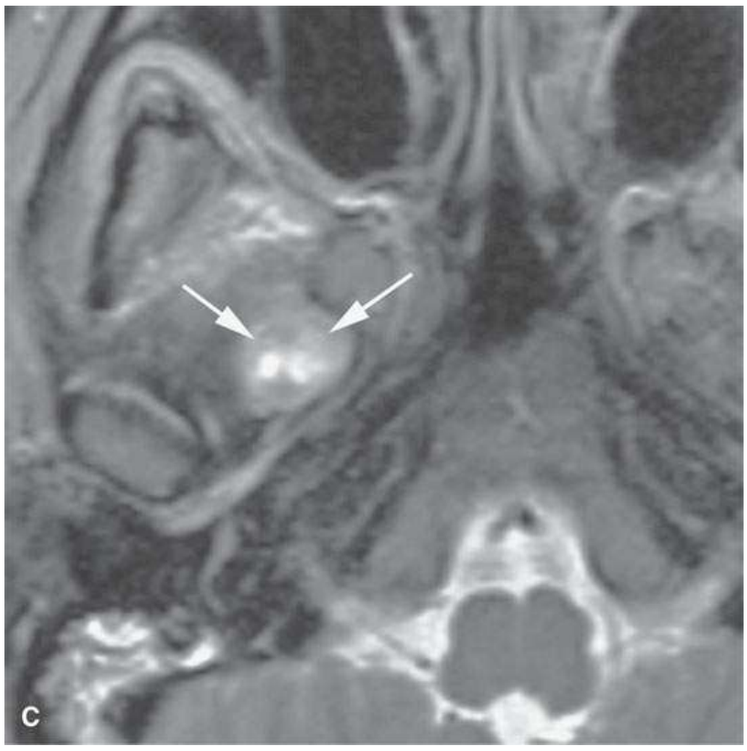

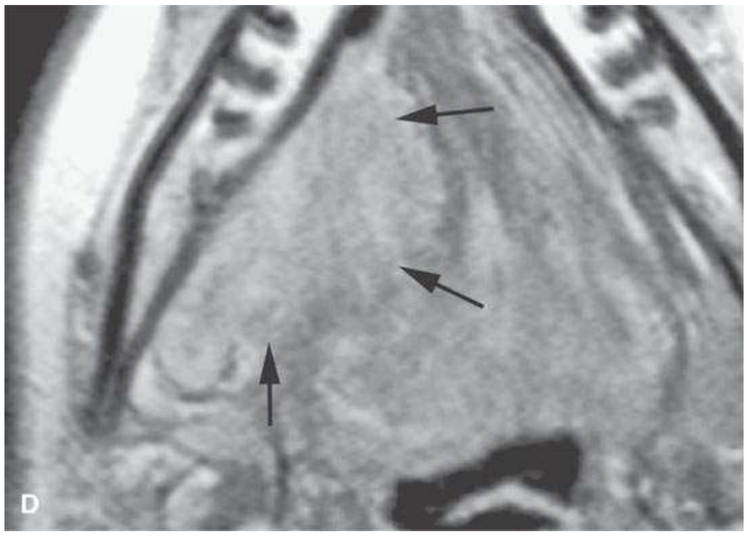

FIGURE 21.11. A young woman with facial pain and what was believed to be a transcranial meningioma based on outside prior imaging studies. This magnetic resonance imaging study showed a primary malignancy of the floor of the mouth with spread along the lingual nerve to V3 and then the trigeminal ganglion. It was believed to be a neurogenic sarcoma on the basis of the imaging but turned out to be a rhabdomyosarcoma of the floor of the mouth with perineural spread of tumor. The imaging findings dramatically altered the treatment plan. **A:** Contrast-enhanced T1-weighted (T1W) image shows tumor spreading along V3 *(arrows)* to its junction with the trigeminal nerve ganglion *(arrowheads)*. **B:** Contrast-enhanced T1W image shows tumor spreading along the lingual nerve *(arrows)*. **C:** T2-weighted image shows tumor spreading along V3 to the foramen ovale *(arrows)*. **D:** Contrast-enhanced T1W image shows the tumor's origin in the floor of the mouth *(arrows)*.

In cancer patients, imaging can also provide an objective assessment of all cervical and retropharyngeal nodes proven for some time, although itself an imperfect method, to be far more accurate than the physical examination (Fig. 21.12).The extent of nodal disease is often crucial to both therapy and prognosis, and high-quality, detailed imaging can improve the accuracy of clinical staging of cervical and retropharyngeal nodal metastasis (Fig. 21.13).

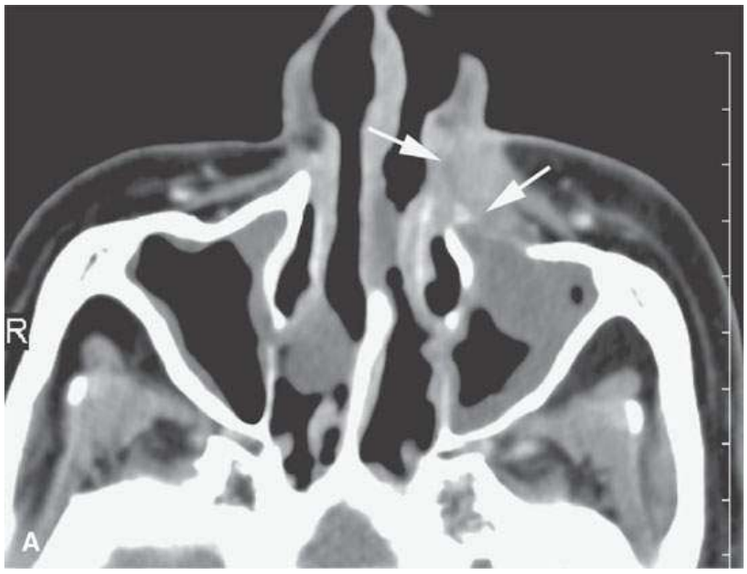

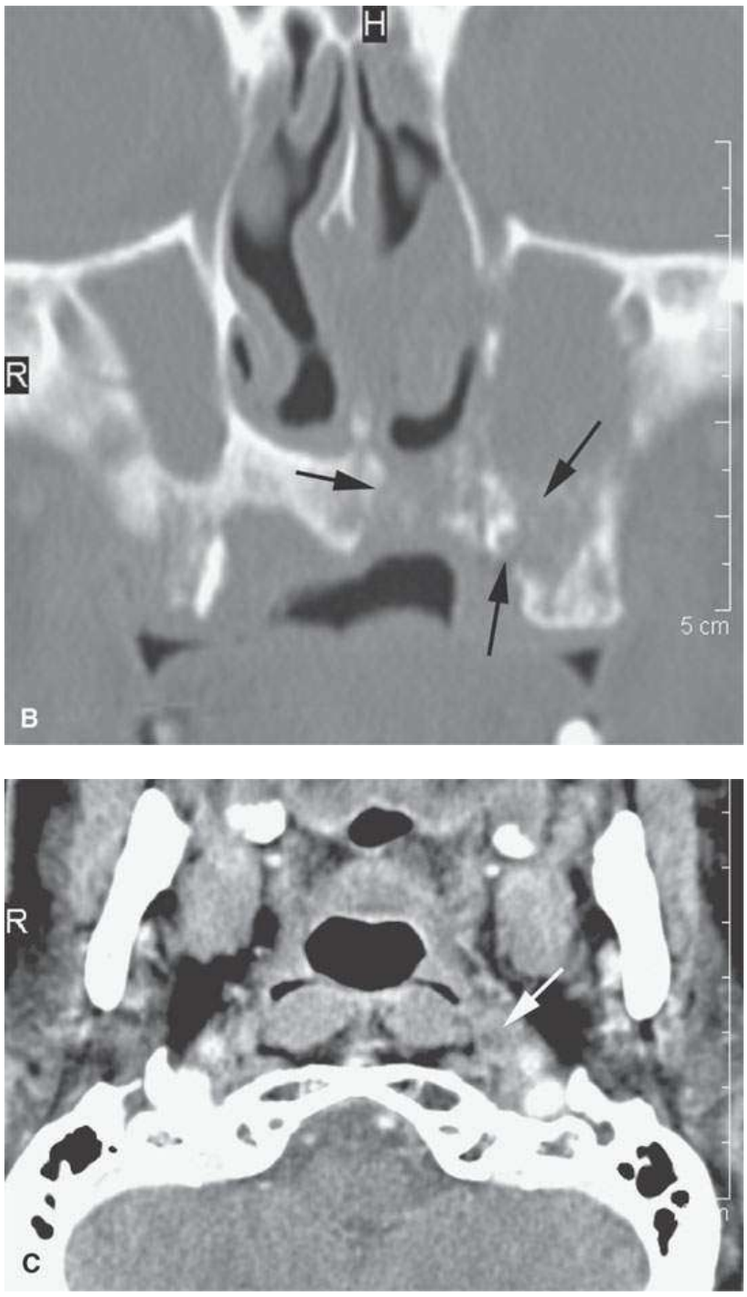

FIGURE 21.12. Contrast-enhanced computed tomography in a patient with nasal vestibule cancer invading deeply and into bone (*arrows* in **A** and **B**). The metastatic retropharyngeal node (*arrow* in **C**) significantly altered the postsurgical radiotherapy treatment plan.

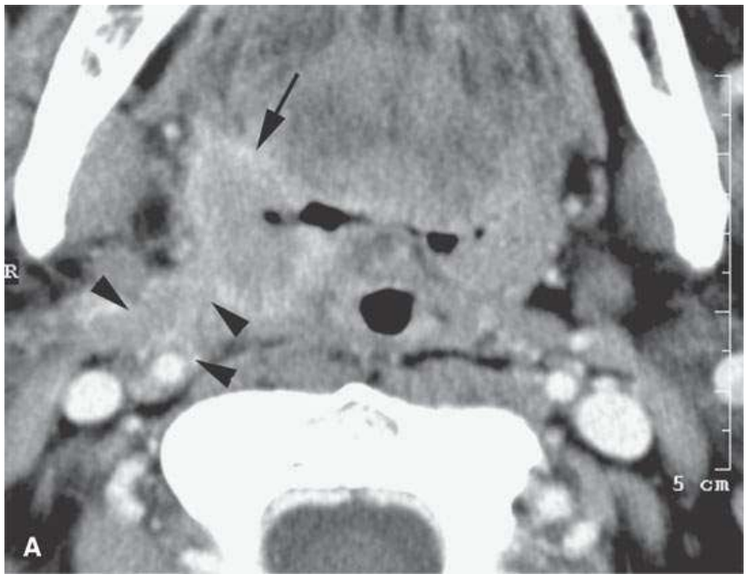

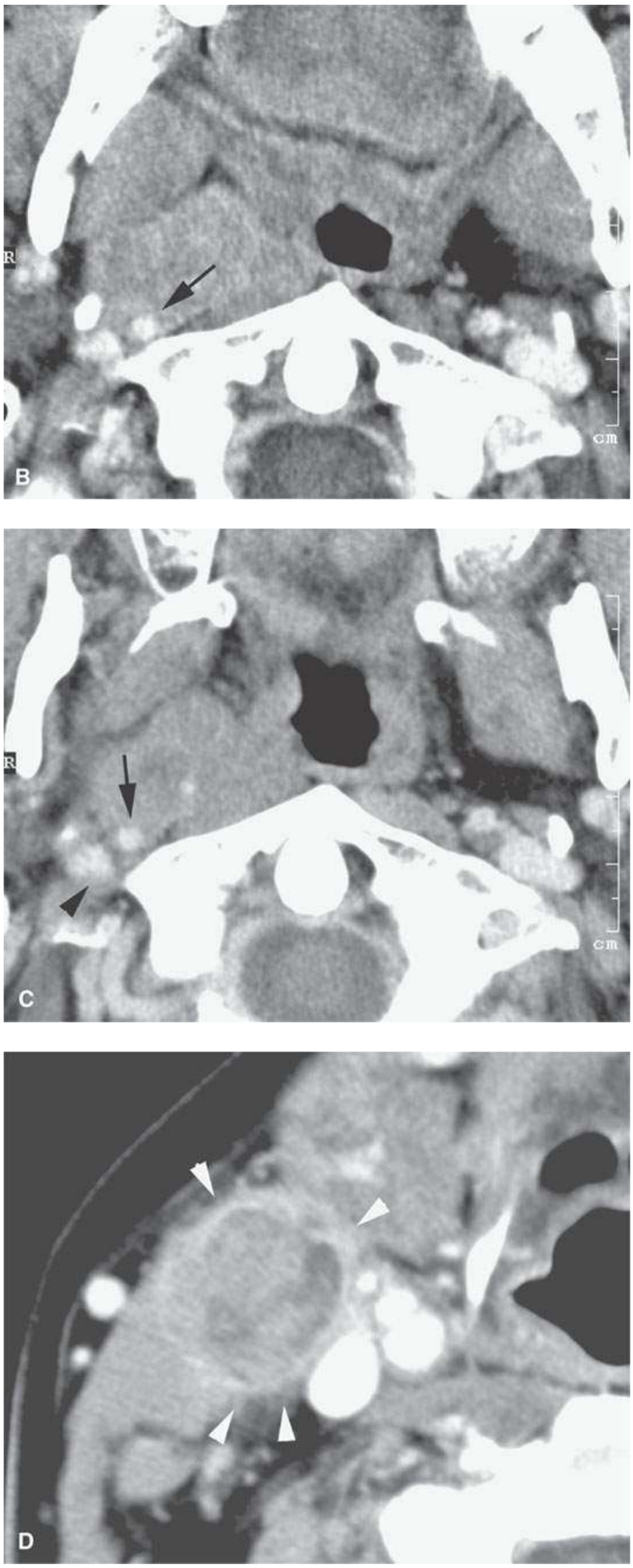

FIGURE 21.13. Contrast-enhanced computed tomography in a patient with tonsillar squamous cell carcinoma**. A:** The indistinct margins are a sign of aggressive behavior**.** The tumor breaks out of the tonsillar bed to invade along the stylopharyngeus muscle to the carotid sheath *(arrowheads)***. B, C:** The tumor continues to spread in the parapharyngeal space along the carotid sheath within the retrostyloid parapharyngeal space *(arrows)***. D:** The metastatic lymph node also reflects the aggressive nature of the cancer showing extranodal spread manifesting as indistinctness in the perinodal soft tissues *(arrowheads)***.**

Finally CT, MRI, and FDG-PET may be used to follow patients under treatment to monitor tumor response and try to detect recurrent or persistent disease before it becomes symptomatic and, hopefully, at a time when salvage therapy for cure is possible (Fig. 21.14**).** Each of these issues will now be considered in more detail.

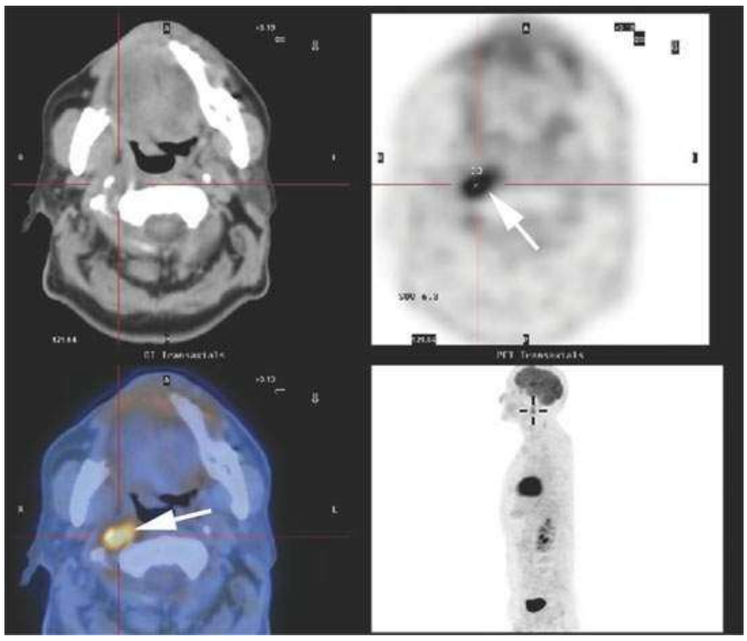

FIGURE 21.14. A patient treated for head and neck cancer developed right suboccipital headaches about 1 year after treatment. Fluorine-18 2-fluoro-2-deoxy-D-glucose positron emissio tomography (FDG-PET) study showed the failure to be in the retropharyngeal node on the right *(arrow)*.

BASIC TUMOR MORPHOLOGY AND SPREAD PATTERNS: MAINLY COMPUTED TOMOGRAPHY AND MAGNETIC RESONANCE APPEARANCE

Frequently, the decision must be made to use either CT or MR as the primary tool for evaluating a particular tumor or site. Several factors contribute to making this choice. The contrast between tumor and normal tissue is one of the more important factors. On non–contrast-enhanced CT, most tumors appear to be roughly the same density as muscle. Vague areas of fluid density somewhat less than the "tissue density" of muscle may be visible within the mass. This trend is of little practical use since non–contrast-enhanced CT is hardly ever used to evaluate cancer. Contrast between fluid and solid elements of the tumor and the much lower density fat will be excellent on CT. Contrast between tumor and lymphoid tissue such as the tonsils and adenoids will generally be poor. The tendency for poor contrast between tumor, muscle, and lymphoid tissue severely limits the value of non–contrast-enhanced CT. If contrast-enhanced computed tomography (CECT) is not possible, then contrast-enhanced magnetic resonance (CEMR) is the preferred imaging tool.

On CECT, most tumors will accumulate iodine to a greater extent than surrounding muscle; thus, CECT improves tumor to muscle contrast (Figs. 21.14 and 21.15). Many tumors will invoke an inflammatory response at their interface with normal tissues. This enhancing margin further improves tumor to muscle contrast and may help in evaluating the aggressiveness of a lesion particularly at tumor–muscle and tumor–fat interfaces. Similar improvement in contrast between tumor and lymphoid tissue may occur, but lymphoid tissue, when inflamed, will also enhance, so there is no guarantee of improved tumor–lymphoid tissue contrast (Fig. 21.15). An exception is the proven value of CECT in demonstrating focal metastatic deposits in normal size, untreated lymph nodes; in these cases, the reactive node parenchyma typically enhances to a greater degree than metastatic foci (Fig. 21.16). Marked enhancement may suggest a more uncommon etiology than the ubiquitous epithelial malignancies that involve the head and neck regions (Fig. 21.17). The degree of enhancement as a marker of perfusion and surrogate for capillary and angiogenesis on CECT has more recently been offered, at least experimentally, as a factor that might help predict response to radiotherapy.

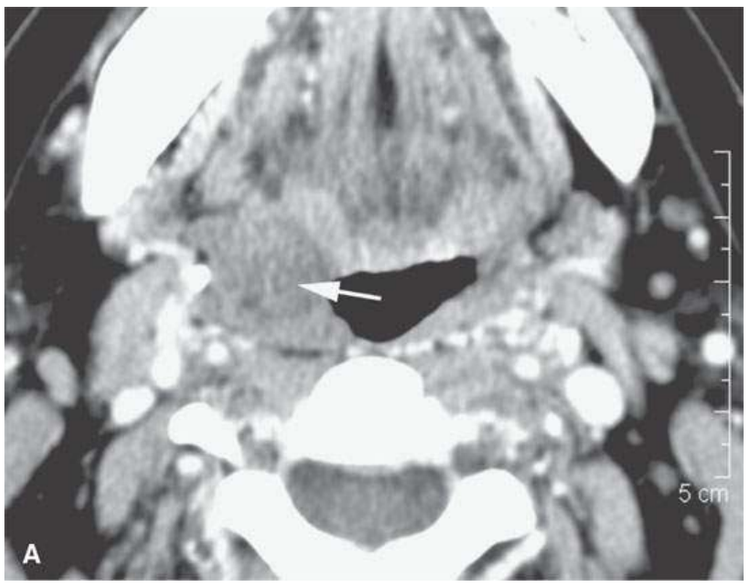

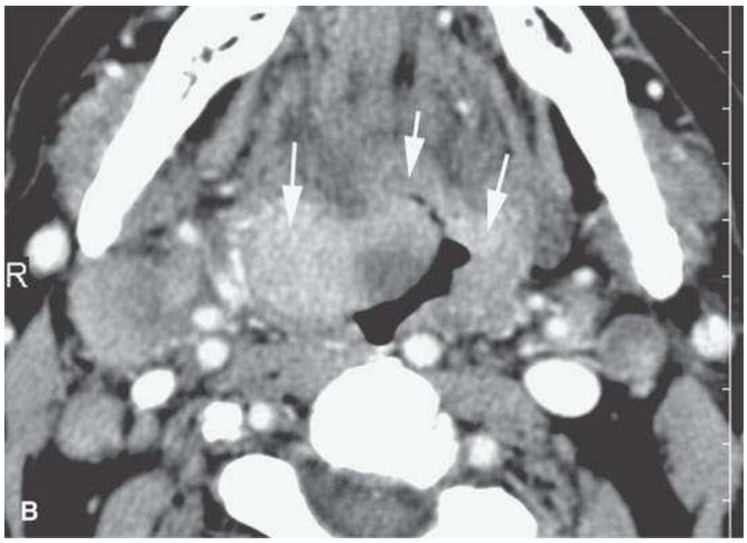
R
B

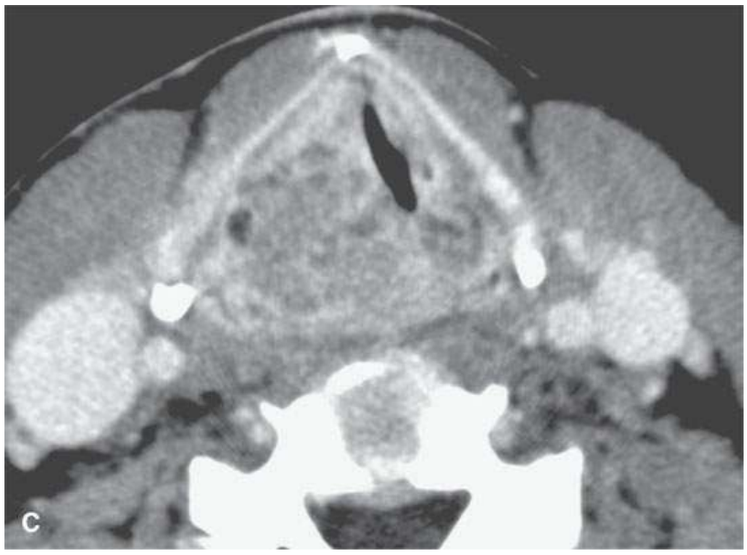
C

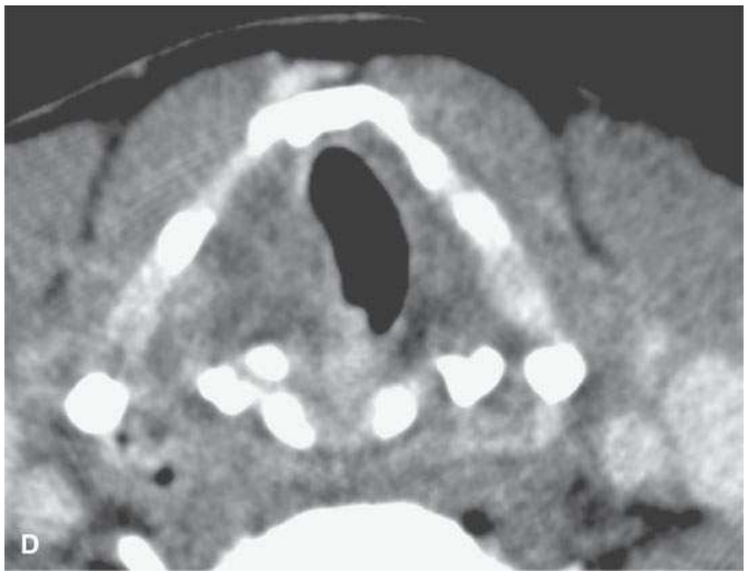
D

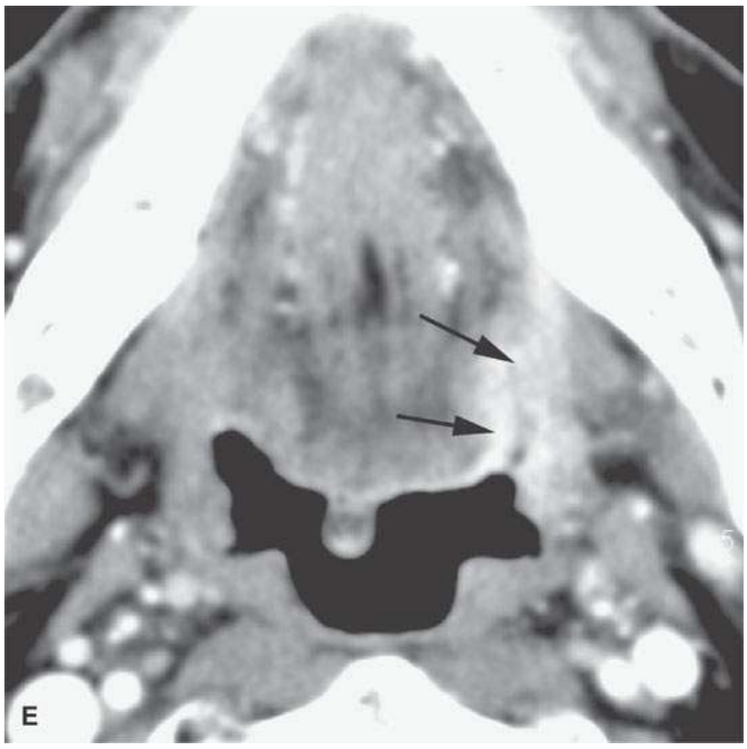

FIGURE 21.15. Contrast-enhanced computed tomography showing the range of enhancement possible in various epithelial-origin mucosal-based cancers. **A:** Adenoidcystic carcinoma of the tongue base. Note how this microcystic lesion is slightly lower in density than muscle *(arrow)*. **B:** Tongue base squamous cell carcinoma (SCCA) showing areas of variable enhancement *(arrows)*. C, D: Mixed pattern of enhancement in this poorly differentiated laryngeal cancer. **E:** Fairly brisk enhancement in this posterior oral tongue SCCA that was ulcerative clinically *(arrow)*.

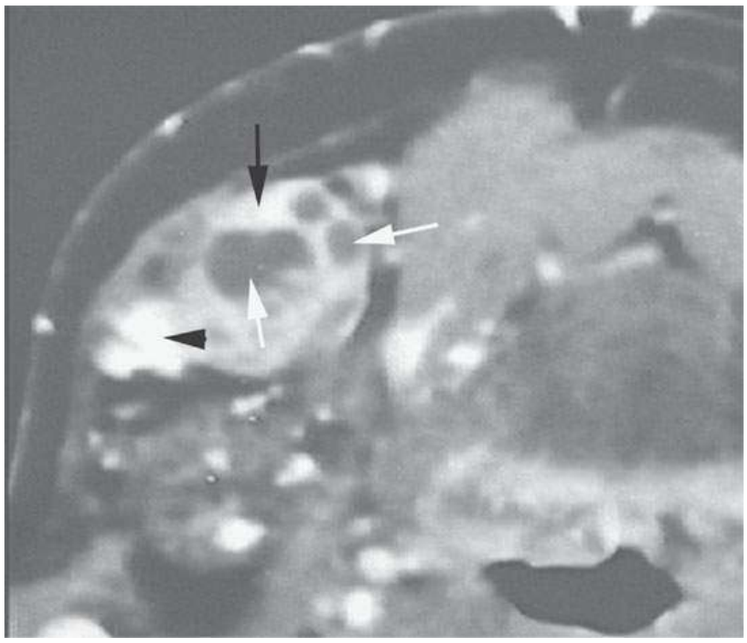

FIGURE 21.16. Contrast-enhanced computed tomography of squamous cell carcinoma metastatic to a level 1 lymph node showing focal enhancement *(black arrow)*, focal lucencies *(white arrows)*, and focal calcification or keratin debris *(arrowhead)*)—all indicators of metastatic disease.

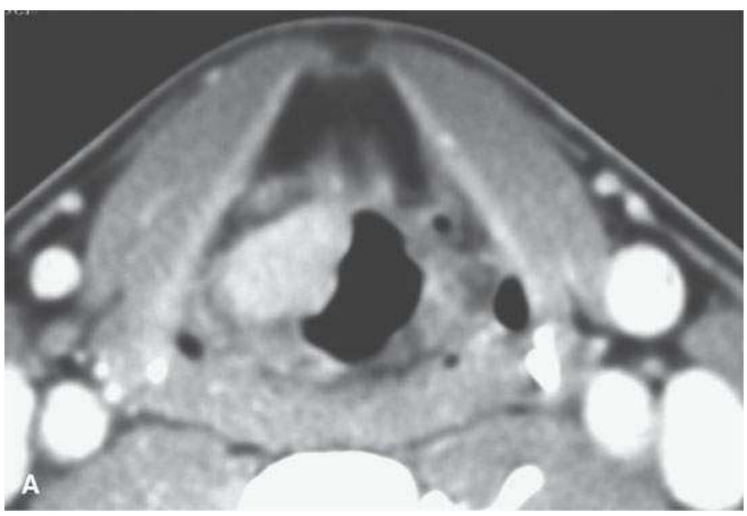

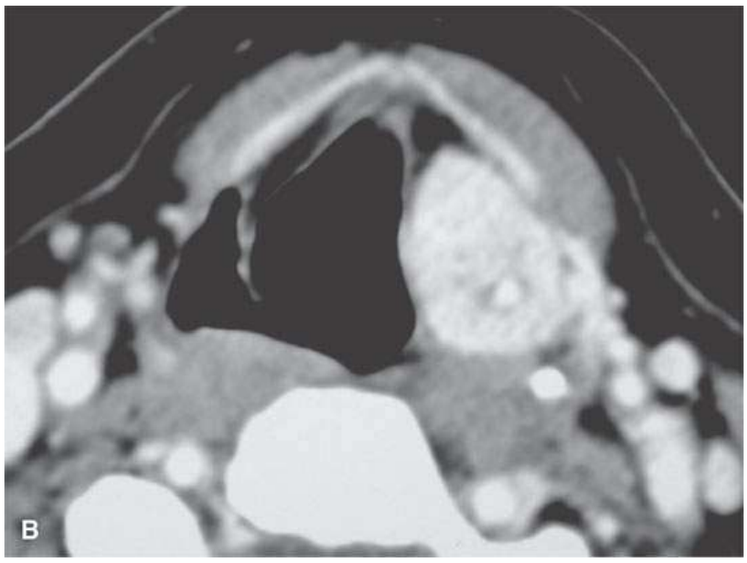

FIGURE 21.17. Contrast-enhanced computed tomography of two markedly enhancing lesions, with the degree of enhancement being somewhat unusual for an epithelial tumor. **A:** Submucosal laryngeal leiomyosarcoma. **B:** Paraganglioma of the aryepiglottic fold. Note the very large superior laryngeal vascular pedicle *(Arrowsarrows)*.

A main benefit of MRI is that image contrast is based on several intrinsic factors (T1, T2, proton density, flow) as opposed to one (electron density), as with CT as discussed in Chapters 1–3). Intravenous contrast may also be used with MR, but contrast between tumor and normal tissues can be varied by simply manipulating the pulse sequences. Non–contrast-enhanced T1-weighted (T1W) MR images generally provide suboptimal contrast between tumor and muscle or lymphoid tissue and excellent contrast between tumor and fat (Fig. 21.18 and Table 21.1). Short TI inversion recovery (STIR) images may improve tumor to muscle contrast while maintaining good tumor to fat contrast but are also limited in usefulness for technical reasons. T2-weighted (T2W) fast spin echo (FSE) images provide excellent tumor to muscle contrast; however, T2W FSE images inherently diminish the tumor to fat contrast unless they are fat suppressed using frequency selective fat suppression (Fig. 21.18). Exceptions to this are tumors with areas of necrosis, or micro- or macrocystic components, where these "cystic" components stay relatively hyperintense to fat even on T2W FSE images (Fig. 21.19). Most nonnecrotic solid neoplasms will show signal intensities that roughly parallel that of fat and lymphoid tissue on T2W sequences; however, some may be closer to muscle, especially if there is a relatively fibrous stromal component or the tumor is inherently fibrous (Fig. 21.9C). Contrast between tumor and lymphoid tissue may be poor on T2W MR (Fig. 21.18). The most obvious example of this is lymphoma, but this tendency is found with most other tumors (Fig. 21.20 and Table 21.1)

TABLE 21.1 **CONTRAST BETWEEN AN "AVERAGE" LESION*a* AND ADJACENT STRUCTURES/TISSUES**

Sequence Type	Muscle	Fat	Lymphoid Tissue	Sublingual and Submandibular Glands	Parotid Gland	Vascular Plexes	Sinus Secretions	Cerebrospinal Fluid	Brain
T1	O	±	O	O	O	O	O	±	O
T1 FS[b]	±	±	O	O	O	O	O	±	O
T1 + Gd	±	–	–	–	–	–	±	±	±
T1 + FS + Gd	±	±	–	–	±	–	O	±	±
SD	±	O	O	O	O	O	O	–	±
SD + Gd	±	–	–	–	–	–	O	O	±
T2	±	O	O	–	O	O	±	O	±
FSET2[c]	±	–	O	–	–	O	±	O	±
FSET2 + FS	±	±	O	–	±	O	±	O	±

O, not predictable but helpful at times; +, predictably good contrast in most cases; FS, fat suppression; Gd, gadolinium; –, potentially misleading and must usually compare with one or two other sequences to be sure that the pathology is not going unnoticed; SD, spin density; FSE, fast spin echo.

a"Lesion" includes a benign/malignant tumor and inflammatory/infectious processes arising extracranially.

*b*Fat suppression done with frequency selective saturation pulse.

*c*FSET2 represents fast spin echo T2 *without* fat saturation.

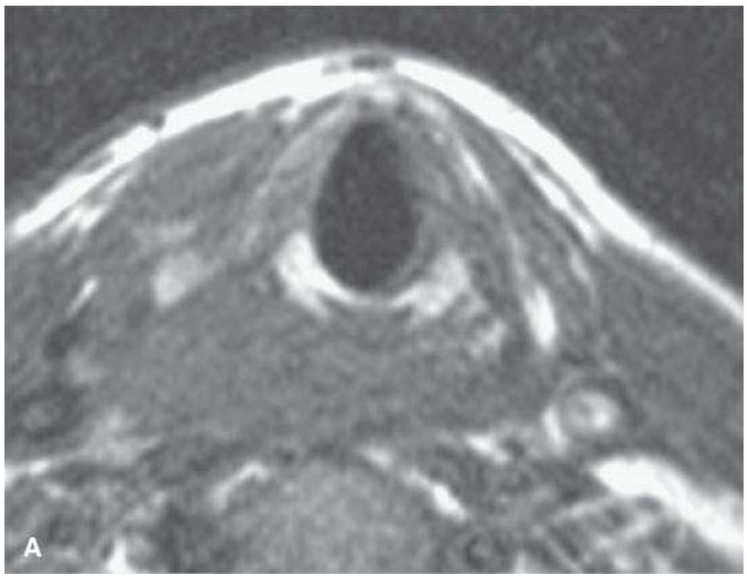
A

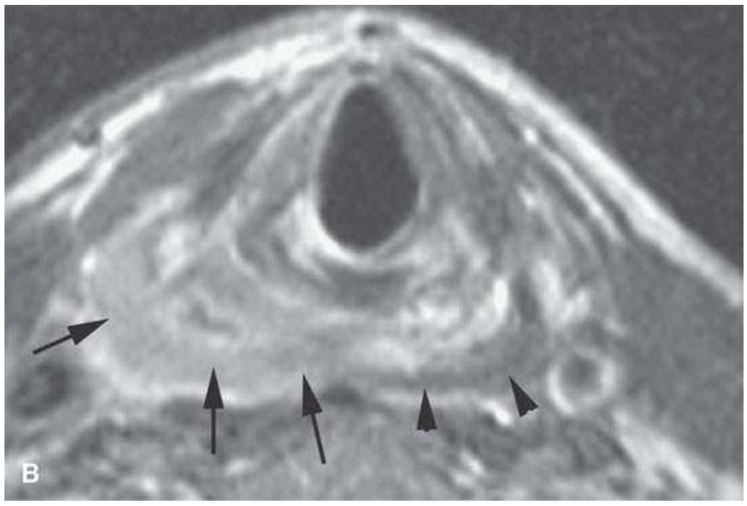
B

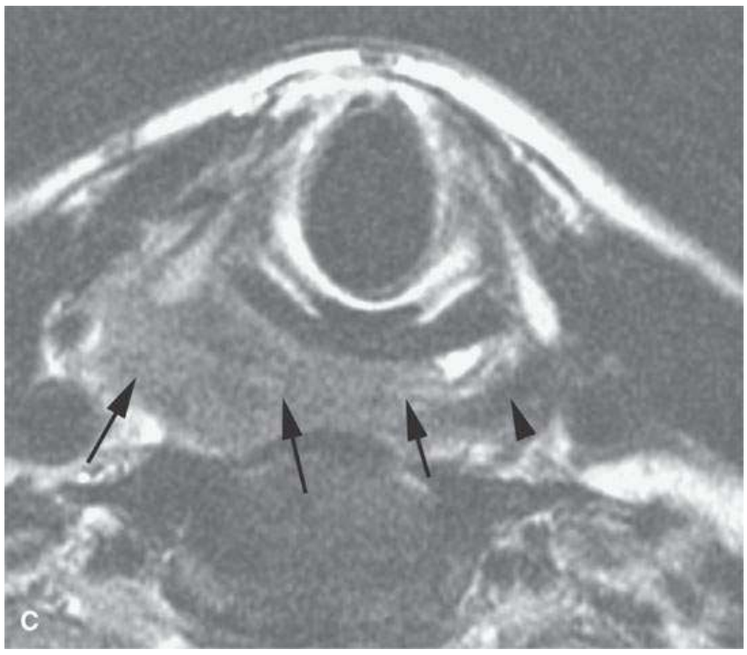
C

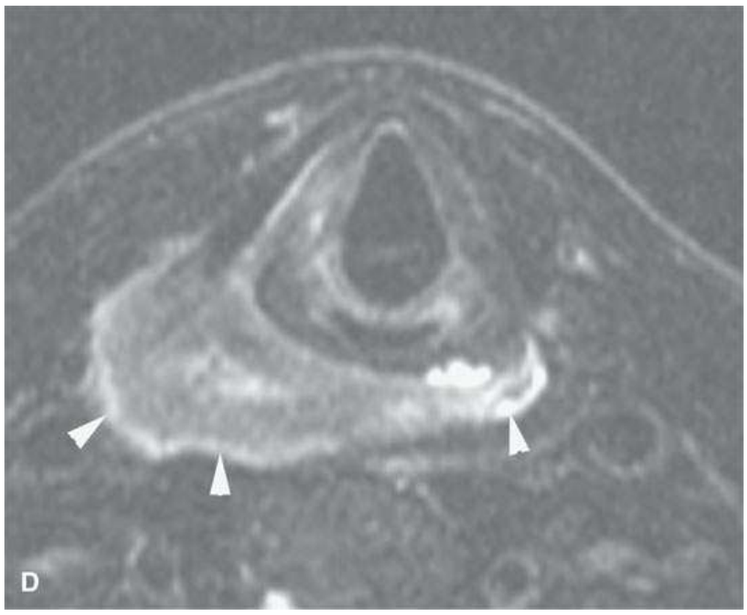
D

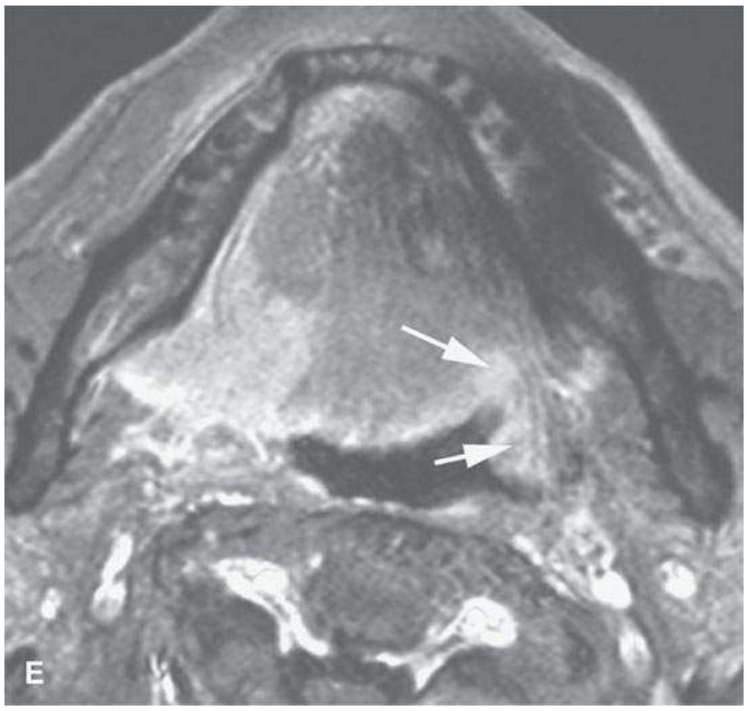
E

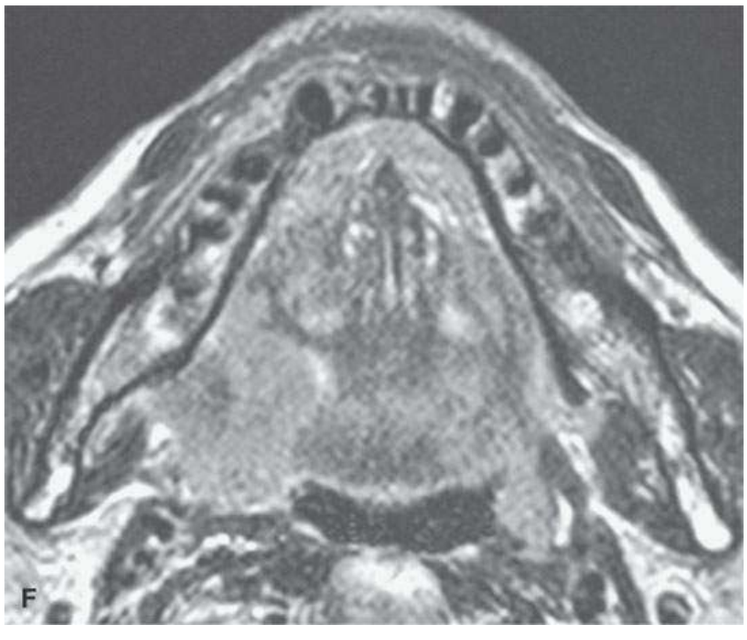
F

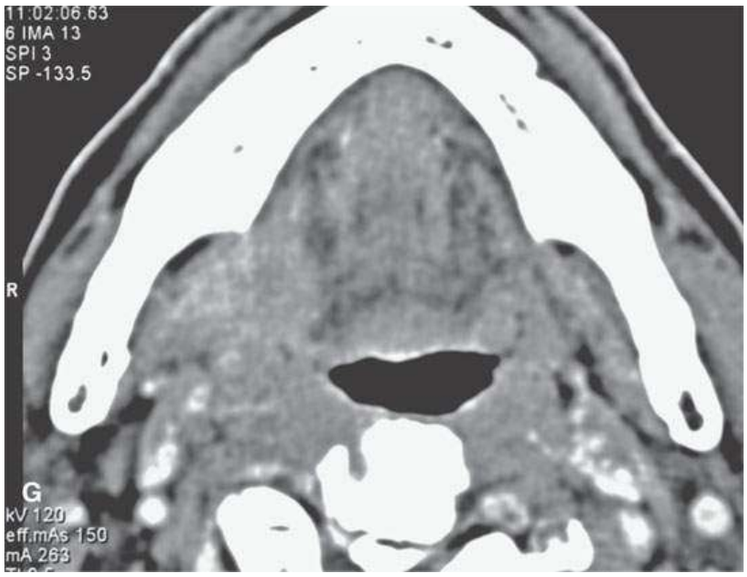

FIGURE 21.18. General trends of contrast enhancement of squamous cell carcinoma (SCCA) and malignancies in general as seen on magnetic resonance imaging in a pyriform SCCA (aA—dD) and tongue base SCCA (eE—gG)**. A:** Non–contrast-enhanced T1-weighted (T1W) image shows poor tumor to muscle contrast**. B:** Contrast-enhanced T1W image shows enhancing tumor *(arrows)* contrasts well with muscle *(arrowheads)***. C:** T2-weighted (T2W) image shows fairly good tumor *(arrows)* to muscle *(arrowhead)* contrast**. D:** Fat-suppressed T2W image improves on the contrast seen in (cC) and shows peritumoral edema better *(arrowheads)***. E:** Contrast-enhanced fat-suppressed T1W image shows excellent tumor to muscle contrast but relative poor contrast with normal lymphoid tissue *(arrows)***. F:** T2W image shows good tumor to muscle contrast but relatively poor contrast with normal lymphoid tissue *(arrow)***. G:** Contrast-enhanced computed tomography for comparison with (e E) and (fF)**.**

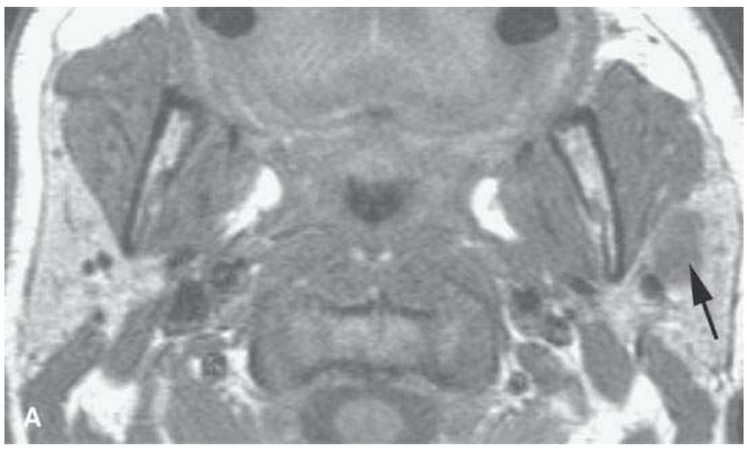

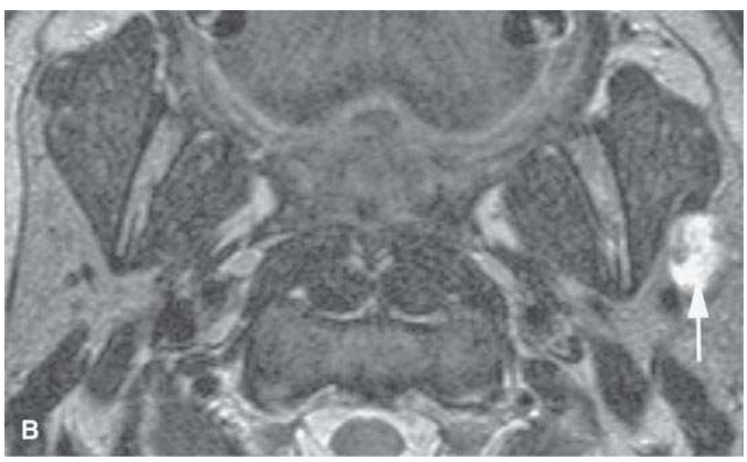

FIGURE 21.19. Magnetic resonance imaging of a patient with a benign mixed tumor of the parotid *(arrows)*, with the microcystic nature of the tumor better appreciated by the increased signal intensity on the T2-weighted image in (bB) compared with the noncontrast T1-weighted image in (A)**.**

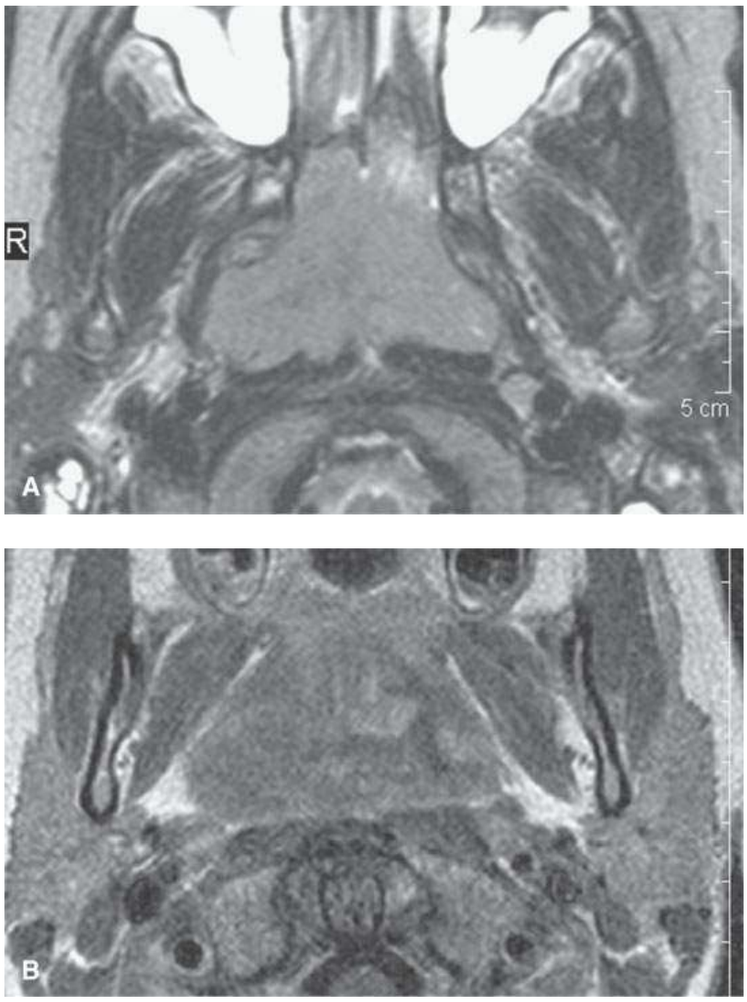

FIGURE 21.20. Magnetic resonance imaging of a patient with Burkitt lymphoma showing that on the T2-weighted image in (aA), the tumor is about the same signal intensity and normal lymphoid tissue but on the T1-weighted contrast-enhanced image **(B)** shows an inhomogeneous pattern different from that usually seen in normal lymphoid tissue.

Gadolinium CEMR behaves in a manner similar to that described for CECT. Tumor to muscle contrast is improved on contrast-enhanced T1W images with the margins and internal morphology of the lesion becoming more apparent (Fig. 21.18). However, since fat is bright on T1W images, CEMR will diminish the contrast between tumor and surrounding fat. This may cause a significant problem in evaluating tumors in extracranial locations or those invading bones containing fatty marrow such as the mandible and skull base (Fig. 21.8).

Fat suppression techniques can be used with T1 or T2W pulse sequences to overcome some of the difficulties with tissue contrast that were just discussed. Fat suppression techniques are not a cure-all, and the ideal single pulse sequence for evaluating all head and neck neoplasms does not yet exist. Also fat suppression techniques all suffer from problems with susceptibility artifacts.

In summary, the contrast between various tumors and surrounding tissue will vary with the tumor histology, size, growth pattern, and natural history of the lesion. Some specific factors that will influence the appearance of particular tumors to be discussed in subsequent sections of this chapter include cellular elements, stromal elements, an acinar or microcystic morphology, macrocystic components or necrosis and cyst contents, hemorrhage, naturally occurring paramagnetic substances, calcification or ossification, growth pattern and peritumoral reactive changes, prior treatment, and the use of intravenous contrast enhancement. The physical basis of some of these factors is considered in the technical section and other discussions in Chapters 1 through 5 and 10 through 12.

While FDG-PET is useful for decision making in some head and neck cancer patients, it is not on its own sufficient for showing the extent of the primary tumor, including bone destruction and perineural spread. The physiologic data from FDG-PET can be fused to CT and MRI data sets or acquired simultaneously to help refine the gross anatomic limits of metabolically active tumor.

US is only of limited use in evaluating primary malignant and benign tumors. It is used primarily in the thyroid and major salivary glands. Some practices find it useful in the routine evaluation of cervical nodes. Its use in exploring the elastic properties of tumors as a measure of their invasiveness or simply for differential diagnosis is in the early stage of clinical investigation.

INTERNAL MORPHOLOGY OF NEOPLASMS

Most tumors grow as a discrete mass. They are generally shaped like a sphere or solid ellipse, even when malignant, but may be modified by surrounding anatomy; the growth patterns that result are discussed subsequently (Fig. 21.21). The mass will have an internal appearance on CT or MR based on the major factors discussed previously and technical factors related to image acquisition.

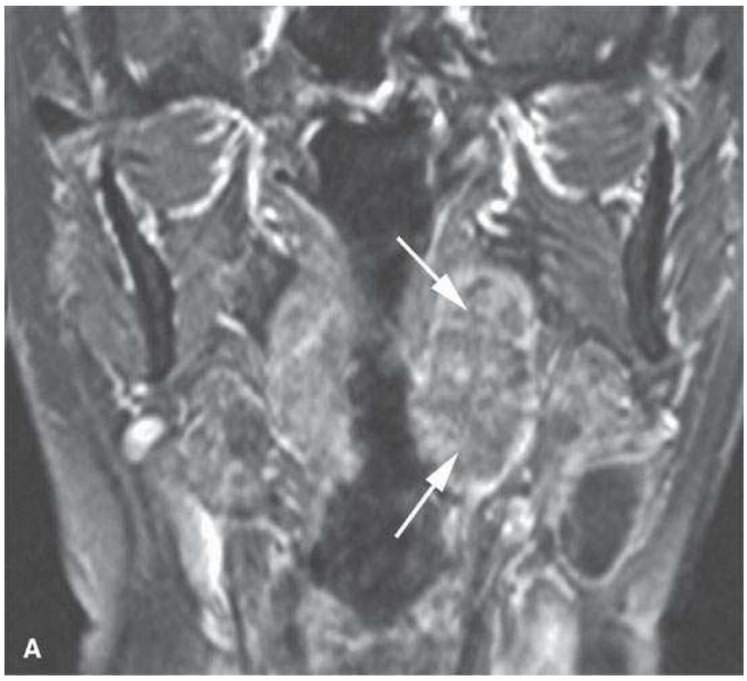
A

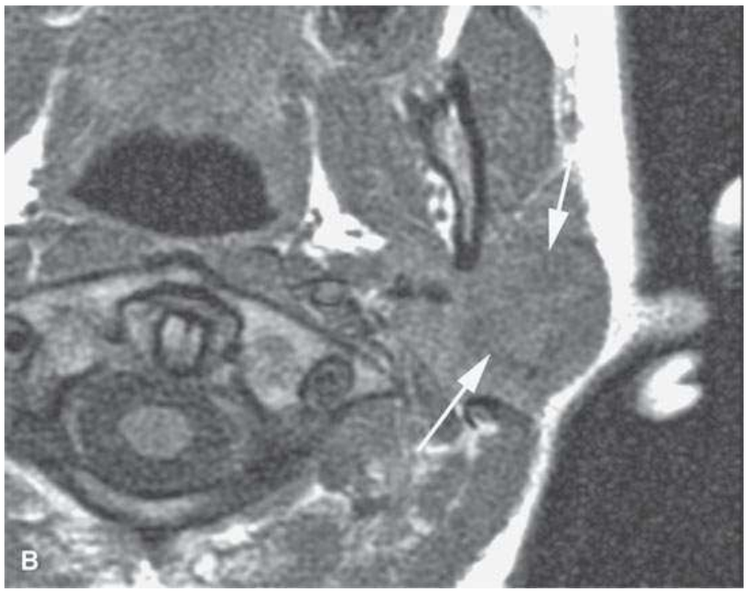
B

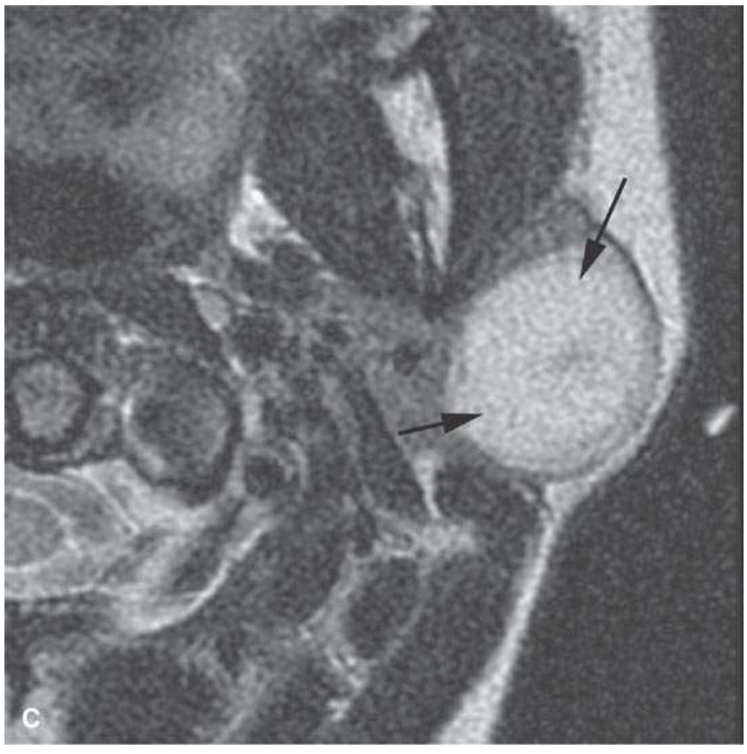
C

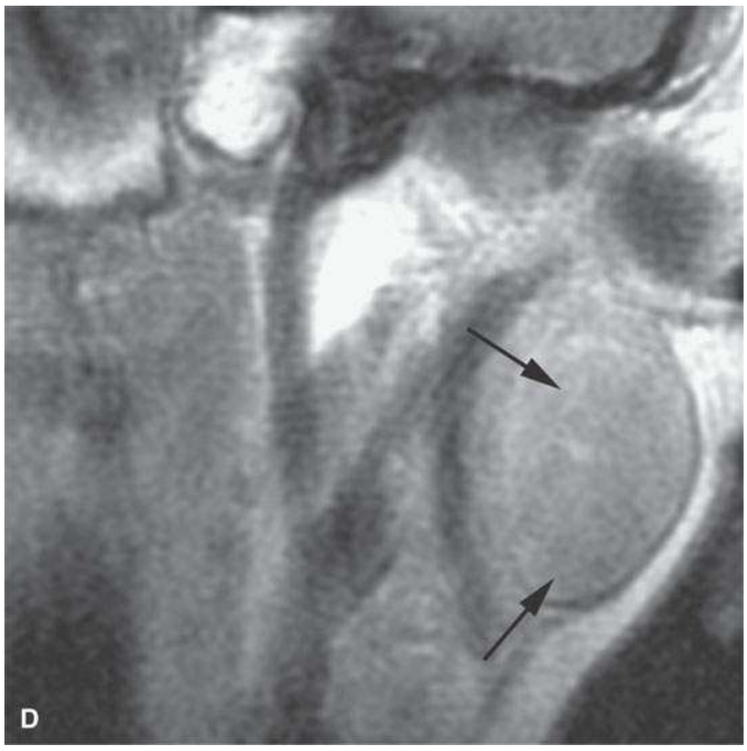

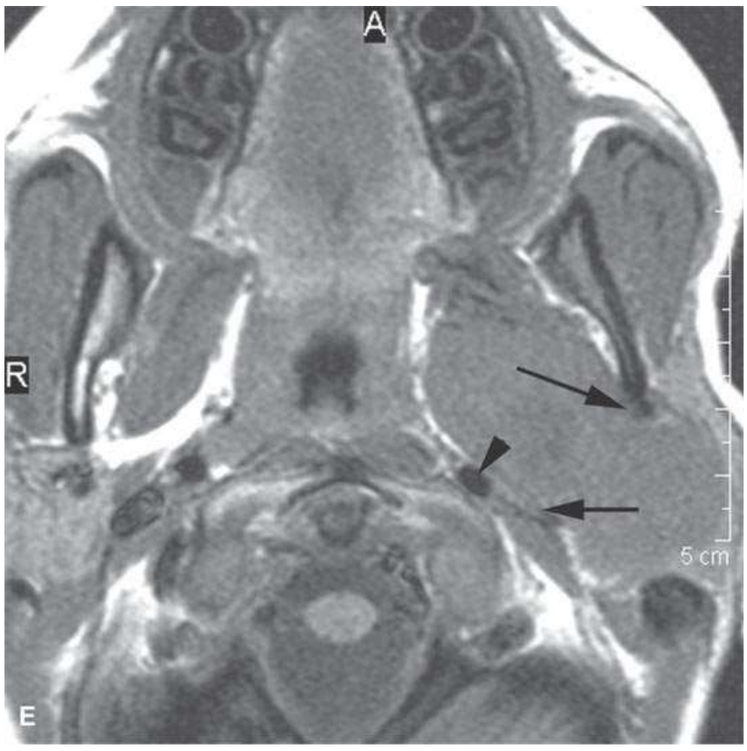

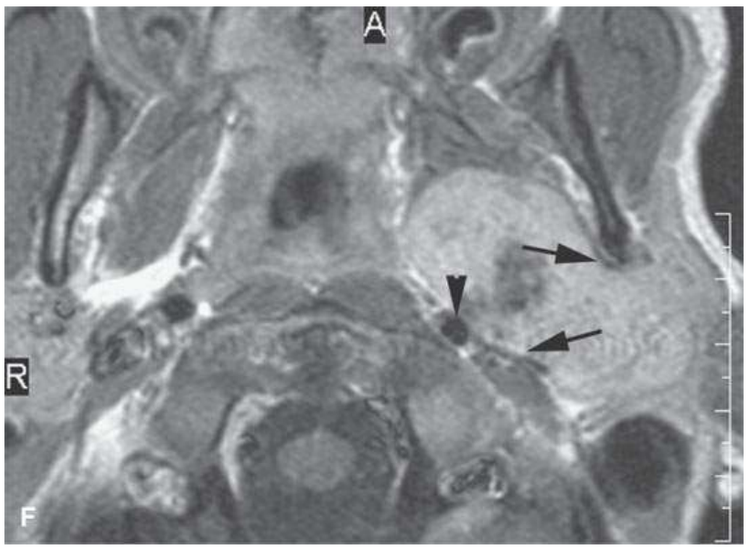

FIGURE 21.21. Magnetic resonance imaging studies showing the general tendency of tumors to grow as a spheroid unless constrained by surrounding anatomy. **A**: Contrast-enhanced T1-weighted (T1W) image of a tonsillar squamous cell carcinoma *(arrows)*. B–D: Magnetic resonance and acinic cell parotid cancer *(arrows*))—non–contrast-enhanced T1W, T2-weighted, and contrast-enhanced T1W coronal, respectively. E, F: Non–contrast-enhanced T1W and contrast-enhanced T1W images of a parapharyngeal benign mixed tumor with the large egg-shaped tumor conforming in its midsection *(arrows)* as it extends through the stylomandibular tunnel. Note the tendency of the mass to displace surrounding structures such as the carotid artery *(arrowhead)* in a manner that suggests its site of origin and in that alone suggests a narrow differential diagnosis.

Homogeneously solid tumors on gross appearance may show tremendous differences histologically. Such differences in microscopic structure will usually affect the MR appearance of the lesion to a far greater degree than the CT appearance. Tumors composed of tightly packed cells, with relatively little water in the cytoplasm and little stroma, will usually be isodense to muscle on non–contrast-enhanced CT and isointense to slightly hyperintense to muscle on non–contrast-enhanced T1W images (Figs. 21.1A and 21.4A). T2W FSE images will show such a lesion to be roughly isointense to fat, slightly hyperintense to muscle, and likely slightly less intense than lymphoid tissue (Figs. 21.1, 21.2, 21.5, 21.17, and 21.18). These trends are those most commonly present in squamous cell carcinoma (Table 21.1). The tumor cells may also have a large amount of watery cytoplasm. A good example is the heavily mucoid-laden cell population of a chordoma. The more voluminous or watery cytoplasm cause such tumors to have higher signal intensity on heavily T2W images than the more common variety of tumor cell population (Fig. 21.22). Densely cellular tumors with limited stromal volume tend to show restricted diffusion.

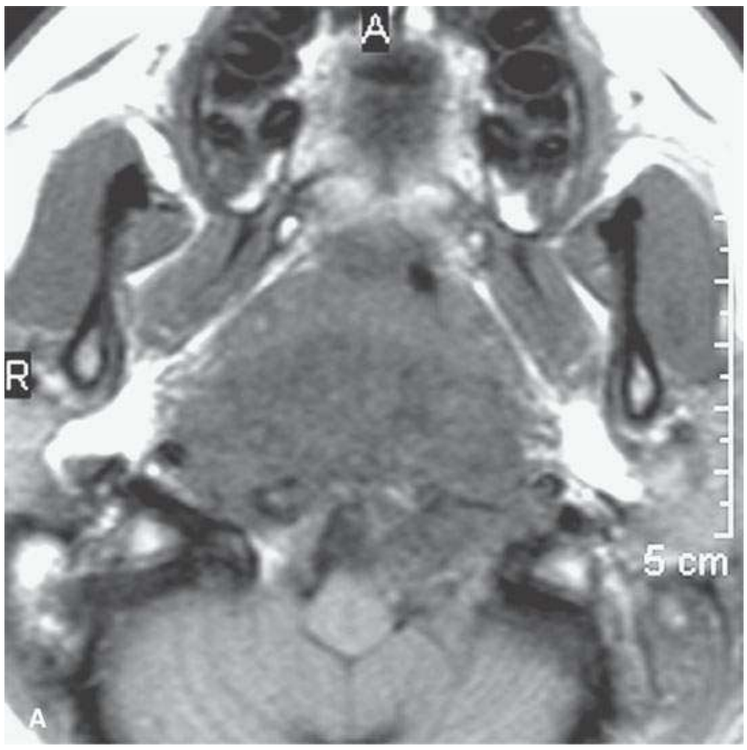

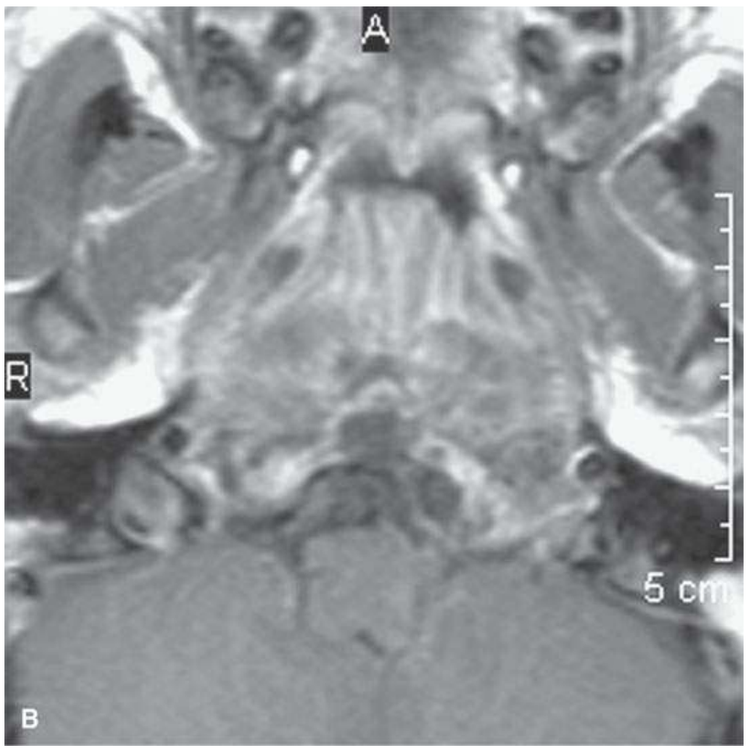

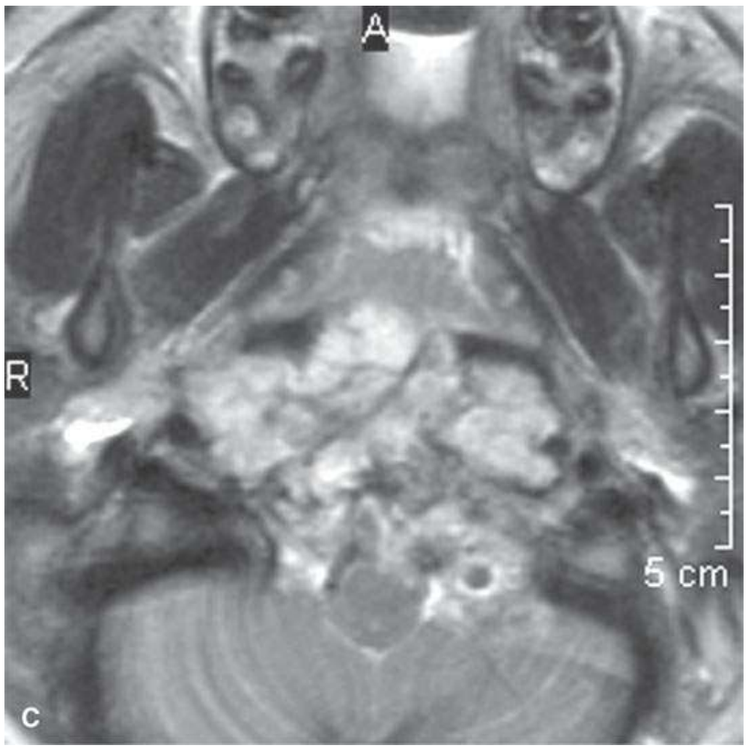

FIGURE 21.22. A–C: Magnetic resonance imaging of a chordoma of the lower clivus, with the "watery" nature of the tumor cells and stroma much more apparent by the way of its signal intensity approaching and matching that of cerebrospinal fluid in some areas on the T2-weighted image in (cC) than on the non–contrast-enhanced (aA) and contrast-enhanced (bB) T1-weighted images.

Tumor cells may be mixed with a neoplastic or reactive stroma. The appearance of CT and T1W images may due to differences in stromal elements as well as the neoplastic cell population. For instance, a water-rich stroma may cause the lesion to appear somewhat hypointense to muscle on T1W images. Variations in stromal structure can greatly alter the appearance on T2W images. At the extremes of this are the very watery mucoid matrix of chordoma that causes the tumor to appear bright (Fig. 21.22) and often partially calcified fibrous matrix of fibro-osseous lesions that make them appear sometimes muscle equivalent on heavily T2W images (Fig. 21.23). Reactive fibroproliferative processes that may mimic tumor can have even a more densely collagenous makeup and profoundly low signal intensity on T2W images—a characteristic that is distinctly uncommon in all but a very few benign and malignant neoplasms (Fig. 21.24). One can extrapolate from these extreme examples the varied appearances that result from lesser amounts of fluid, cells, or fibrosis in a tumor matrix or stroma.

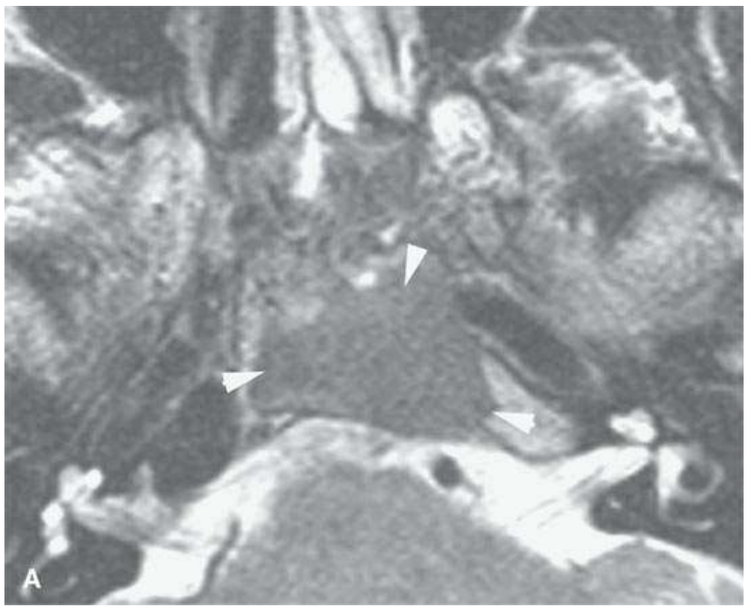

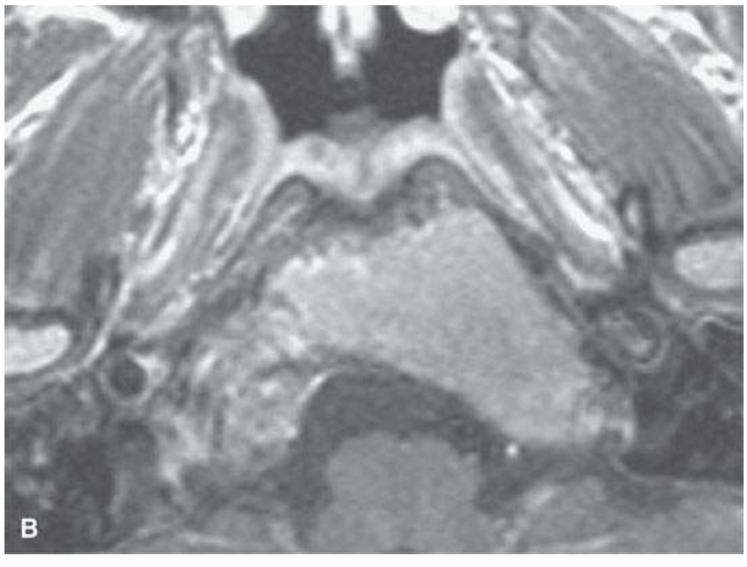

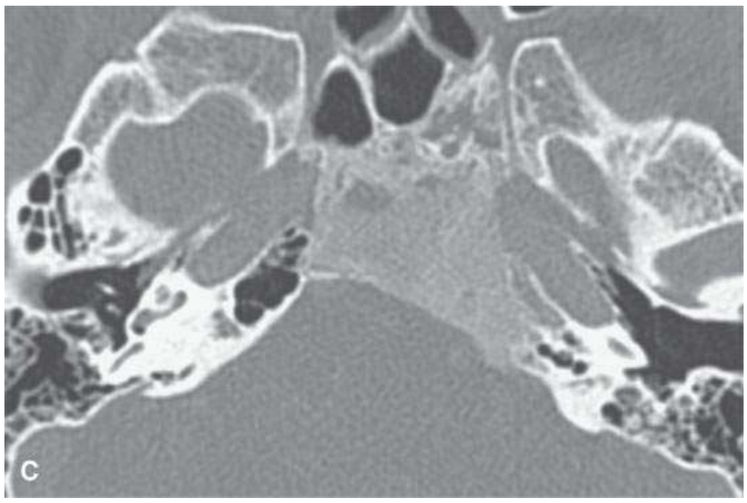

FIGURE 21.23. Magnetic resonance imaging of fibrous dysplasia of the lower clivus, with the fibrous and mineralized matrix nature of the process *(arrowheads)* much more apparent on the T2-weighted image by way of its diminished signal intensity relative to fat and near to that of muscle in (aA) than in the contrast-enhanced (bB) T1-weighted image**. C:** Computed tomography for comparison**.**

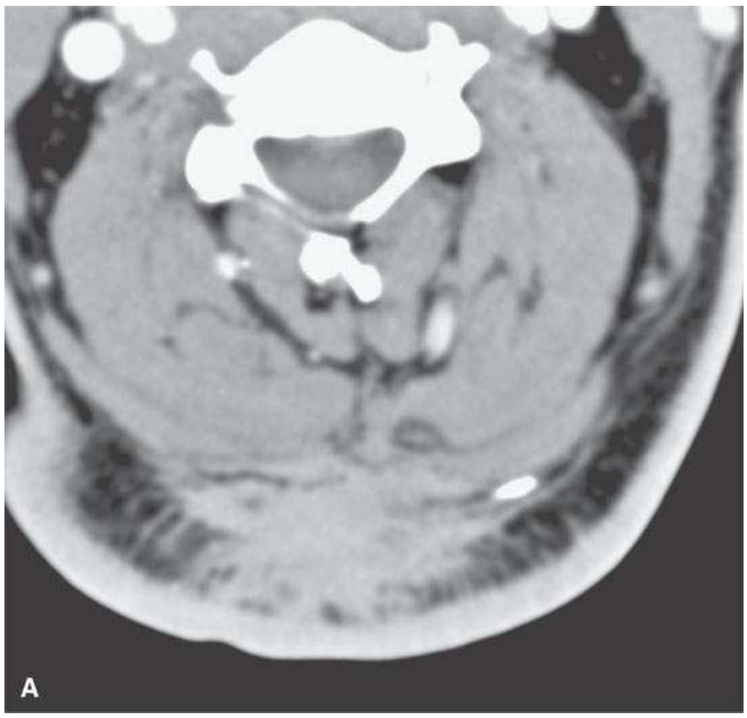

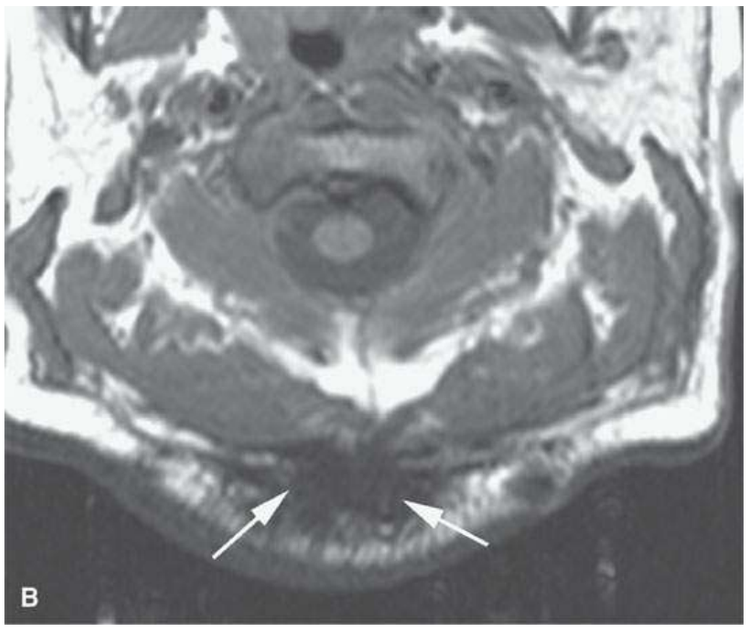

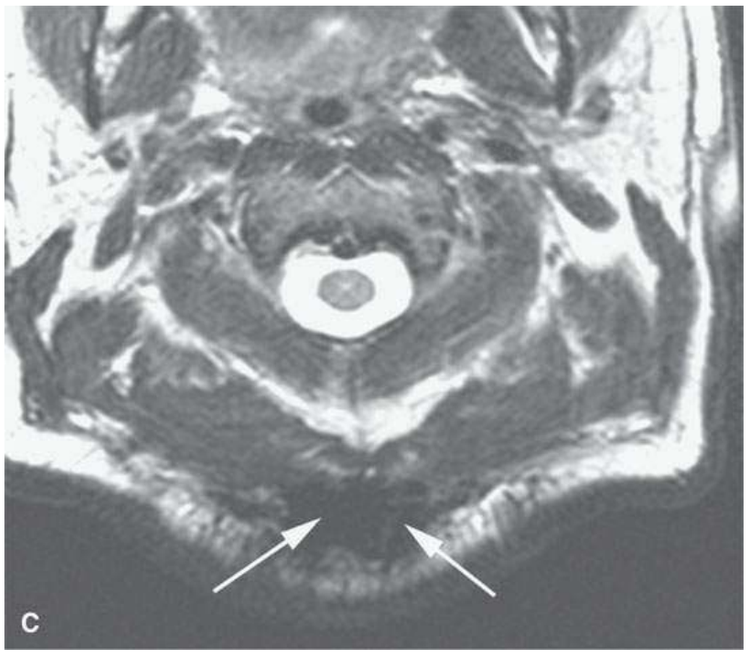

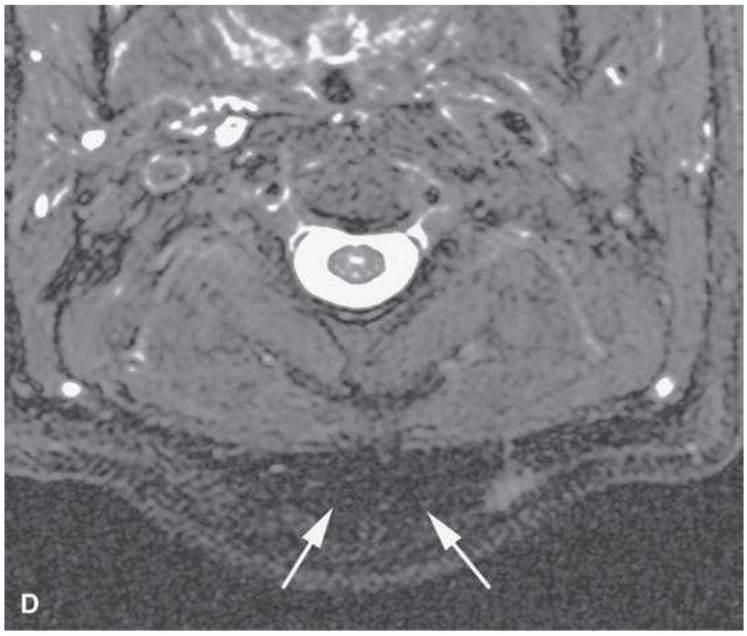

FIGURE 21.24. A–D: A patient with very intense fibroproliferative changes, with the fibrous nature of the mass much more obvious on magnetic resonance imaging (b-dB–D) than computed tomography (CT) (aA) based on its markedly diminished signal intensity relative to muscle on all pulse sequences *(arrows)*. On CT, its density is actually slightly greater than that of muscle. Also note the very aggressive margins in this benign process compared with the pushing, well-defined margins of many malignancies illustrated in this chapter.

Tumors may be nearly entirely or partially microcystic. A classic example is the proliferative hemangioma (Fig. 21.25). These true neoplasms may appear slightly hypointense to muscle on T1W images. The effect of the increased fluid in myriad microscopic vascular spaces is most noticeable as markedly increased signal intensity on heavily T2W images. This reasoning can be extrapolated to thyroid adenomas and papillary-follicular carcinoma and epithelial salivary gland tumors (Chapter 22) among others. These tumors may contain colloid, microcysts, acini, or vascular spaces filled with fluid-rich contents that will have high signal intensity on T2W images with the actual signal intensity seen dependent on the relative amount of macromolecules and bound and unbound water present in the respective “cystic spaces.”

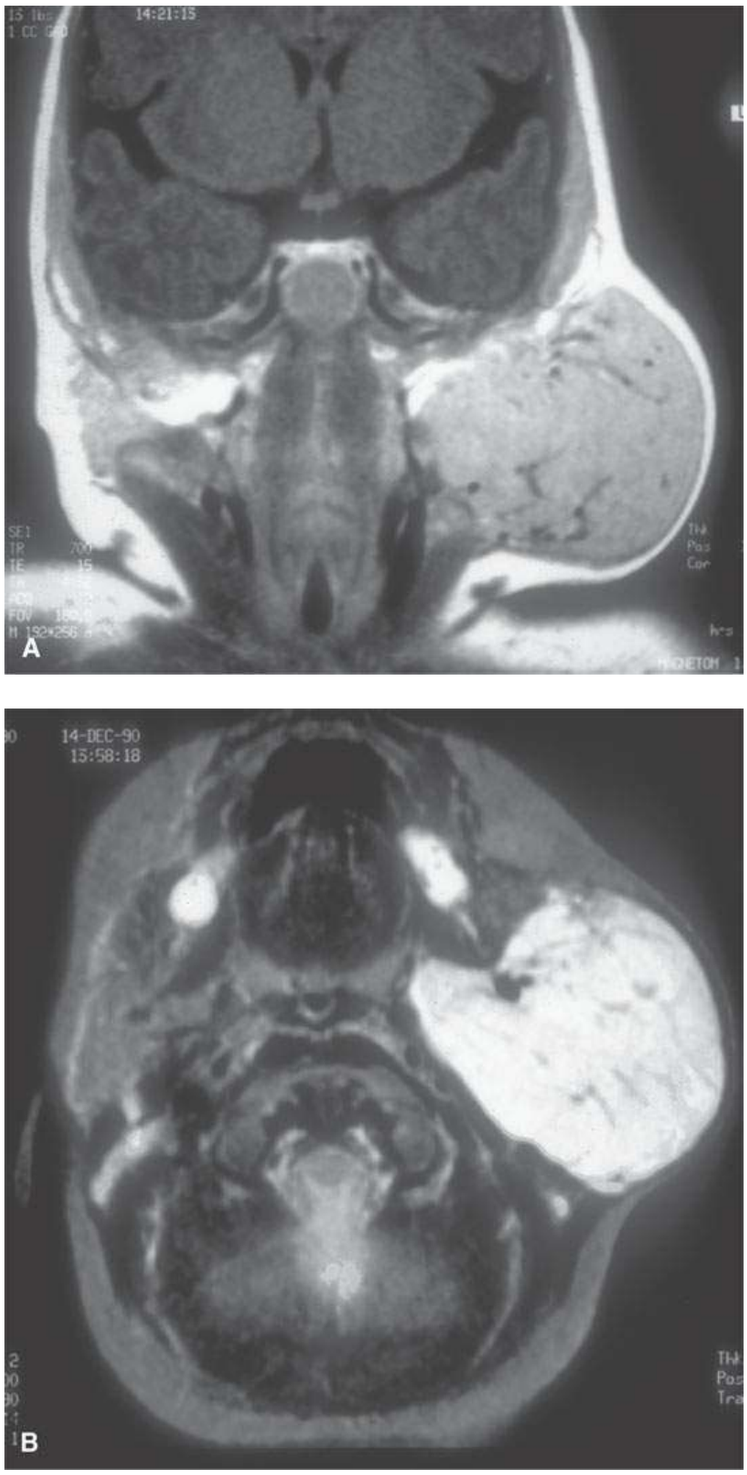

FIGURE 21.25. Magnetic resonance imaging of a parotid proliferative hemangioma, with the contrast-enhanced T1-weighted image in **(A)** reflecting the blood pool nature of its many tiny cystic spaces filled with relatively static blood and the T2-weighted image in **(B)** showing the intensely bright signal again reflecting the basically microcystic nature of the mass.

Both benign and malignant tumors may show focal areas of necrosis and hemorrhage. Some tumors are commonly macrocystic, such as mucoepidermoid carcinoma (Fig. 21.26). The differences in possible origins of macrocysts mean that a cystic cavity may vary in appearance from a smooth, thin-walled, and unilocular lesion to a thick, multiseptated, irregular-walled cavity. The density or signal intensity of a hemorrhagic cavity depends on the state of blood product evolution and macromolecular content of the fluid. Tumoral cysts and bleeding are discussed more specifically with regard to the reasons for their varied appearance in Chapters 10 and 11.

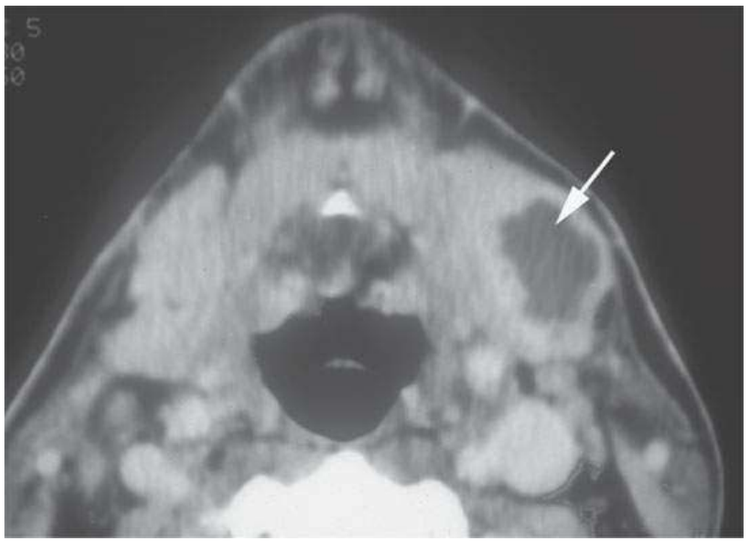

FIGURE 21.26. Contrast-enhanced computed tomography of macrocystic changes *(arrow)* in a mucoepidermoid carcinoma.

GENERAL TRENDS IN GROWTH PATTERNS OF BENIGN AND MALIGNANT NEOPLASMS

Growth patterns within the soft tissues as well as associated findings such as bone erosion and perineural extension seen on imaging studies are a valuable aid to the differential diagnosis. Taken with the history, physical examination, and gross morphology of the lesion, a particular growth pattern can often suggest a specific diagnosis. For example, a highly vascular lesion in the posterior nasal cavity and nasopharynx growing into the pterygopalatine fossa, with regressive remodeling of surrounding bone, in an adolescent male with nosebleeds is virtually always a juvenile angiofibroma (Fig. 21.7). Lack of extension into the pterygopalatine fossa or an aggressive pattern of bone destruction in the same clinical situation strongly suggests a different diagnosis such as a malignant tumor (Fig. 21.27) or an alternative benign neoplasm (Fig. 21.28) or other disease process. Growth patterns may also reflect the rate of growth of a lesion, but morphologic features of a slow-growing lesion do not necessarily indicate that the disease is benign.

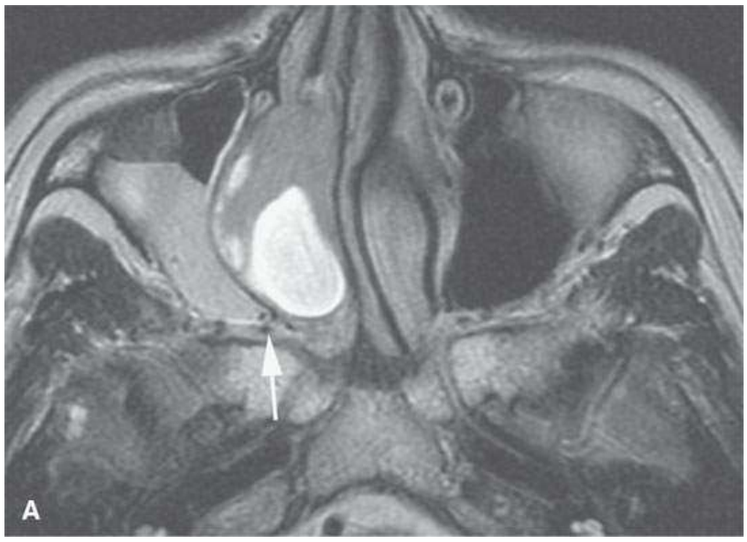

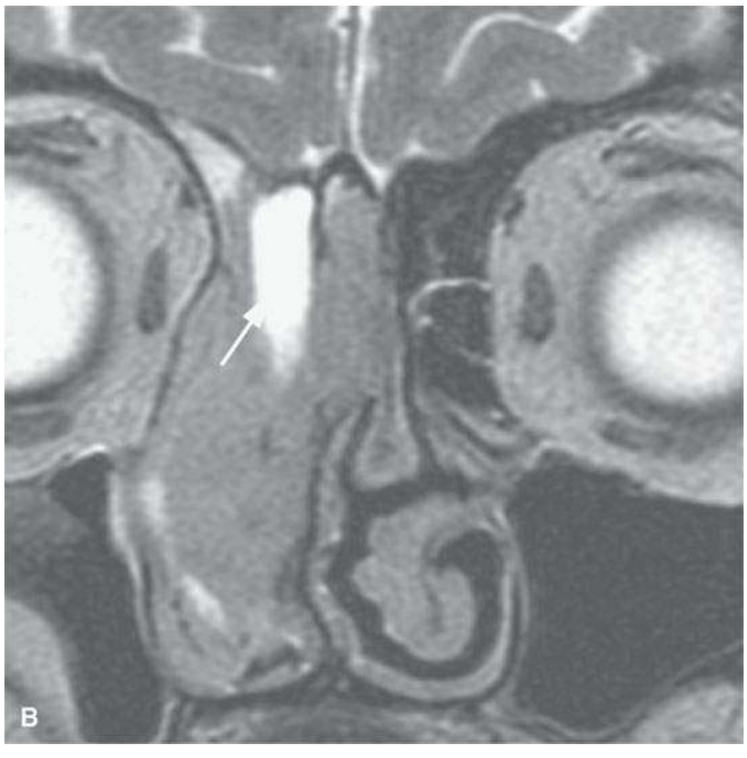

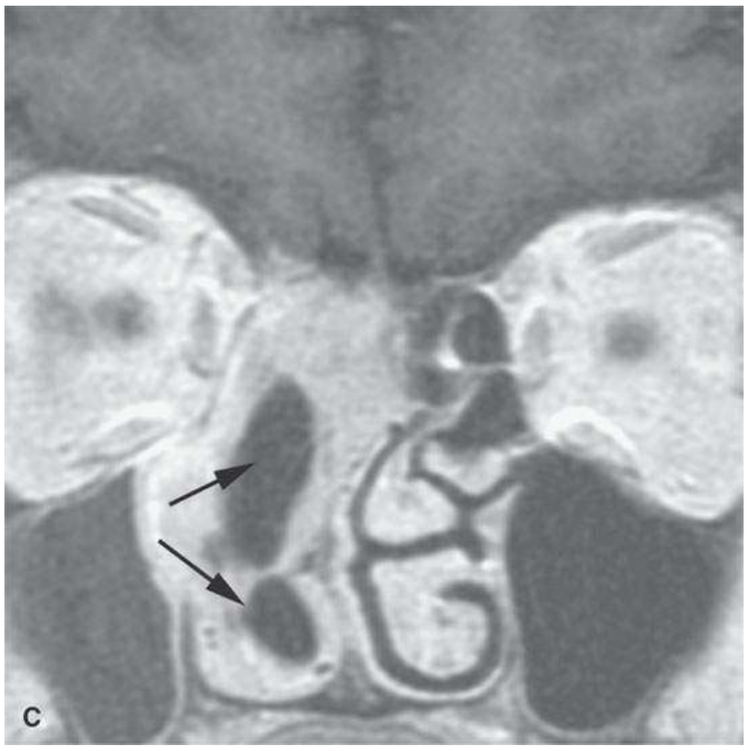

FIGURE 21.27. Contrast-enhanced magnetic resonance in a young male believed to have a juvenile angiofibroma clinically but the study showing no extension into the pterygopalatine fossa (*arrow* in **A**) in this leiomyosarcoma**.** B, C: Cystic regressive changes *(arrows)* in an otherwise homogenous and diffusely enhancing mass without obvious flow voids**.**

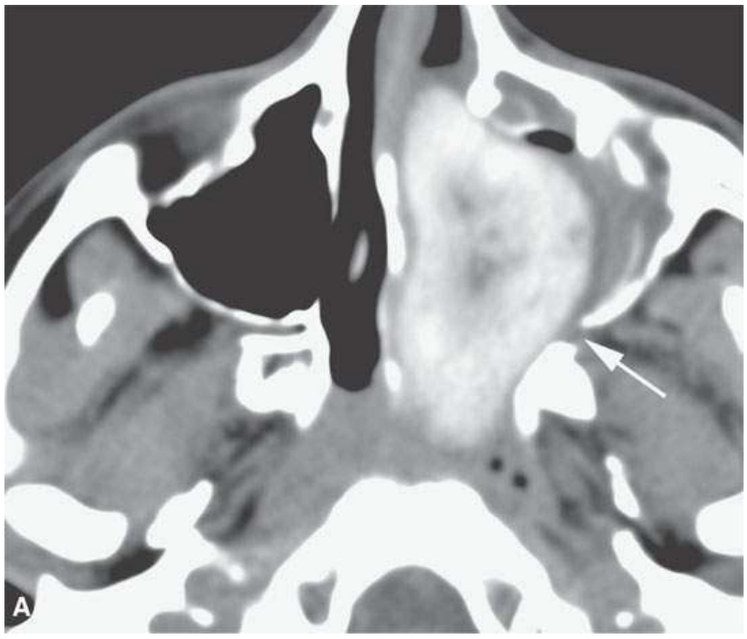

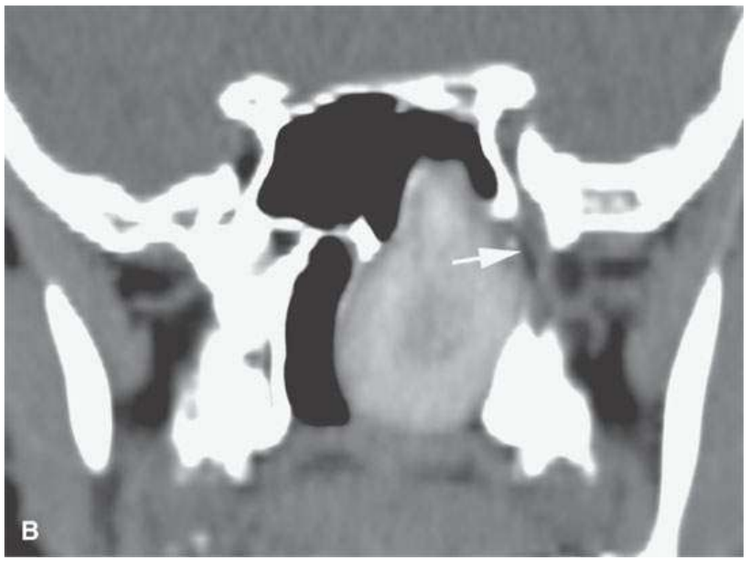

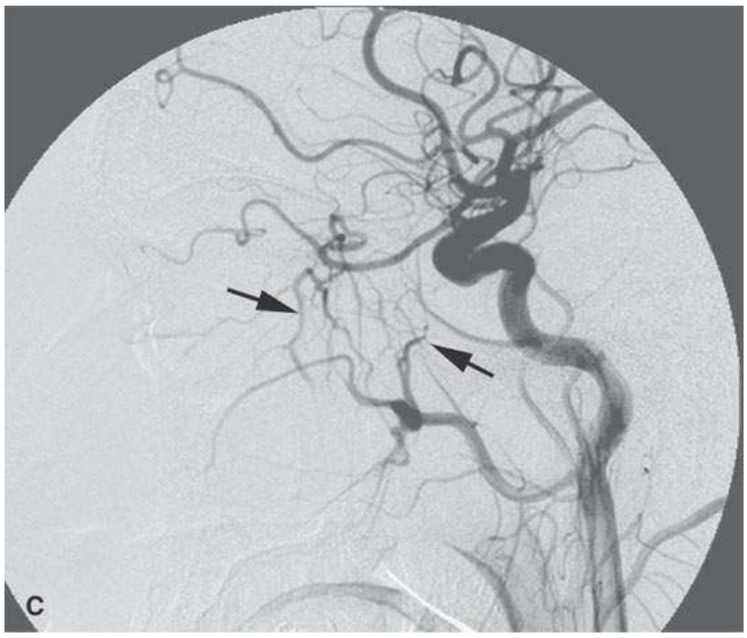

FIGURE 21.28. A, B: Non–contrast-enhanced computed tomography in a young male believed to have a juvenile angiofibroma clinically but the study showing no extension into the pterygopalatine fossa (*arrow* in **A**) in this benign fibro-osseous lesion. **C:** The angiogram shows pathologic vascularity (between the *arrows*), but this is not that typical of a juvenile angiofibroma.

One should resist the temptation to universally link gross morphology and growth patterns to histology. Benign inflammatory lesions may have an aggressive growth pattern and malignant tumors may have a very indolent appearance. This tendency for dysjunction between histology and morphology is predictable in some situations. One specific example is the erosive appearance of bone seen in the jugular fossa in the glomus jugulare variety of paraganglioma, even though these tumors are almost always histologically benign (Fig. 21.29). Another is the sometimes very smooth contour of an adenoidcystic carcinoma of the parotid gland, even though many >1 cm in size will already have disseminated via perineural spread at the time of presentation (Fig. 21.30). The gross morphology and growth patterns of other tumors will be discussed subsequently in conjunction with those specific histologic classifications in Chapters 22 through 42. This discussion begins with a consideration of the general pattern of growth of benign and malignant tumors and their influence mainly on the CT and MR appearance of a lesion.

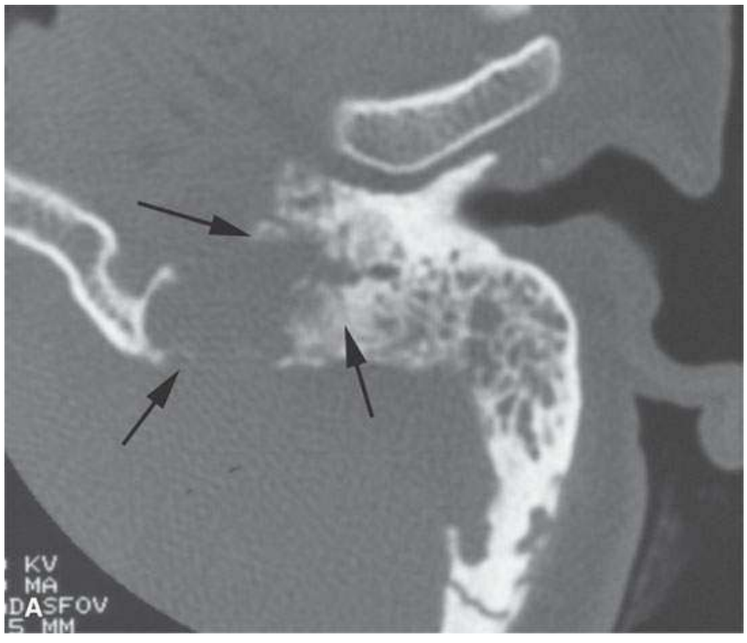

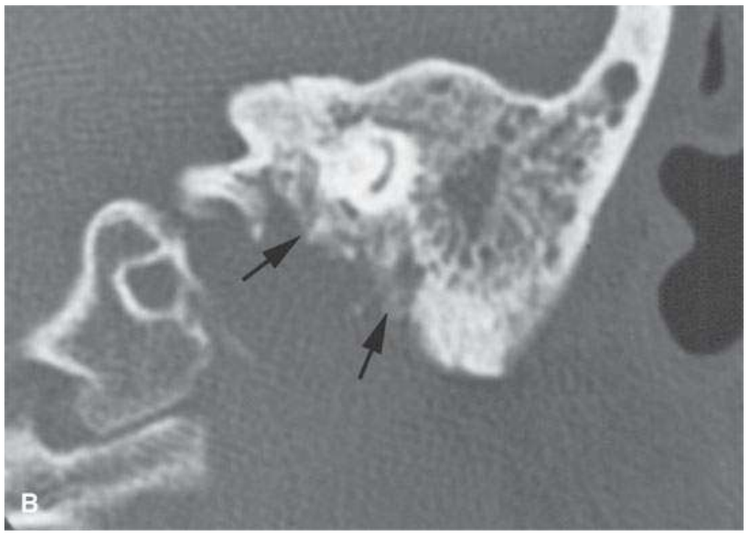

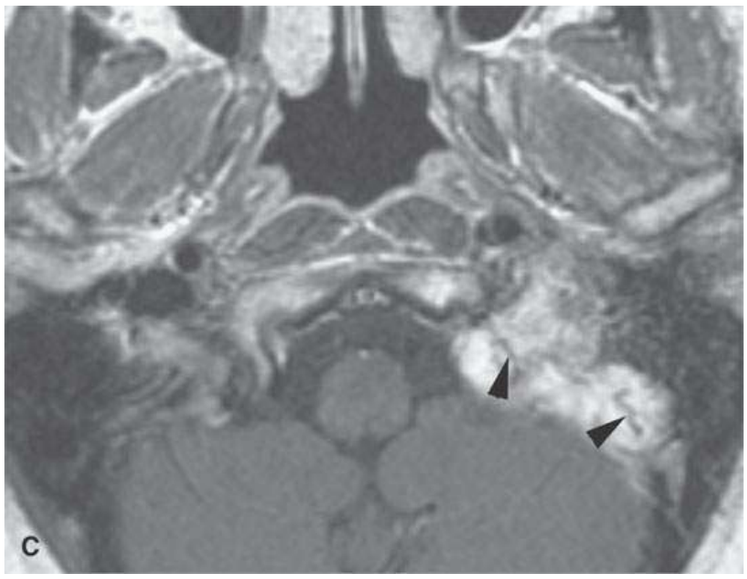

FIGURE 21.29. Computed tomography images showing erosive rather that remodeling type changes (*arrows* in **A** and **B**) in this benign glomus jugulare tumor. Contrast-enhanced T1-weighted image in (cC) shows the enhancing mass with flow voids *(arrowheads)*.

GROWTH PATTERNS OF BENIGN NEOPLASMS

Benign tumors may be thought of as focal and relatively firm spheres like a handball (Figs. 21.21, 21.21, and 30.21) or more diffuse with a consistency more like putty or partially dried clay (Figs. 21.27 and 21.28). Each type will grow according to its consistency and the influence of surrounding anatomy. All will grow along the paths of least resistance. Most firm tumors will cause their surroundings to remodel once in a tight space to accommodate the increased tumor volume (Figs. 21.7, 7.21, and 27.21). The softer ones will grow in a more insinuating pattern like slowly spreading toothpaste oozing into an accommodating adjacent space and then spreading out once more accommodating soft tissue surroundings are reached. The oozing pattern is more often seen in developmental masses such as the venolymphatic malformations discussed in Chapter 9 and in the neoplastic category exemplified by the plexiform neurofibroma (Fig. 31.32). Mixtures of these patterns are possible.

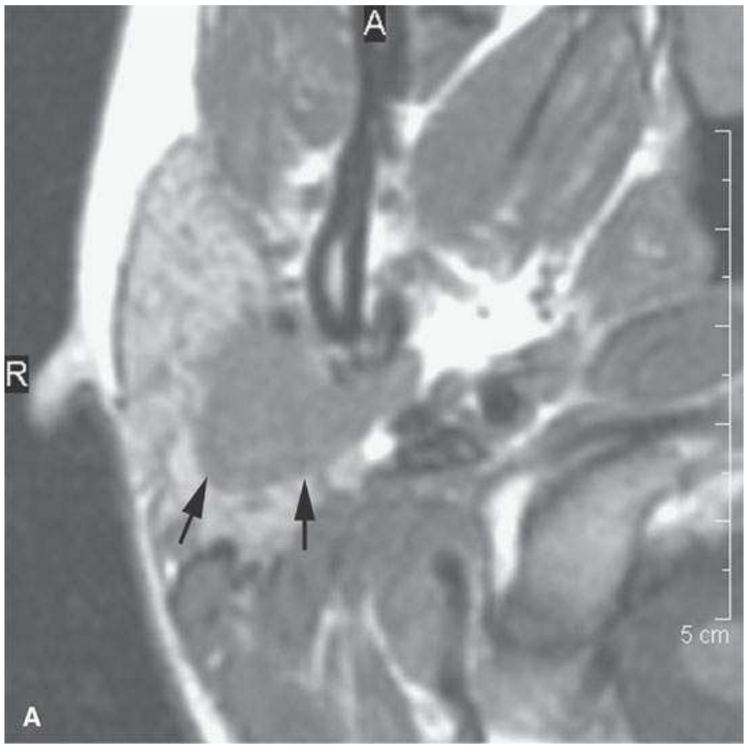

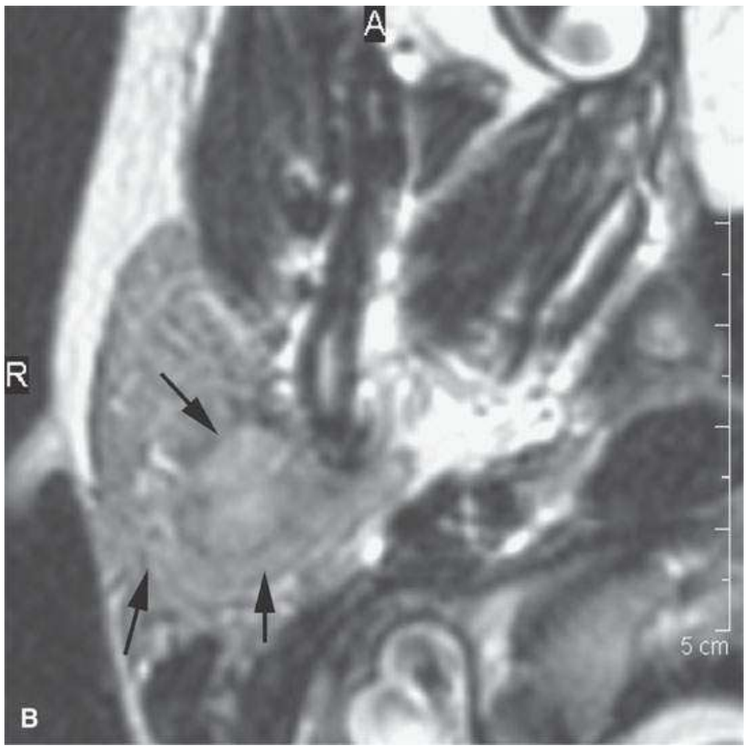

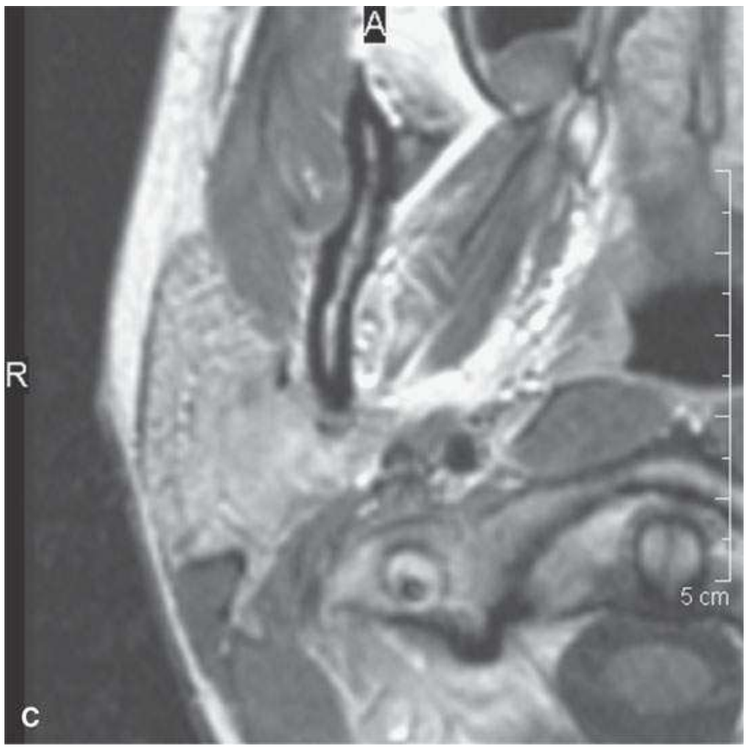

FIGURE 21.30. Magnetic resonance imaging of a patient with adenoidcystic carcinoma of the parotid gland. The margins *(arrows)* of the malignant tumor are very well defined on the T1-weighted (aA) and T2-weighted (T2W) (bB) images. With contrast (cC), the mass becomes isointense to the rest of the gland. The lesion also remains obviously hypointense to fat and fluid on the T2W images, suggesting both its malignant nature and the fact that this is likely not the "cribriform" variety of adenoidcystic carcinoma that has a microcystic microscopic morphology.

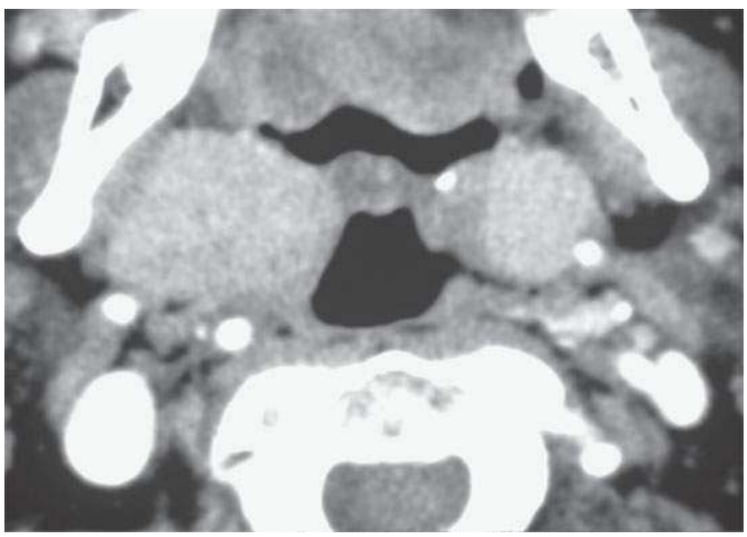

FIGURE 21.31. Contrast-enhanced computed tomography of a patient with multiple rhabdomyomas of the parapharyngeal space showing the tendency for unrestrained tumors to grow essentially spherically.

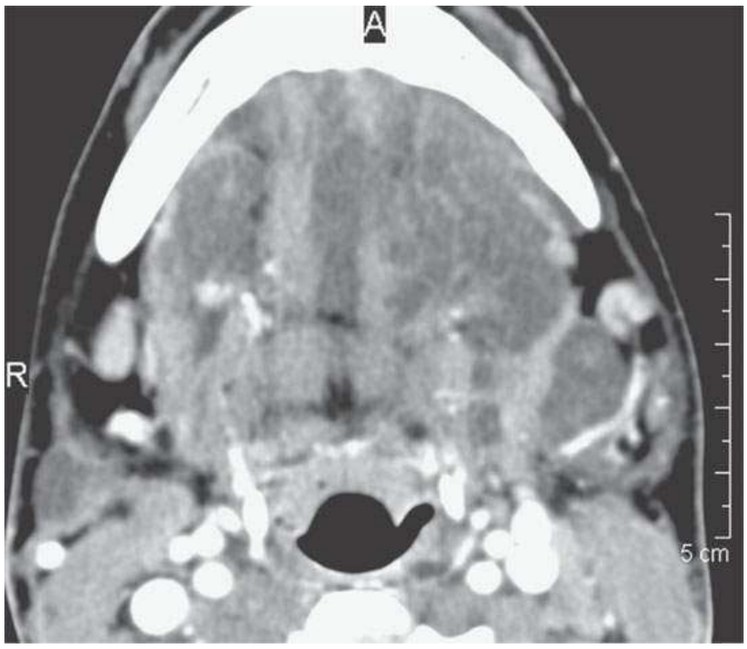

FIGURE 21.32. Contrast-enhanced computed tomography of a neurofibromatosis type 1 patient with a plexiform neurofibroma "oozing" in and around the pre-existing space between and around the muscles of the floor of the mouth and submandibular spaces.

A firm mass in a compartment, at least in part bordered by bone, will cause regressive remodeling of the bone. The remodeling is caused by constant pressure of tumor on bone (Figs. 21.7, 21.27, 21.28, and 21.33). The bone responds by turning over at a more rapid rate than usual. Malignant tumors cause bone erosion by this mechanism as well as by producing substances that activate osteoclasts. In most benign tumors, the stimulus is probably mechanical rather than biochemical. The demineralization allows the bone to soften and accommodate the mass. If the mass grows slowly enough, the bone will remineralize at its interface with the tumor but will usually be thinner than the original bone. No bony rim may be visualized, especially in the central skull base. The central skull base is relatively quick to become dehiscent appearing and slow to restore mineralization, especially when the etiology of the bone "thinning" is benign. The resulting appearance is that of an expanded space such as that of the pterygopalatine fossa in a juvenile angiofibroma, jugular fossa in a schwannoma, and the sinus and orbit in fibro-osseous tumors. In fact, there is no real expansion; it is a regressive change made to accommodate a process, taking place on a timetable of months to years. A good example of how benign lesions may show disparate bone remodeling morphology is the smooth "expanded" appearance of the jugular fossa seen in schwannomas arising at this site (Fig. 29.26) contrasted with the more aggressive erosion seen in paragangliomas that are also benign (Fig. 21.29). The value of this comparison is to realize that changes are not always specific or pathognomonic or even always reflective of the lesion's timetable, since paragangliomas normally grow slowly. Most benign lesions grow at a rate that produces >1 to 3 mm per year of enlargement in any particular cross section typically measured as the greatest short axis on axial images for efficiency and simplicity, although volume of growth can be calculated if desired.

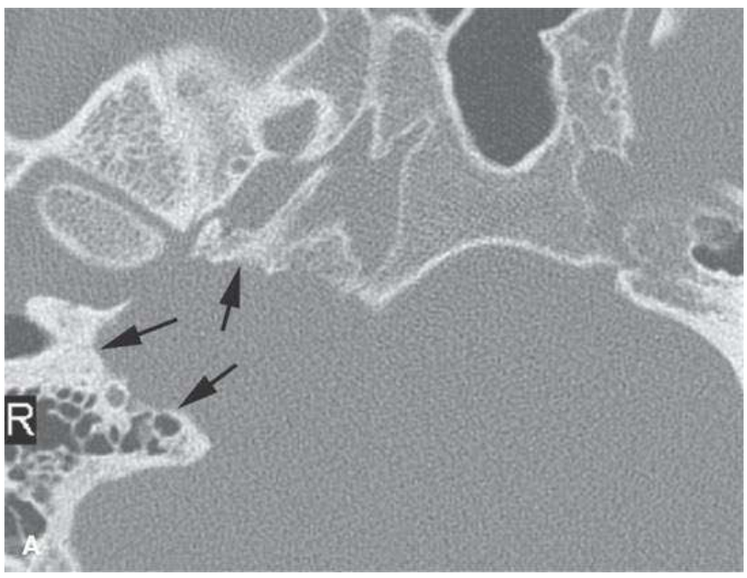

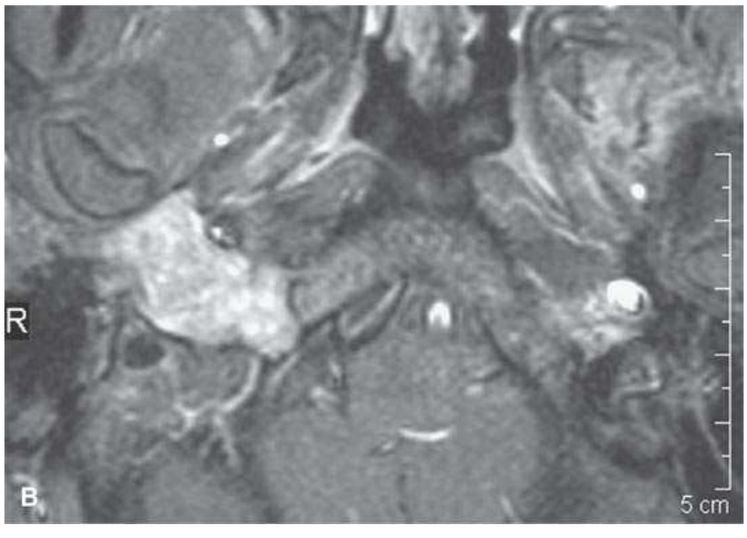

FIGURE 21.33. Images of a patient with a jugular fossa schwannoma. **A**: Computed tomography shows smooth regressive remodeling *(arrow)* of the walls of the jugular fossa (contrast with the pattern in Figure 21.29). **B**: Contrast-enhanced T1-weighted image for comparison.

In soft tissue spaces, benign and less aggressive malignancies will simply push aside adjacent soft tissues such as muscles and neurovascular structures. The vectors of such displacements are very valuable in predicting the type of lesion and site of origin. Perhaps the best examples of this are masses of the parapharyngeal space (Fig. 21.21).

Softer benign lesions seem to surround bone and soft tissue structures and produce less displacement and regressive remodeling per unit volume of tumor than more firm tumors. The classic examples are the developmental venolymphatic malformation or its cousin the proliferative hemangioma. All of these tendencies are relative, and crossover is not uncommon. For example, the juvenile angiofibroma is a relatively firm lesion that oozes into and through tight spaces, and its expansion in the tighter foramina and spaces bordered by bone is less voluminous than in the spaces occupied by soft tissues. The variations of tumor volume at different locations are influenced by the tumor's need to expand by displacement of soft tissues versus regressive remodeling of adjacent bone. The areas of more resistance may be thought of as channeling growth toward those that are more accommodating.

Most importantly, one must always realize that slow-growing malignancies can show patterns identical to benign tumors. Malignancies may also arise in pre-existing histologically benign neoplasms such as carcinoma ex pleomorphica arising in a benign mixed tumor. Also, a malignant tumor can cause secondary benign processes such as an obstructing sinonasal cancer producing a mucocele. Imaging studies must always be carefully scrutinized for findings suggesting that an otherwise benign-appearing process may be malignant or caused by an associated malignant tumor. The types of findings to be on the lookout for as evidence for malignancy are discussed in the next sections. Such a warning to a knowledgeable clinician may result in potentially lifesaving shifts in the surgical approach to a lesion. Cutting across cancer or incisional biopsy of a malignancy can significantly compromise a chance for cure in some lesions.

GROWTH PATTERNS OF MALIGNANT TUMORS

Primary Tumor: Local Spread

Malignant tumors can have a gross appearance and spread pattern identical to benign tumors and inflammatory lesions, as was discussed in detail previously in this chapter. It is very important to study the general trends of spread or malignancies and keep them in mind as a framework for understanding the natural history of cancer at specific sites. The trends discussed here are reflected in the organization of the table outlining the spread patterns of head and neck malignancies in Appendix C.

Cancer spreads locally by direct extension. This may be mucosal and/or deep spread. Deep spread is usually channeled along planes of least resistance, although aggressive malignancies respect no boundaries, including cortical bone. Muscle bundles, deep fibrofatty tissue spaces and planes, neurovascular structures, and the periosteal surfaces and medullary spaces of bone all serve as conduits for the spread of cancer (Figs. 21.13, 13.21, and 34.21).

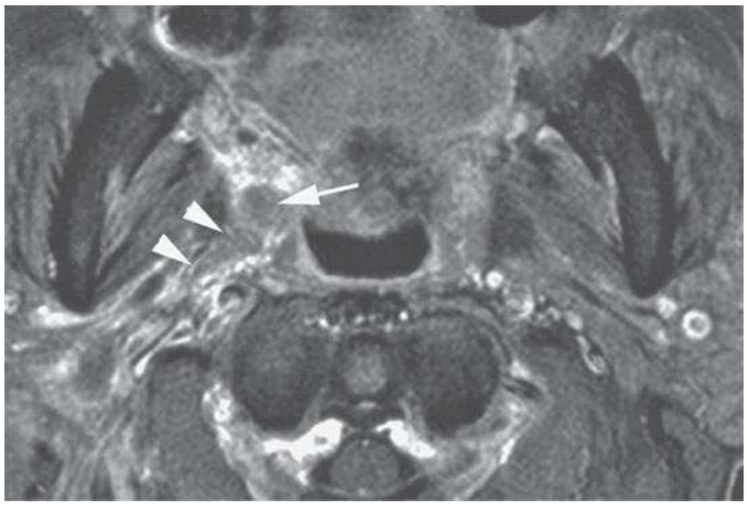

FIGURE 21.34. A patient with tonsillar carcinoma. Contrast-enhanced fat-suppressed T1-weighted computed tomography image shows the lesion to grow from the tonsil *(arrow)* along the stylopharyngeus muscle into the parapharyngeal space *(arrowheads)*.

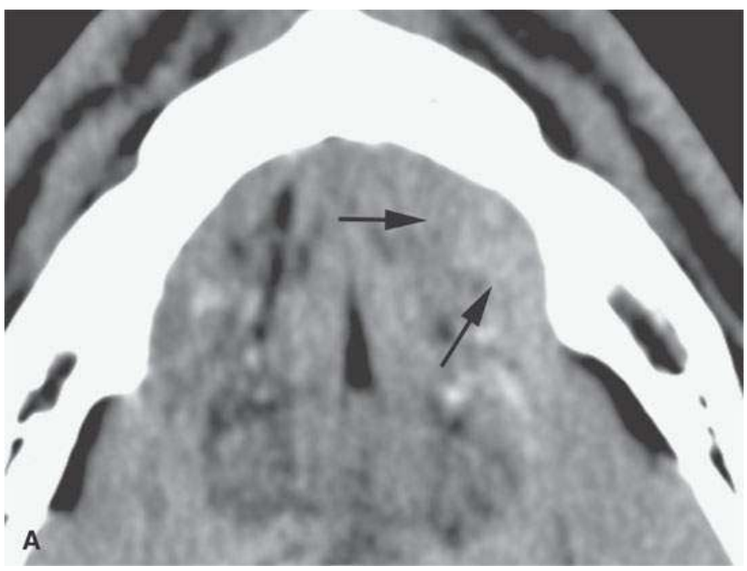

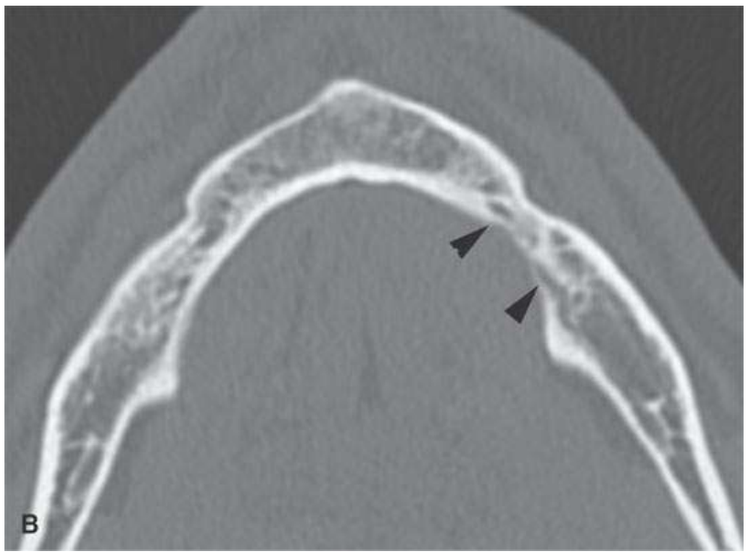

FIGURE 21.35. Contrast-enhanced computed tomography study of a patient with squamous cell carcinoma of the floor of the mouth. The cancer (*arrows* in **A**) is "directed" along the periosteum of the lingual plate of the mandible. The bone appears saucerized *(arrowheads)* due to the effects of tumor **(B)**, but no tumor was found beyond the periosteum and into bone at surgery.

The arrangement of the anatomic structures in at any specific head and neck site will predispose to particular spread patterns. This concept was, perhaps, most comprehensively introduced to the English speaking literature by Lederman and Ballantyne in the 1950s and 1960s.[4–7] Similarly, comprehensive discussions of infectious diseases appeared earlier in the century. The important observations of these physicians and anatomists interested in the natural history and pathoanatomic correlates of cancer spread in the upper aerodigestive tract can now be appreciated, in vivo, on CT and MR. Such imaging data is increasingly used to improve treatment plans and subsequent outcomes. Specific examples of more refined uses of such data are now seen in intensity modulated radiation therapy and endoscopic skull base surgery.

Mucosal spread is studied by the endoscopist. CT and MR provide basically no consistently reliable distinction between tumor and inflammatory mucosal changes and normal lymphoid tissue that lines the upper aerodigestive tract. In fact, these imaging tools are relatively insensitive to mucosal disease when compared with endoscopy. Many interpretive errors on CT and MR come from a lack of understanding of this limitation. The normal variations that frequently lead to overcalling masses or needless equivocation will be discussed fully in conjunction with the pharynx, oral cavity, larynx, trachea, and esophagus.[8,9] The guiding principle for those discussions is that the mucosa should generally be left to the endoscopist, and the strength of MR and CT and, to a lesser extent, US and FDG-PET imaging is in their depiction of deep spread and regional lymph node involvement. The superficial lumps, bumps, and attendant variation in airway contour seen on CT and MR images may be used as a clue for focused observation of adjacent deep structures that can lead to the detection of significant pathology that might otherwise go unrecognized (Figs. 21.1–21.4). One of the best examples of this is the detection of carcinomas that begin on the squamous mucosa deep within the crypts of the palatine and lingual tonsils (Figs. 21.1 and 21.2). These lesions may be completely hidden from the endoscopic view and can grow deeply in the absence of a visible mucosal component. On CT and MR, such a lesion may show obliteration of the parapharyngeal space or spread into the intrinsic muscles at the tongue base. On T2W MR, the even more subtle sign of penetration of the pharyngeal constrictor muscles may be seen as early evidence of deep invasion (Fig. 21.1). While such subtle changes may be due to inflammation, benign aggressive disease such as Wegener granulomatosis, or normal variation, in the proper clinical situations a locally invasive mass should be considered cancer until proven otherwise (Fig. 21.36). Sometimes, a mucosal lesion will be seen on imaging that is missed in the mucosal areas sometimes hidden from the endoscopist, such as the pyriform sinus apex and laryngeal ventricle (Fig. 21.37).

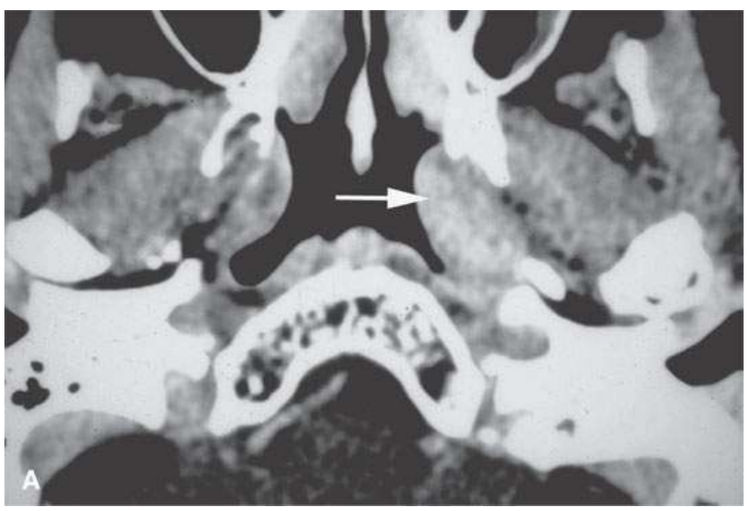

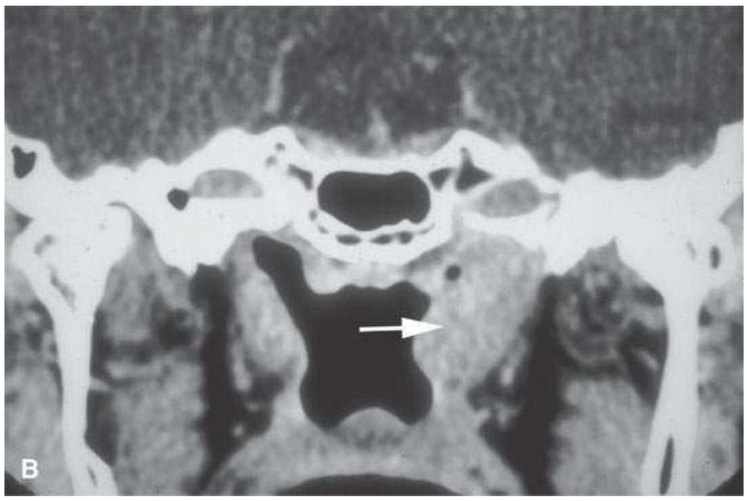

FIGURE 21.36. Contrast-enhanced computed tomography in the axial **(A)** and coronal **(B)** planes of Wegener granulomatosis of the nasopharynx mimicking nasopharyngeal carcinoma as an infiltrating mass surrounding the eustachian tube *(arrows)*.

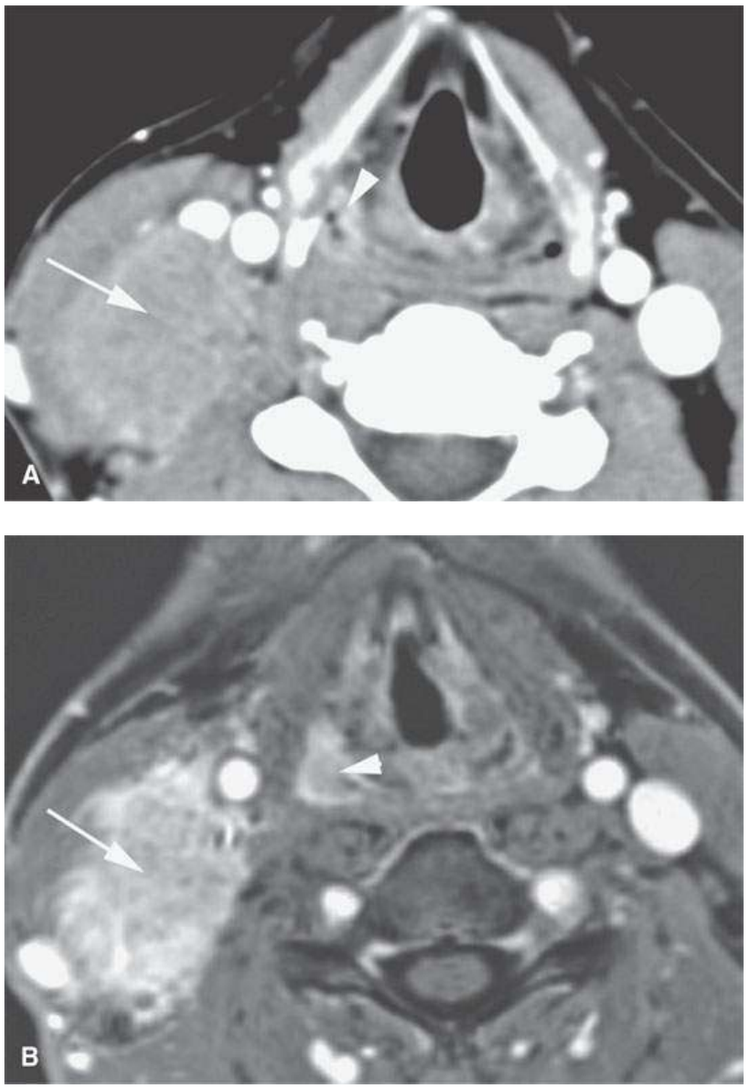

FIGURE 21.37. Contrast-enhanced computed tomography (aA) and contrast-enhanced fat-suppressed T1-weighted image **(B)** showing metastatic level 3 adenopathy *(arrow)* due to a pyriform sinus apex primary *(arrowheads)* not found at endoscopy but picked up on these imaging studies.

Once a primary mucosal tumor gains access to the structures and spaces deep to its site of origin, it is free to expand and/or spread in an infiltrative manner. Tumors that originate deep to the mucosa such as adenoidcystic carcinoma of the parapharyngeal space or sarcomas of the pterygoid muscles begin their growth and spread in these areas that are less accessible to physical examination. Such lesions may be detectable only by the absence of a deep tissue plane.8

Cancers that grow as well-defined masses tend to expand within adjacent spaces and follow the paths of least resistance. This is may be with margins that are sometimes referred to as pushing rather than infiltrating. Their well-circumscribed macroscopic appearance, however, belies their true nature, and microscopically the margins of the cancer may be aggressive. As they grow within a space, they will displace or invade adjacent muscles and neurovascular structures (Figs. 21.3, 3.21, and 5.21). Obliteration of a tissue plane between a tumor and vessel or muscle does not necessarily indicate invasion. MR may be somewhat more accurate for evaluating such interfaces, since muscle edema can be taken as evidence of invasion and a sharp interface between a vessel and tumor may exclude adherence or invasion with a high degree of confidence (Fig. 21.13). Focal adherence or fixation to vessels or other structures can never be completely excluded when the plane between them and the mass is obliterated. Fixation to a vessel is only assured when the tumor completely or nearly completely surrounds (subtends an arc of 270 degrees or more) the vessel as seen on high-quality CT and MR examinations (Fig. 21.39).

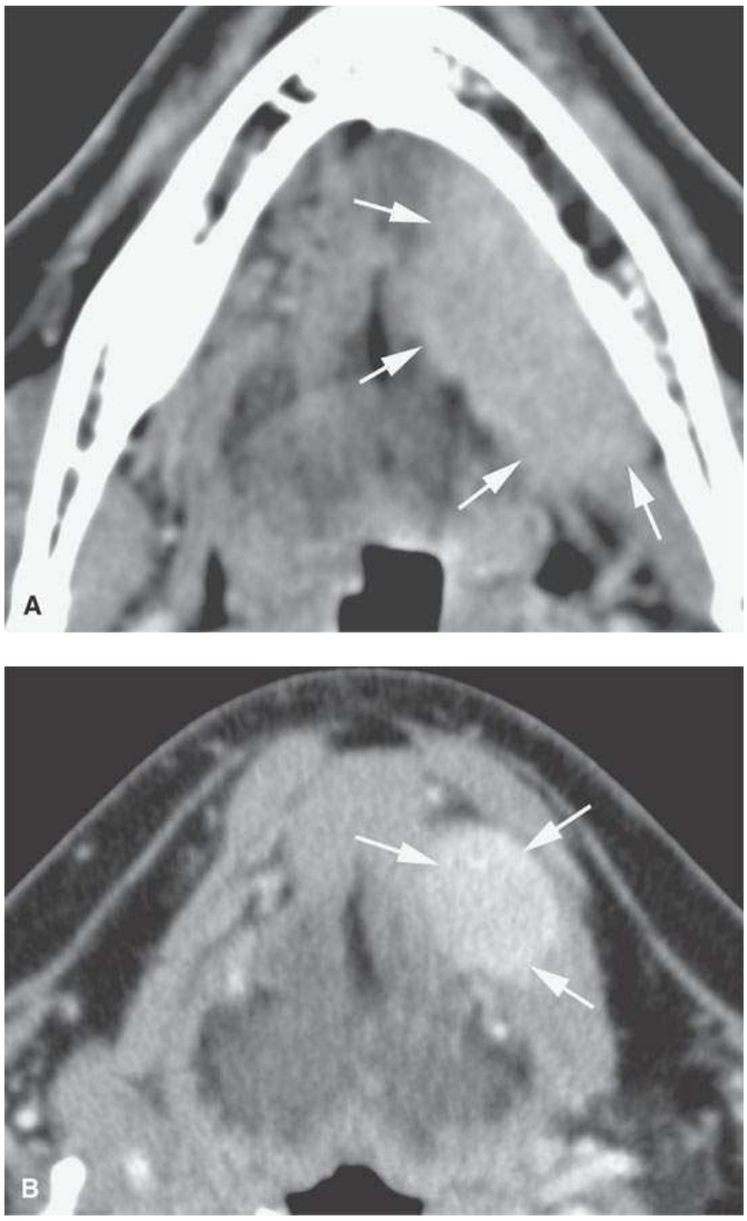

FIGURE 21.38. Contrast-enhanced computed tomography studies of two patients—one with a high-grade mucoepidermoid carcinoma of the sublingual gland (aA) and one with a low-grade mucoepidermoid carcinoma of the sublingual gland (B). Both have "pushing" margins *(arrows)* despite the disparate histologic features.

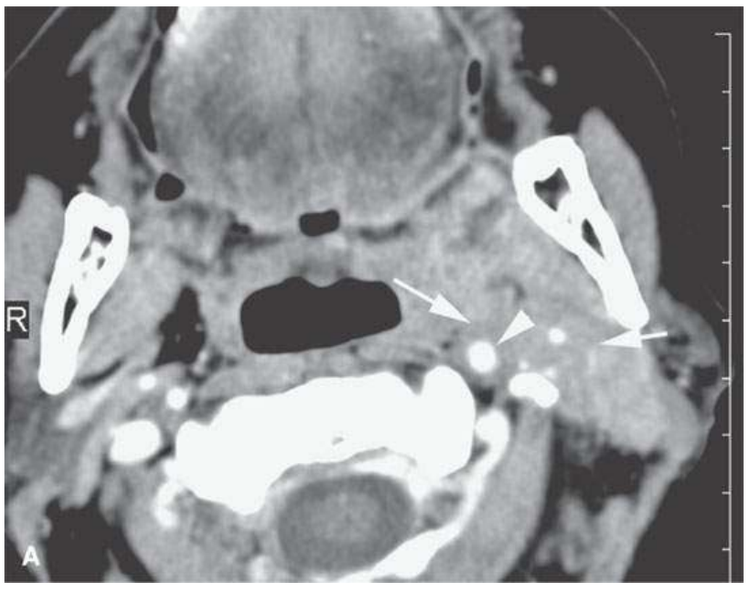

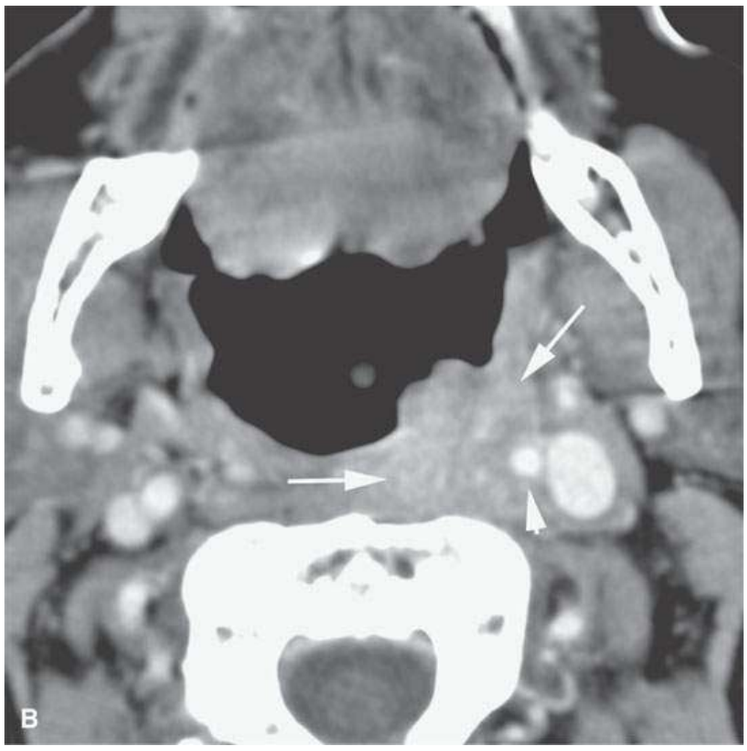

FIGURE 21.39. Contrast-enhanced computed tomography of a tonsillar carcinoma within some areas of hard to define margins and carotid artery encasement *(arrowheads)* as an example on a tumor with infiltrative and pushing margins combined.

Primary tumors may also have an infiltrative as opposed to the just described and illustrated pushing growth pattern. These are usually histologically aggressive lesions (Figs. 21.2, 21.6, 21.13, 21.15, and 21.18). Deep fibrofatty tissue planes serve as freely accessible, low-resistance conduits for such growth. The tendency for these lesions to spread from the origin to the insertion of involved muscles is of particular clinical importance (Figs. 21.6, 6.21, and 15.21). Such extension may not be palpable and is not visible on physical examination, and this growth pattern frequently takes the cancer surprisingly far from its obvious site of origin. Unfortunately, imaging will show the tumor to be far beyond the limits of an oncologically safe surgical procedure with an acceptable morbidity, while the clinician believes that these lesions are more limited. The disparity of findings can lead to suboptimal disposition in some cases if the imaging findings are not taken as reasonably certain. MR and CT are both excellent at showing spread along muscle bundles and within deep tissue planes, although MR is somewhat better because of its superior tissue contrast resolution.

Peritumoral Reactive Changes

Tumors may have a reactive internal stroma. The effects of this stromal composition on tumor morphology as seen on CT and MR were discussed previously. Tumors may also cause a localized or diffuse peritumoral tissue response. In benign tumors and slow-growing malignancies without lymphatic spread, such tissue responses result in little or no obvious morphologic changes beyond the limits of the mass other than a picture of encapsulation or pseudoencapsulation. Peritumoral abnormalities are much more commonly seen in malignant tumors (Fig. 21.40).

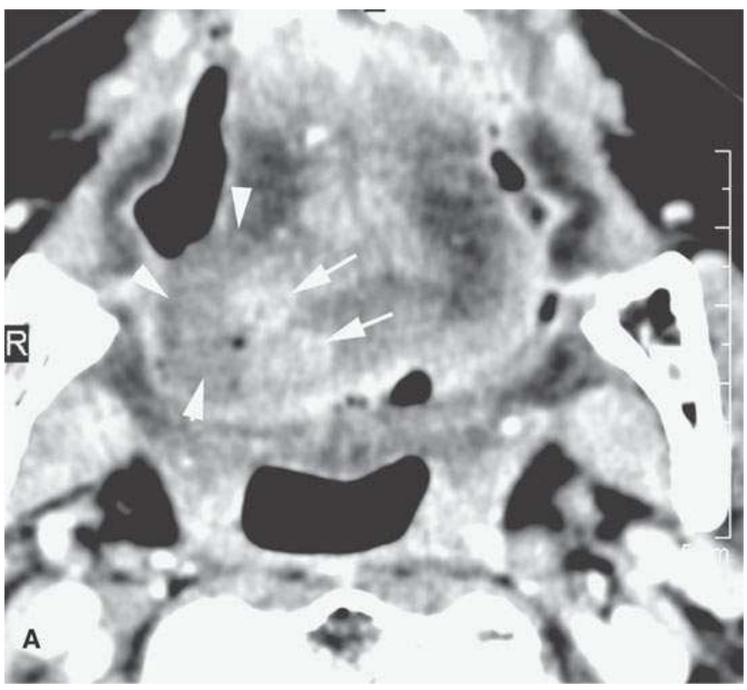

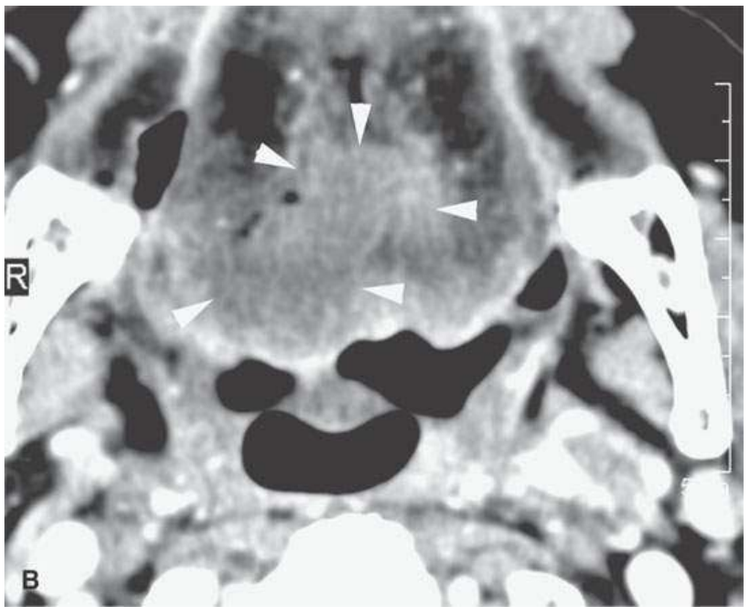
R
B

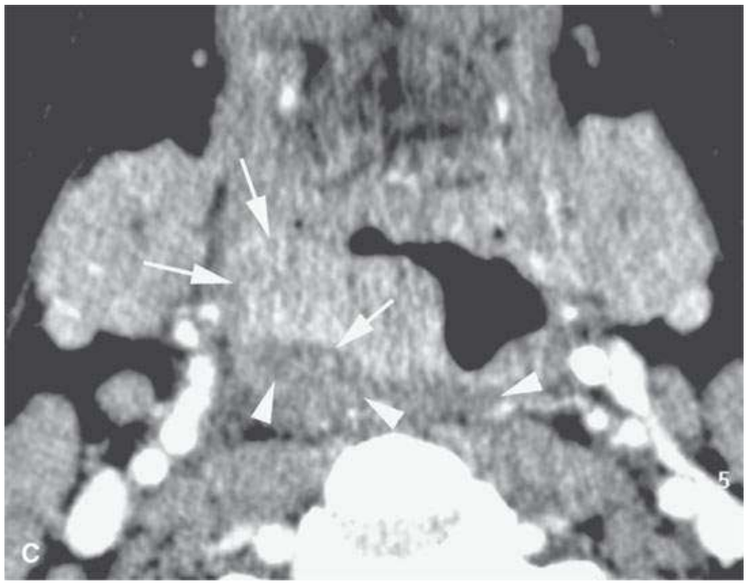
C

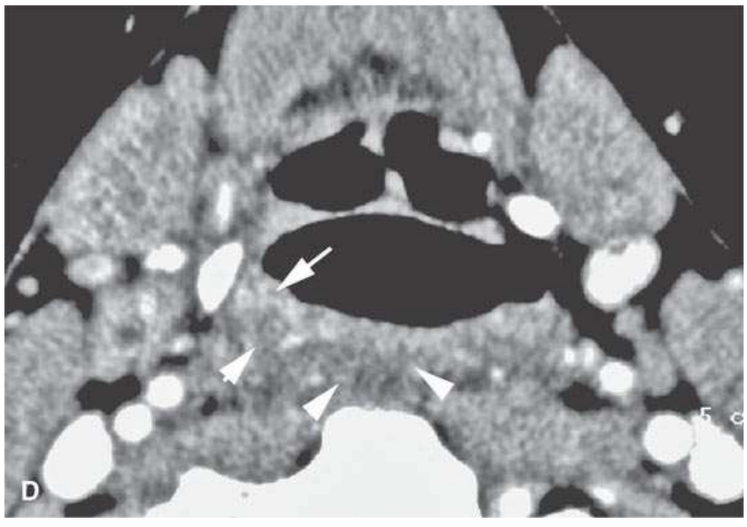
D

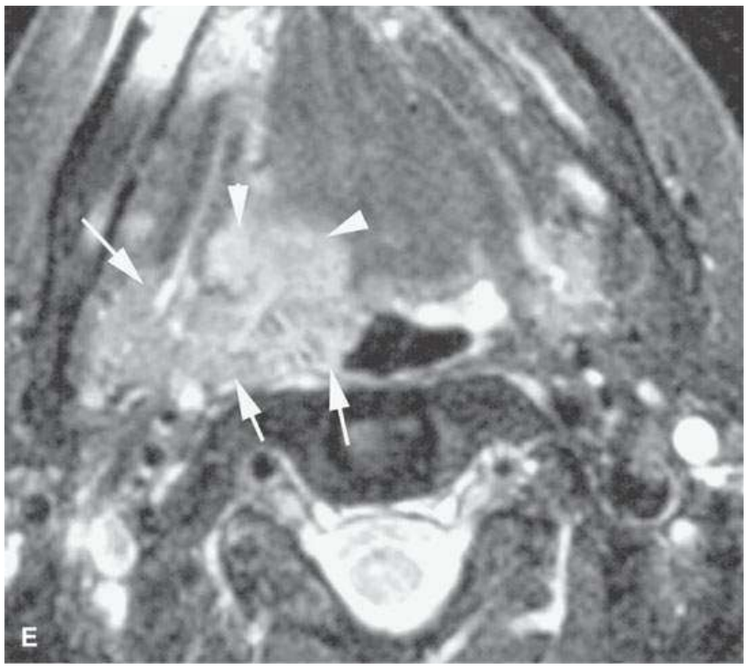

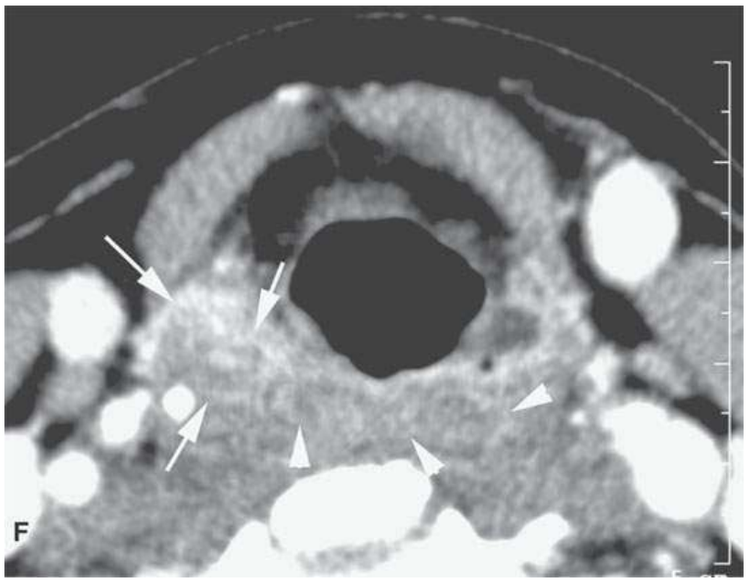

FIGURE 21.40. Four patients with squamous cell carcinoma and zones of tumor-related edema. None had a recent deep biopsy, and none had therapy. In all images, the *arrows* show the gross margins of the tumor, and *arrowheads* indicate zones of likely predominantly reactive edema (see text for the limit of reliability of such assumptions). A, B: Contrast-enhanced computed tomography (CECT) of a patient with oral tongue cancer with a relatively small primary and large zone of predominantly edema. C, D: CECT of a patient with posterior pharyngeal wall cancer with related pharyngeal wall and retropharyngeal space edema. **E**: Fat-suppressed T2-weighted images showing exophytic tumor with likely deep edema perhaps mixed with tumor. **F**: CECT of a relatively small pyriform sinus primary with marked posterior pharyngeal wall and retropharyngeal space edema.

Sometimes, diagnostic imagers are asked to differentiate between the actual limits of a malignant tumor and peritumoral reactive changes, most commonly peritumoral edema. It is never possible to do this with a level of confidence that will allow the "tumor nidus" or gross tumor volume to be treated while excluding the peripheral zone of secondary tumor effects. The main reason for this limitation is that imaging can never exclude microscopic or even macroscopic tumor deposits within the peripheral, more edematous proposed "reactive" zone (Fig. 21.40). This is long-standing general knowledge about brain tumors and has been known about laryngeal and tongue cancer for many years and is due to several basic causes of the phenomenon of peritumoral edema: (a) the edema may simply be a component of a tissue response to the tumor and no tumor cells are present in the peritumoral reactive zone; (b) tumor cells may have seeded the peritumoral soft tissues and are inciting an inflammatory response; (c) tumor cells are clogging local lymphatics and producing lymphedema; (d) there is lymphedema as a reactive response or because of downstream lymphatic obstruction caused by tumor in nodes; and (e) the tumor is infected and the peritumoral reactive changes are related, at least in part, to the superimposed infection. It is virtually impossible to differentiate these circumstances on CT and MR or FDG-PET. There may be one partial exception. Tumors with very exuberant inflammatory response, characterized by extensive enhancement with intravenous contrast, may be secondarily infected. This is especially true in ulcerated carcinoma but is actually very uncommon. When this may be confusing in the clinical decision making, patients can be placed on antibiotics and restudied in 7 to 10 days to see if part or all of the reactive changes on imaging are related to infection. Most often, there will be no change; however, even if the mass shrinks, its margins become sharp, and the contrast enhancement markedly diminishes, one cannot be sure that microscopic tumor emboli were not carried peripherally with the inflammatory response. Needle biopsy is of limited help in determining the cause of a peritumoral reactive zone, since a high rate of sampling error may be anticipated outside of the main tumor volume. In other words, a negative biopsy of a zone of "peritumoral edema" does not exclude the presence of tumor.

The preferred approach to this is to realize the limitations of imaging and most safely presume that all structural changes seen are related to local tumor infiltration whether it microscopic or gross. It is generally oncologically unsafe to presume that the main tumor bulk can be excised even in an en bloc procedure and the "reactive zone" be left untreated or "cleaned up" with radiotherapy. There is a recent belief that FDG-PET can help increase the accuracy of gross tumor volume determination. This is speculative at present and could lead to potentially oncologically unsound radiotherapy planning until it is substantiated in larger patient experiences than currently supported. FDG-PET cannot exclude microscopic disease. There is a parallel to this in orthopedic oncology, whereby the entire anatomic compartment containing gross tumor and peritumoral reactive changes is removed. Surgery with curative intent in the head and neck region tends toward the same approach, but the compartments are sometimes less well defined, and a wide margin of safety is sometimes sacrificed to avoid significant functional losses. These are decisions that only the surgeon, radiation oncologist, and patient can make together. It is the job of the diagnostic imager to establish the extent of disease and warn the clinicians about the inherent limitations in imaging. In our opinion, a clinician should never be told that imaging can separate peritumoral reactive changes from the tumor itself for the reasons just discussed.

Invasion or Reaction of Bone and Cartilage

Spread to bone and cartilage is an extremely important finding in head and neck cancer. Cartilage is relatively resistant to invasion, probably because of its hypovascularity, but nonossified cartilage can be invaded by cancer. This is frequently seen in cancers of the nose and pinna. Invasion of the laryngeal "cartilages" is virtually always at areas of ossification; thus, in reality, it is bone invasion along a penetrating neurovascular bundle. Bone erosion is an important sign of malignancy, but it is not absolutely specific. Bone erosion may be seen in benign tumors and infectious or aggressive inflammatory lesions or as a response to injury. The finding of bone or cartilage invasion by a cancer often significantly alters the approach to therapy (Figs. 21.35 and 21.41–21.44).

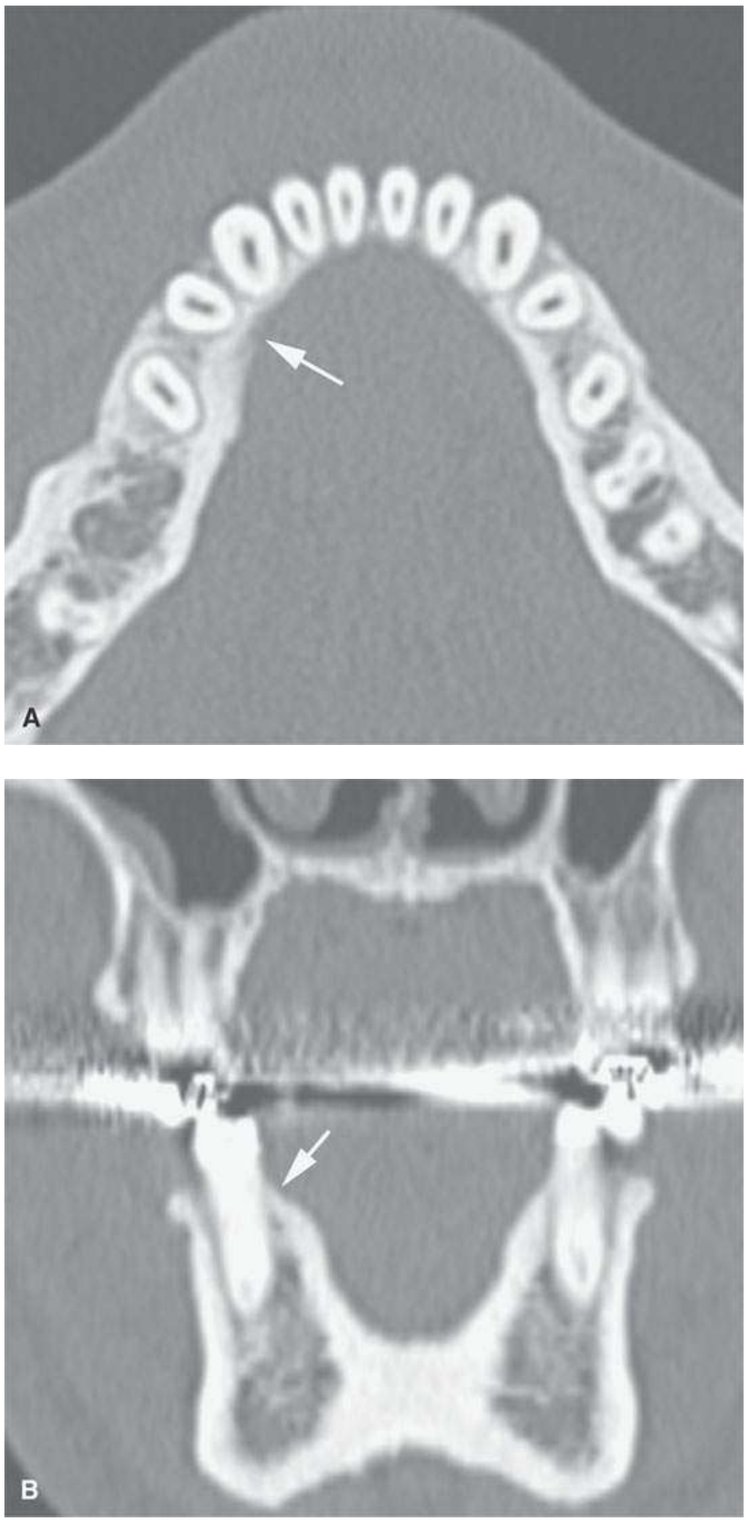

FIGURE 21.41. Computed tomography showing early alveolar ridge bone erosion *(arrows)* by a squamous cell carcinoma of the floor of the mouth. Such limited involvement could not be confidently detected or excluded by magnetic resonance imaging in the vast majority of cases.

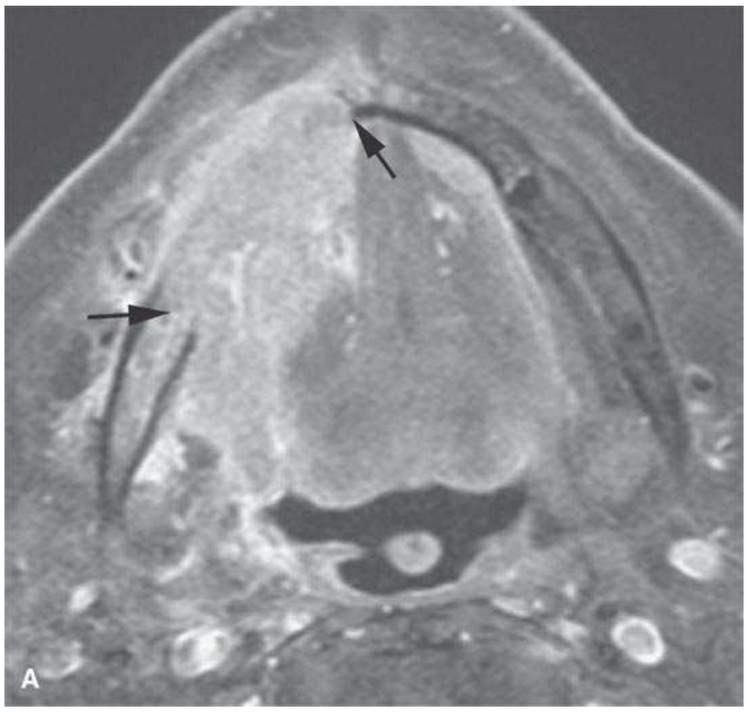
A

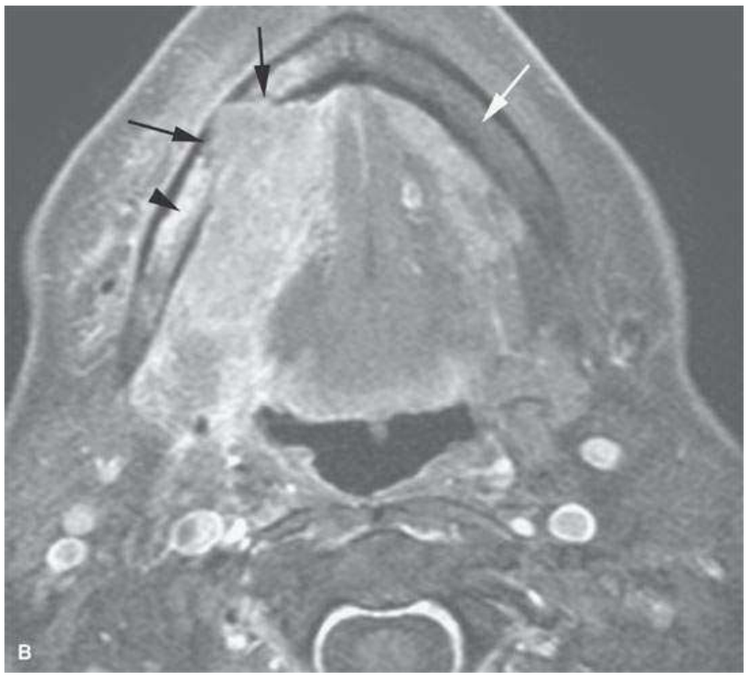
B

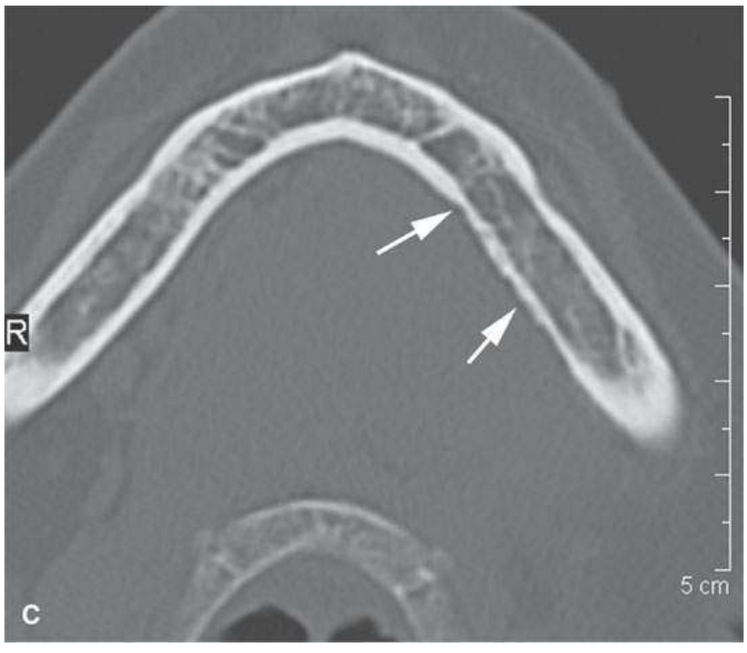
R
5 cm
C

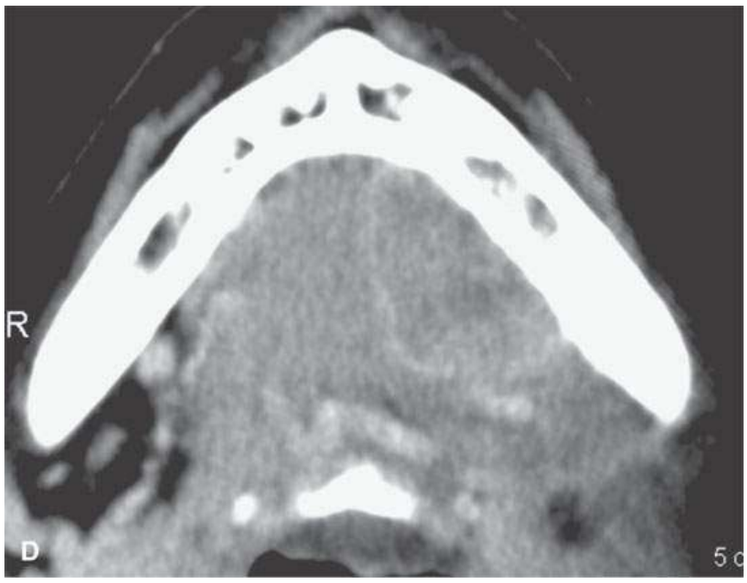

FIGURE 21.42. Two patients requiring segmental mandibular resection. Contrast-enhanced fat-suppressed T1-weighted image in a patient with floor of the mouth cancer. Note how the margins of tumor invasion *(arrows)* match the geography of the bone invasion. There is marrow space increased signal in (Bb) *(arrowhead)* compared to normal side *(white arrow)* that likely represents volume averaging at the depth of invasion but could be due to marrow space edema. Contrast-enhanced computed tomography of a patient with level 1 nodes (dD) fixed to and eroding the mandible (*arrows* in **C**).

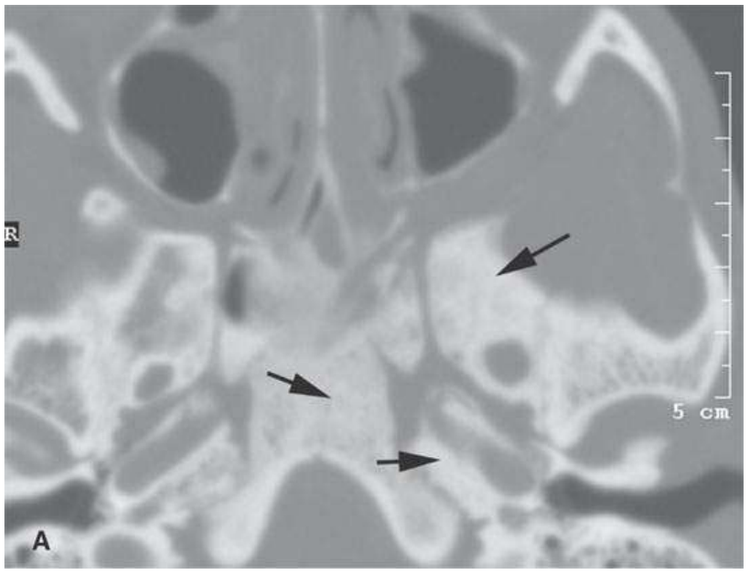

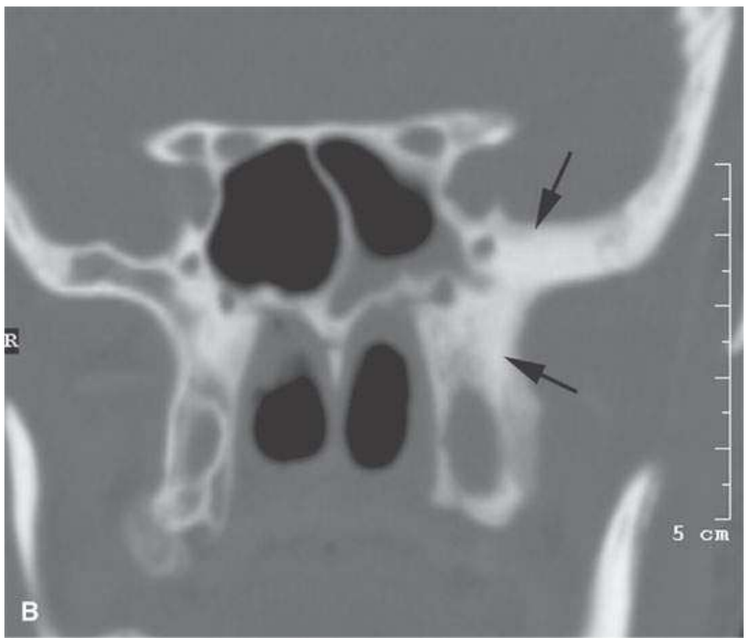

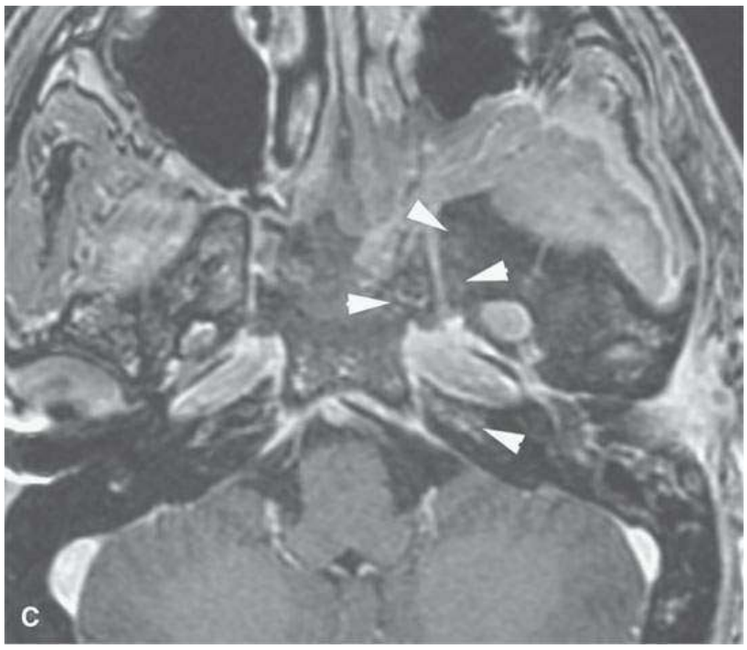

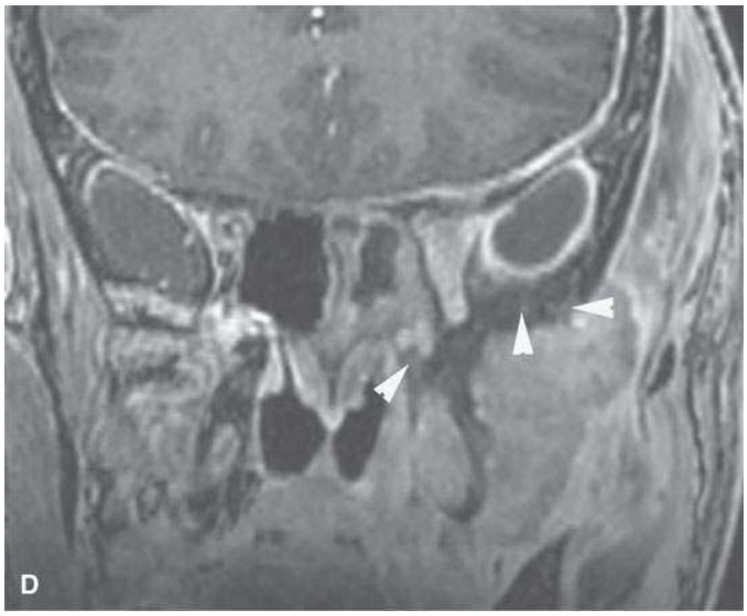

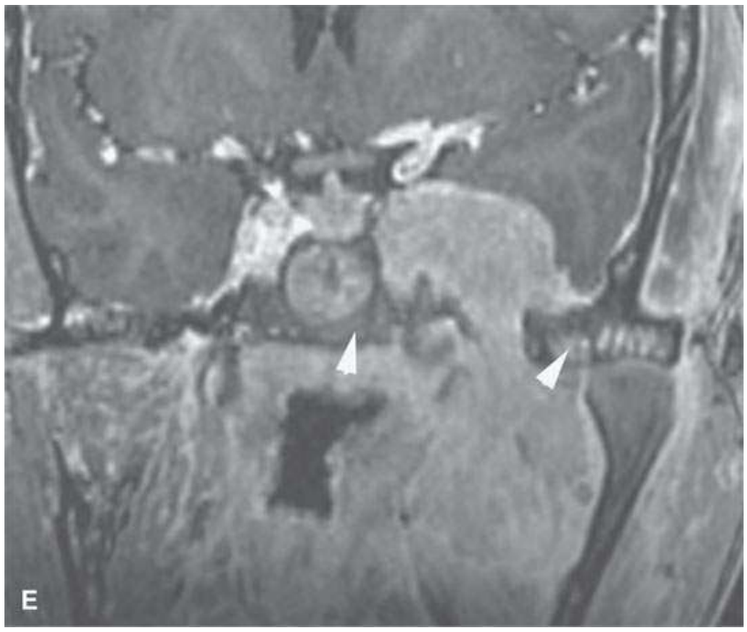

FIGURE 21.43. A patient with nasopharyngeal squamous cell carcinoma**.** A, B: Computed tomography showing marked reactive bony changes *(arrows)* in the central skull base due to adjacent and/or infiltrating tumor**.** C–E: Three-dimensional contrast-enhanced T1-weighted gradient echo images showing the thickened sclerotic bone with subtle evidence of marrow space enhancement *(arrow heads*) due to tumor infiltration and/or reactive changes**.**

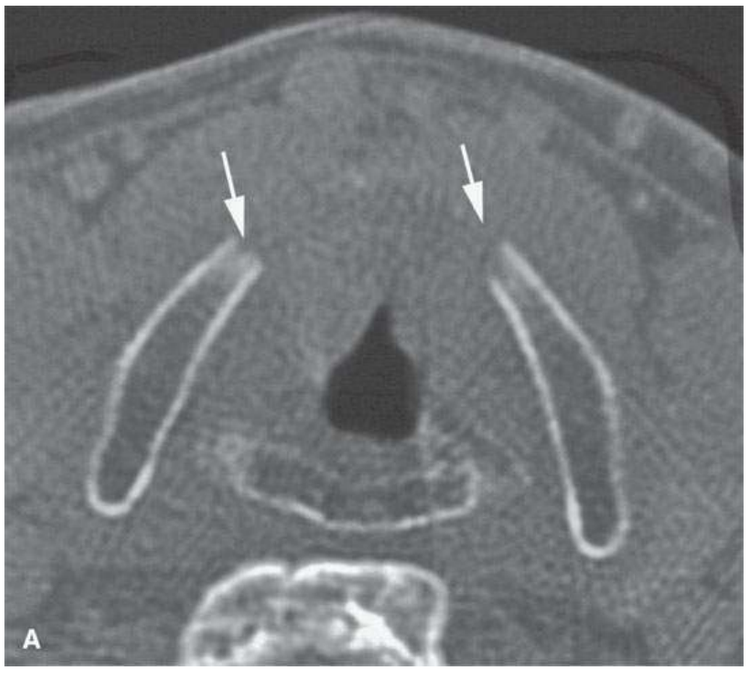
A

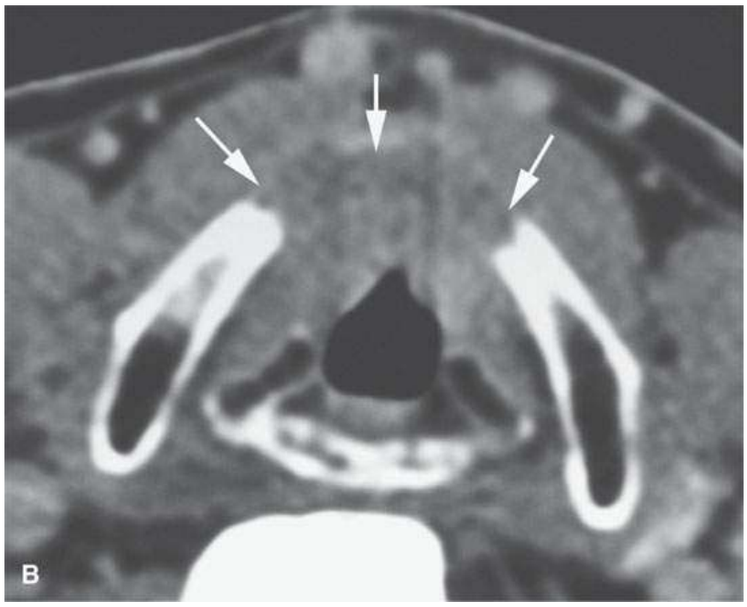
B

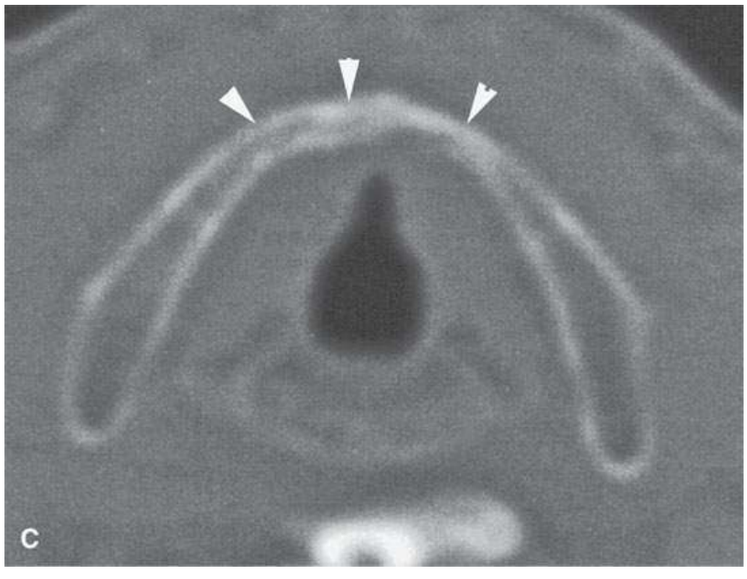
C

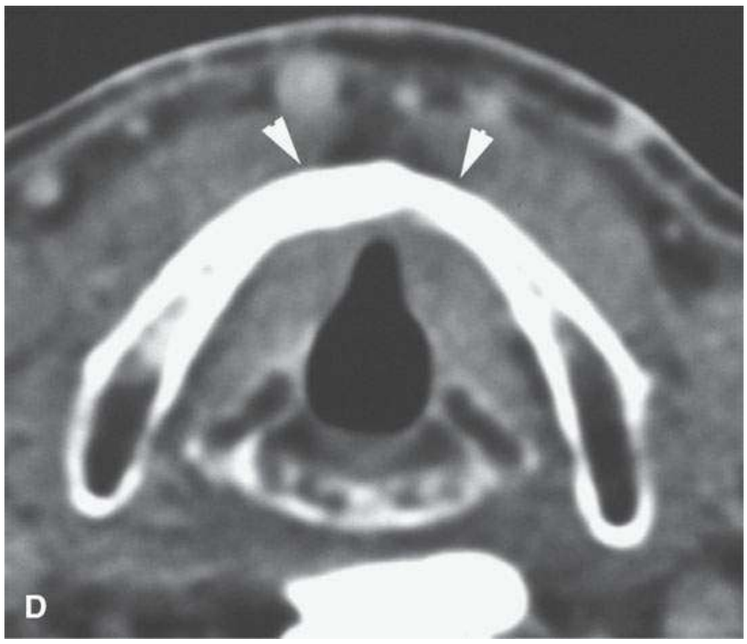

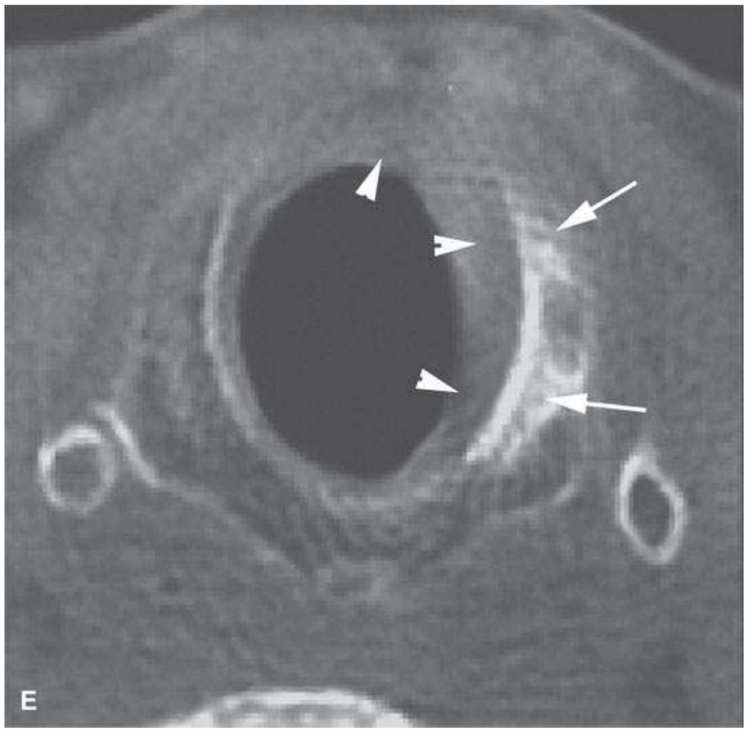

FIGURE 21.44. Two patients with laryngeal cancer. A, B: Pretreatment contrast-enhanced computed tomography (CECT) study showing cartilage erosion (between the *arrows*) due to adjacent cancer. Such gross cartilage erosion would usually suggest that the patient should be treated by total laryngectomy. C, D: CECT following radiotherapy showed the tumor to have responded completely and the cartilage to have remineralized (healed cartilage shown by *arrowheads*). **E:** CECT of another patient with subglottic spread *(arrowheads)* adjacent to the ossified cricoid cartilage. The cartilage sclerosis is reactive to adjacent tumor and a risk factor but not definitive evidence of cartilage invasion.

Cancers growing as well-circumscribed lesions may simply erode bone or, if the growth is slow enough, cause regressive remodeling as described in the previous section on benign tumors (Fig. 21.35). However, bone destruction in head and neck cancer is usually an obvious, aggressive process with certain general trends (Fig. 21.42). The actual erosion is likely due to tumoral factors that activate osteoclasts. Access to bone varies at different sites. In sinonasal cancers, bone is destroyed simply by direct extension. Elsewhere, the point of attack is influenced by some structural factors. The periosteum is relatively resistant to penetration by tumor. In fact, this tendency is part of the rationale for mandibular conservation procedures such as rim mandibulectomy as opposed to segmental resection. Tumor adjacent to bone tends to slide along the periosteum until it encounters a neurovascular channel or point of muscular attachment to enter. The point of attachment of muscles is associated with microscopic breaches in the periosteum and bone. These fissures are weak zones in the otherwise resistant periosteum, and it is here that bone and cartilage invasion may begin. This pattern is seen along the mylohyoid attachment on the lingual surface of the mandible. CT remains the best study to detect invasion at cortical bone soft tissue interfaces (Figs. 21.35 and 21.44). Radionuclide studies, especially with single photon emission computed tomography (SPECT) techniques, may identify suspicious areas, but these studies are notorious for false positives and should be followed up primarily with CT for confirmation. MR has been touted as being capable of demonstrating subtle cortical invasion, but this has never been proven in a study comparing high-resolution CT and MR. Thin-section CT is the best study for detecting early cortical bone invasion.

Once cancer has entered a bone and spreads to its medullary space, continuing spread within the marrow is possible. High-resolution T1W MR is more accurate than CT for showing such involvement, but MR can be difficult to interpret and is fraught with pitfalls such as normal variations of fatty marrow distribution and the effects of reactive sclerosis. CEMR can mask marrow space invasion unless it is combined with fat suppression techniques. Reactive bone changes are not necessarily indicative of bone invasion (Fig. 21.44). When sclerosis is present, bone invasion cannot be excluded and may be present. Volume averaging coupled with adjacent sclerosis may mimic obliteration of a marrow space by tumor. These are significant limitations of imaging the marrow-containing spaces in head and neck cancers. Fortunately, squamous cell carcinoma, the most common lesion in the region, shows relatively little tendency to spread in the marrow space remote from areas of entry through the cortical bone unless it is spreading along a nerve or vessel (Fig. 21.42). Round cell tumors —for instance, plasmacytoma—may pack the marrow with little evidence of periosteal surface destruction, and in such primarily marrow space processes, cortical bone erosion may be primarily endosteal (Figs. 21.45 and 21.46).

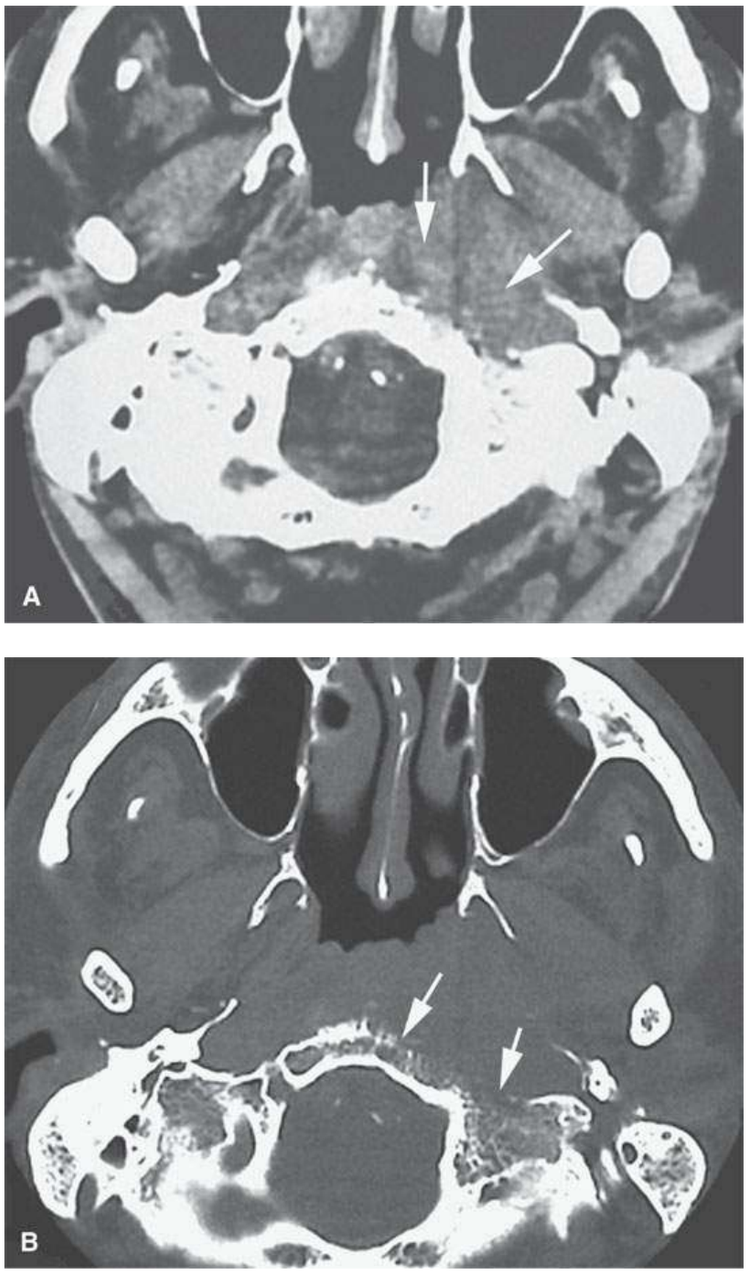

FIGURE 21.45. Non–contrast-enhanced computed tomography showing that the extramedullary plasmacytoma (*arrows* in **A**) causes erosion of the outer cortex of the posterior skull base (*arrows* in **B**).

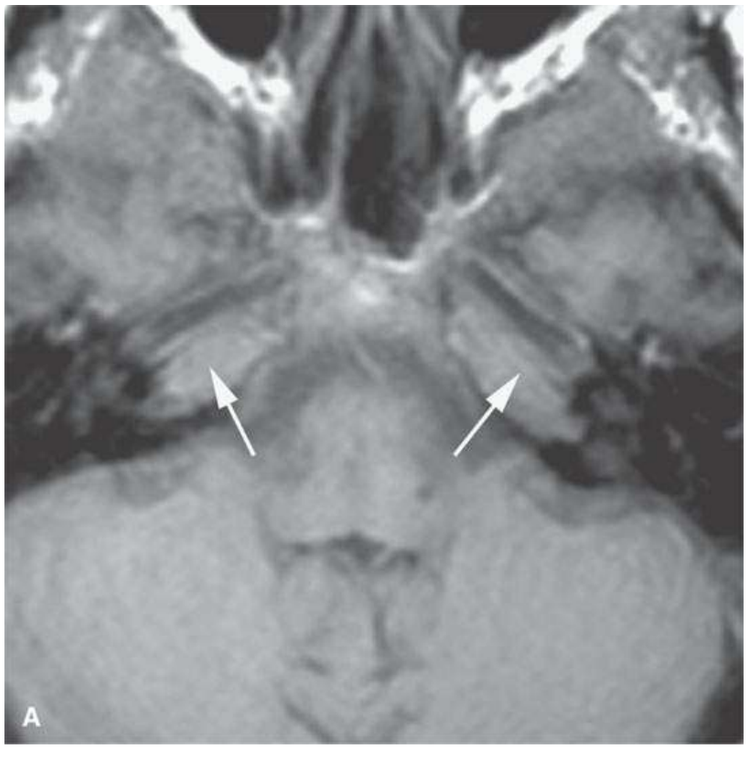

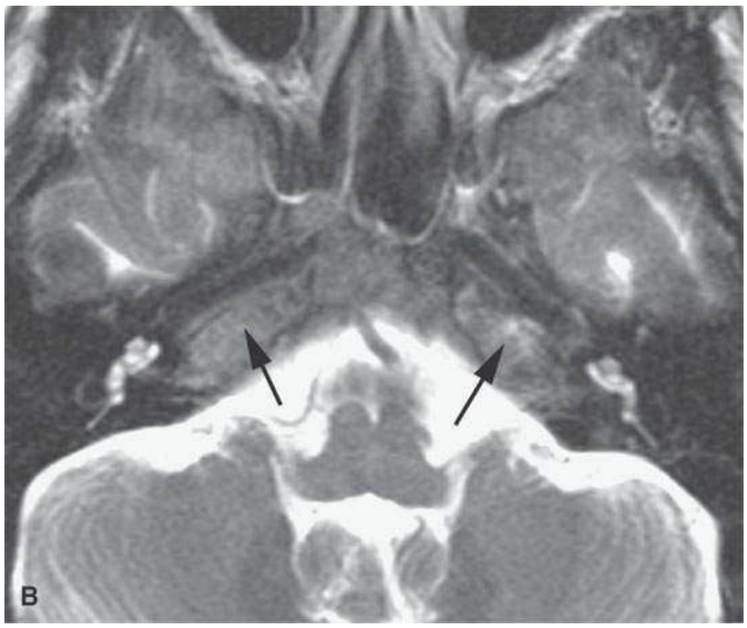

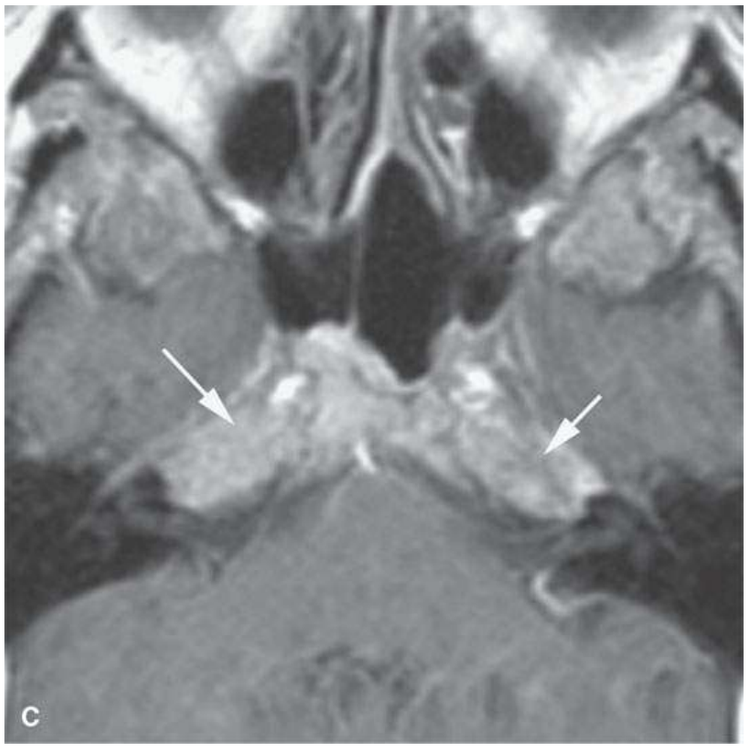

FIGURE 21.46. Contrast-enhanced magnetic resonance shows myeloma spreading freely in the marrow space of the skull base replacing its fat *(arrows)* content as seen on the T1-weighted noncontrast image **(A)** and T2-weighted image **(B)** this infiltration of the fatty marrow made essentially isointense to fat on the contrast-enhanced T1-weighted image in (cC).

Growth Along Nerves and Vessels (Perineural and Perivascular Spread)

Infiltrative growth can also follow neurovascular bundles. This is different from the "perineural" spread that will be discussed subsequently. Like spread along muscle bundles, this pattern of growth can lead to tumor deposits remote from the site of origin (Figs. 21.9–21.11). In fact, the muscle and neurovascular bundles involved can be thought of as spokes extending peripherally from the main bulk of tumor. The actual structures involved depend on the site of origin of the tumor. Some more important examples for aerodigestive tract cancers are the carotid sheath (Fig. 21.47), distal maxillary (Fig. 21.48), palatine (Fig. 21.48), and lingual (Fig. 21.49) neurovascular bundles and the branches of mandibular division of the trigeminal. A final common pathway of several of these is the pterygopalatine fossa and eventually the trigeminal ganglion and even more proximal spread along the trigeminal nerve (Fig. 21.50). Spread involving the auriculotemporal, lingual, and inferior alveolar nerve reaches the trigeminal ganglion via V3 (Fig. 21.48). Spread along the carotid sheath eventually invades the jugular fossa and/or carotid canal. Perineural spread is also commonly encountered in skin and parotid cancers, with the spread following branches of the fifth and seventh cranial nerves from their distal ramifications as far proximally as the brain stem (Figs. 21.50–21.52).

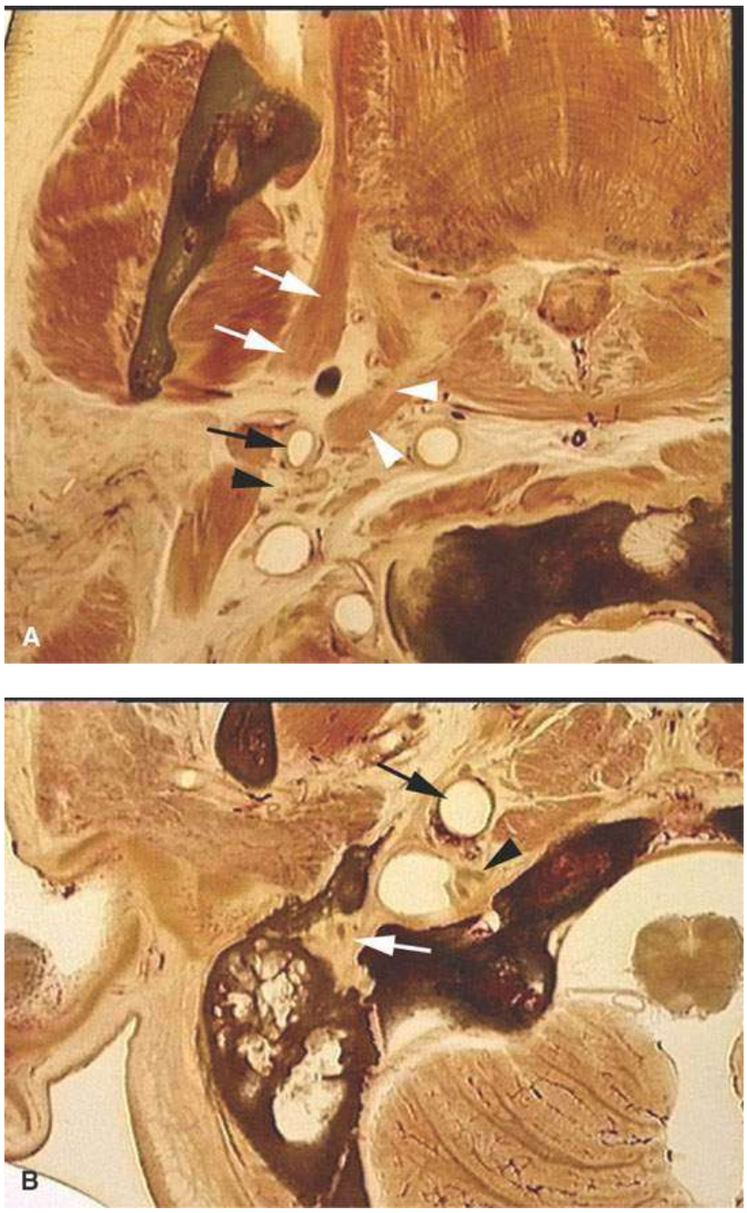

FIGURE 21.47. Anatomic sections. **A:** The styloglossus *(white arrows)* and stylopharyngeus *(white arrowheads)* muscles as possible conduits for tumor spread to the structures within the carotid sheath including the carotid artery *(black arrow)* and cranial nerves *(black arrowheads)*. **B:** The carotid sheath just below the skull base showing the carotid *(black arrow)* and lower cranial nerves *(black arrowheads)*. Also note the facial nerve in the stylomastoid fat pad *(white arrow)*.

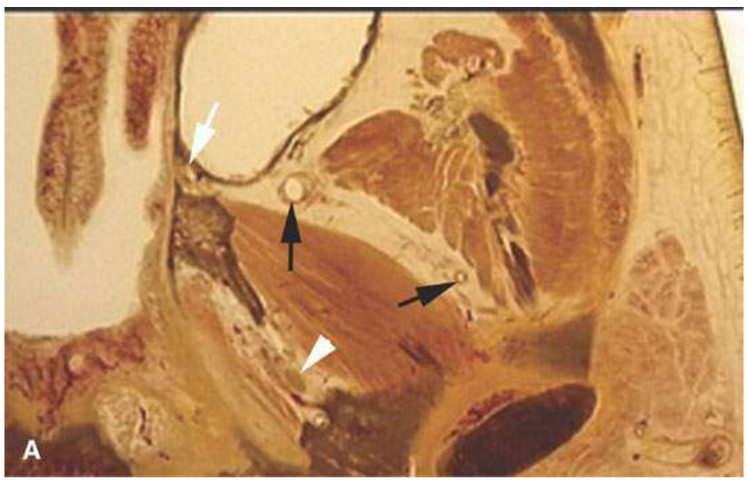

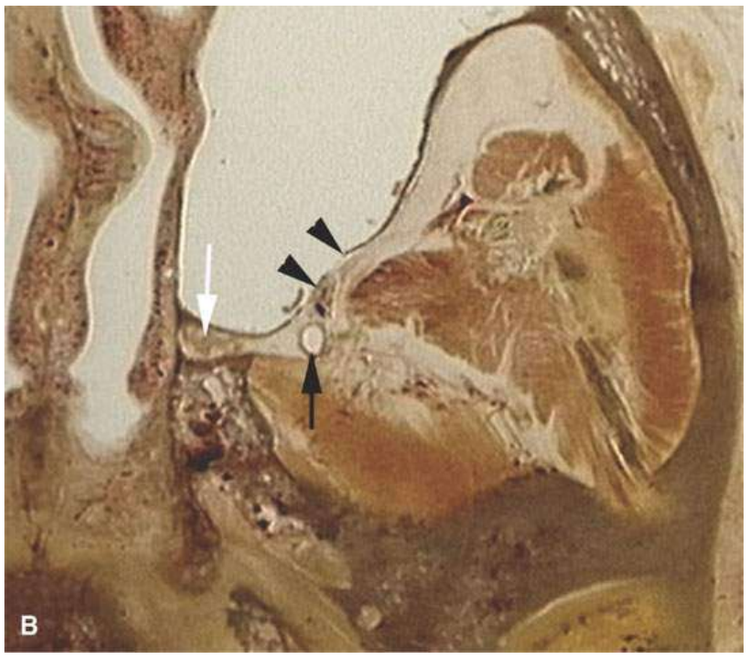

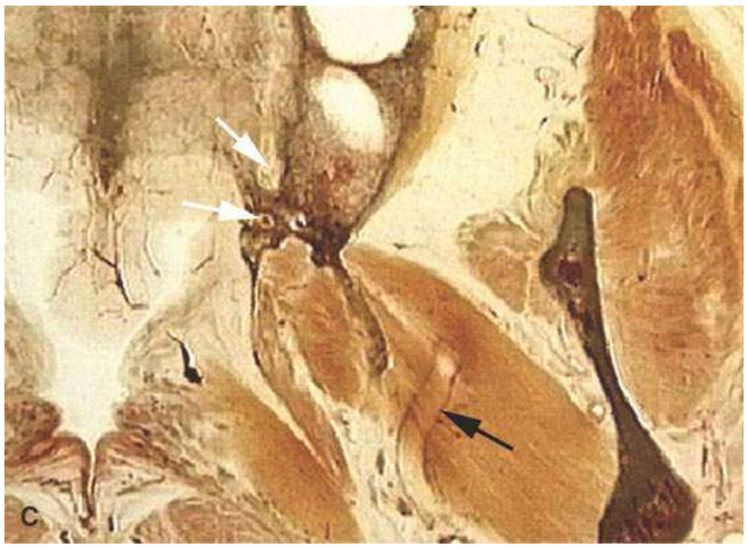

FIGURE 21.48. Anatomic sections showing the potential routes of spread along the distal maxillary neurovascular bundle and its terminal branches. **A:** The maxillary artery and its branches wander through the masticator space *(black arrows)*. Terminal branches lie in the lower pterygopalatine fossa *(white arrow)*. The *white arrowhead* shows V3 in the masticator space. **B:** The distal maxillary *(black arrow)* giving off its posterior superior alveolar terminal branches that ramify in areas of sometimes dehiscent bone along the posterior wall of the maxillary sinus *(arrowheads)*. Nerves in the mid to upper pterygopalatine fossa *(white arrow)*. **C:** The distal maxillary artery *(black arrow)* and palatine foramina *(white arrows)*.

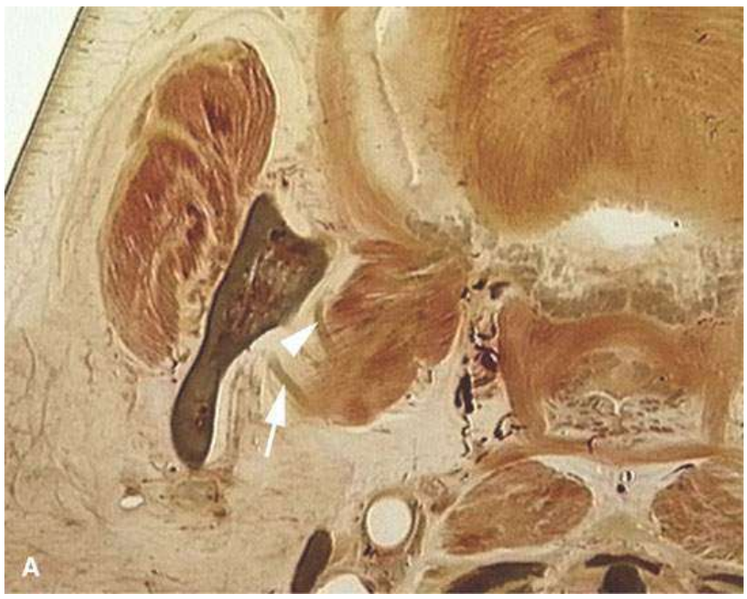

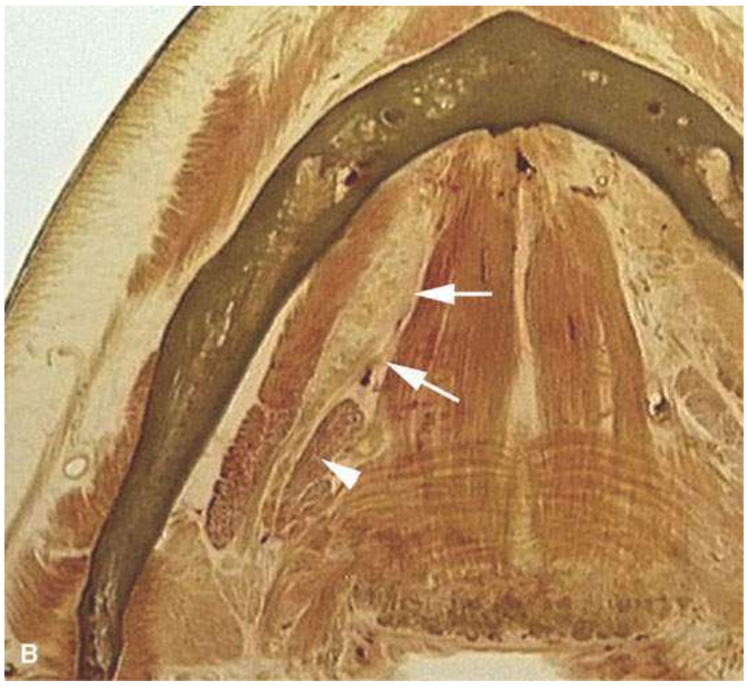

FIGURE 21.49. Distal branches of V3. **A:** The lingual *(arrowhead)* and inferior alveolar nerve *(arrow)* just after they split from V3. **B:** The lingual neurovascular bundle (including the lingual and hypoglossal nerves) eventually courses through the floor of the mouth *(arrows)* both medial and lateral to the hyoglossus muscle *(arrowhead)*.

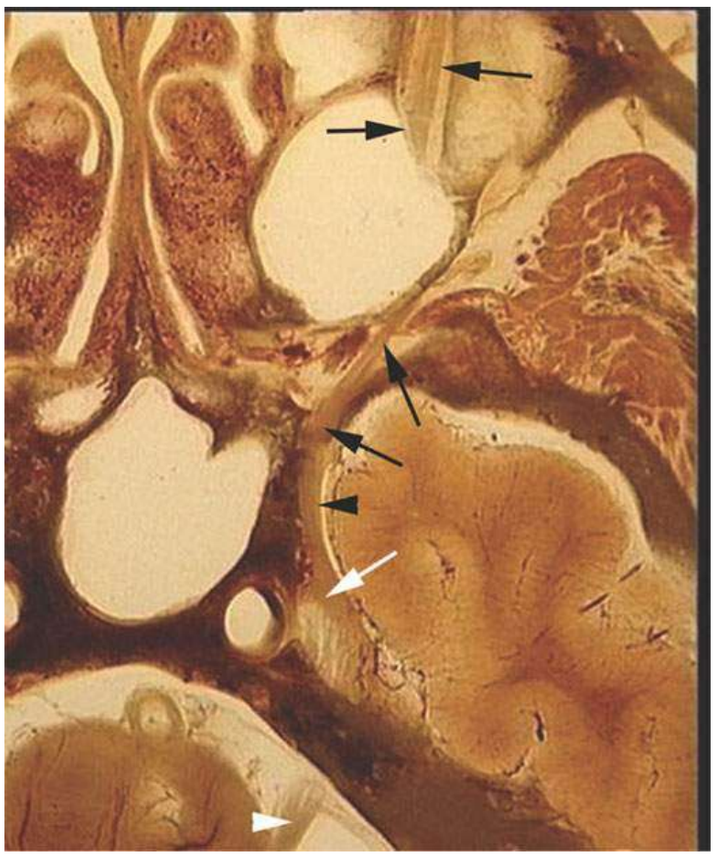

FIGURE 21.50. Anatomic section tracing V2 *(arrows)* from the infraorbital canal to the inferior orbital fissure to the foramen rotundum *(black arrowhead)* to the trigeminal ganglion *(white arrow)* and the main trigeminal nerve *(white arrowhead)* as it enters the brain stem.

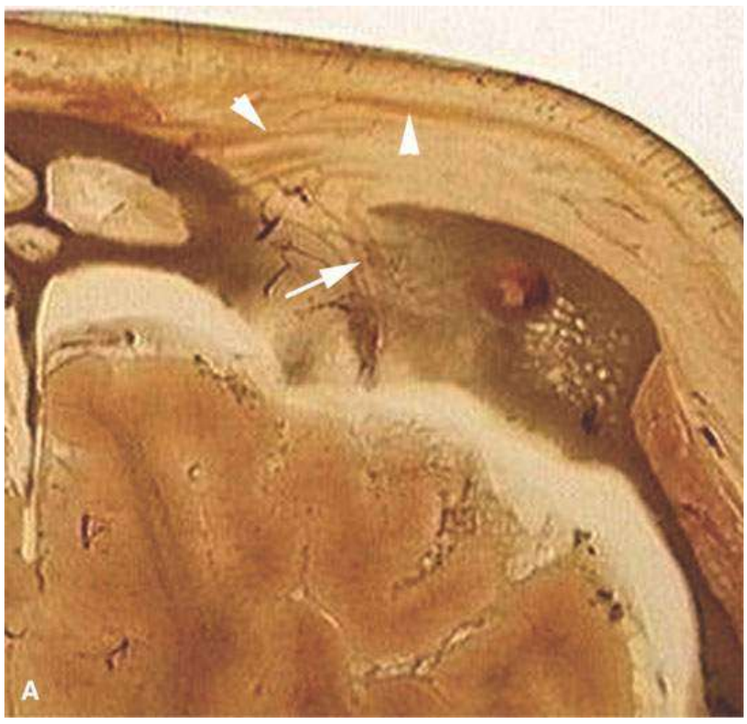
A

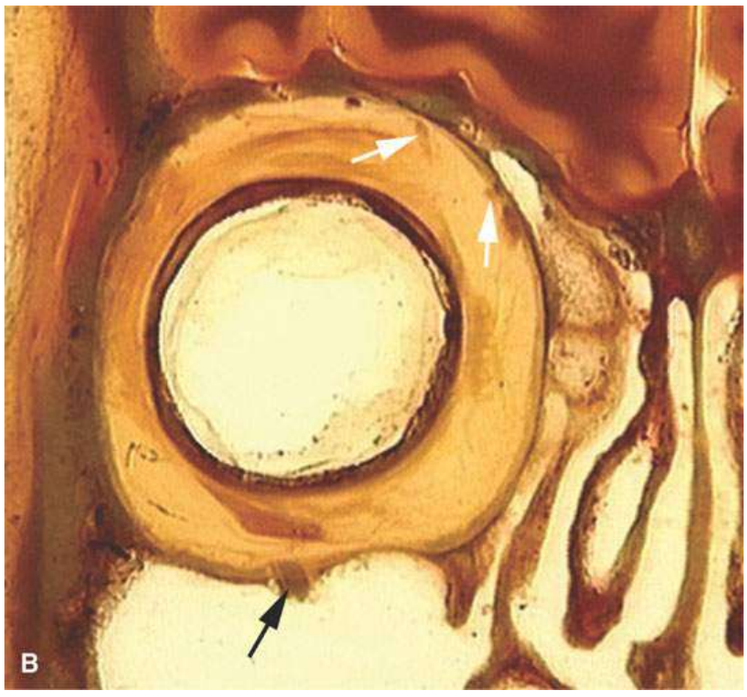
B

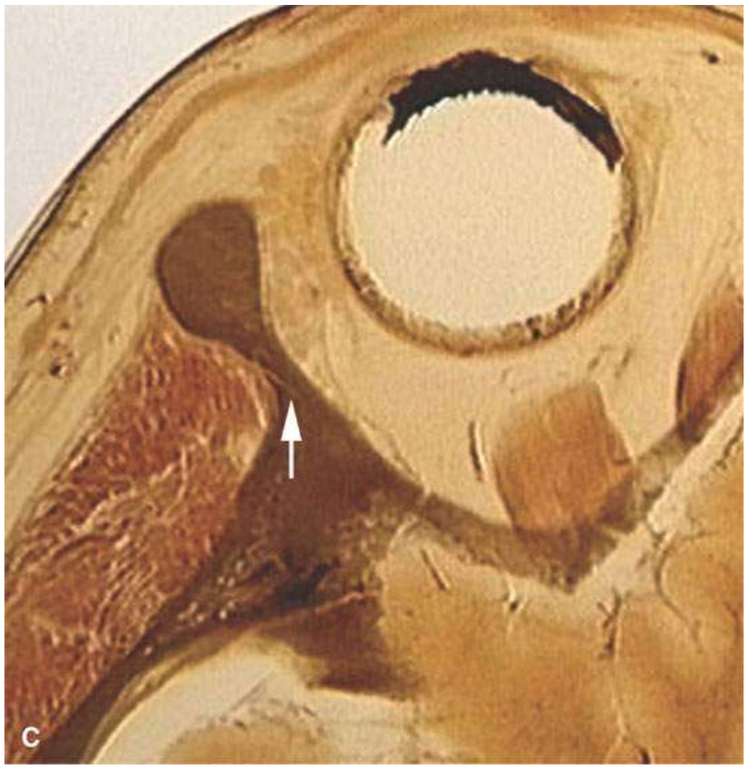
C

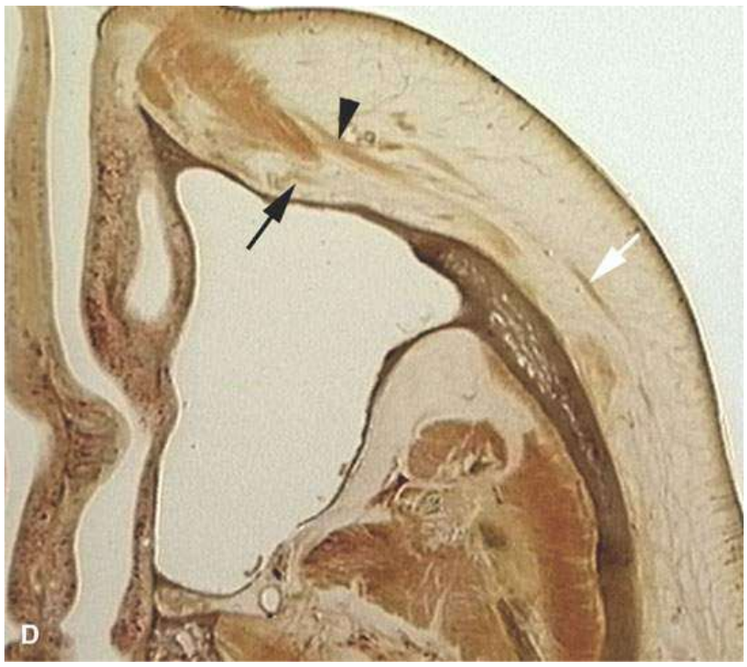

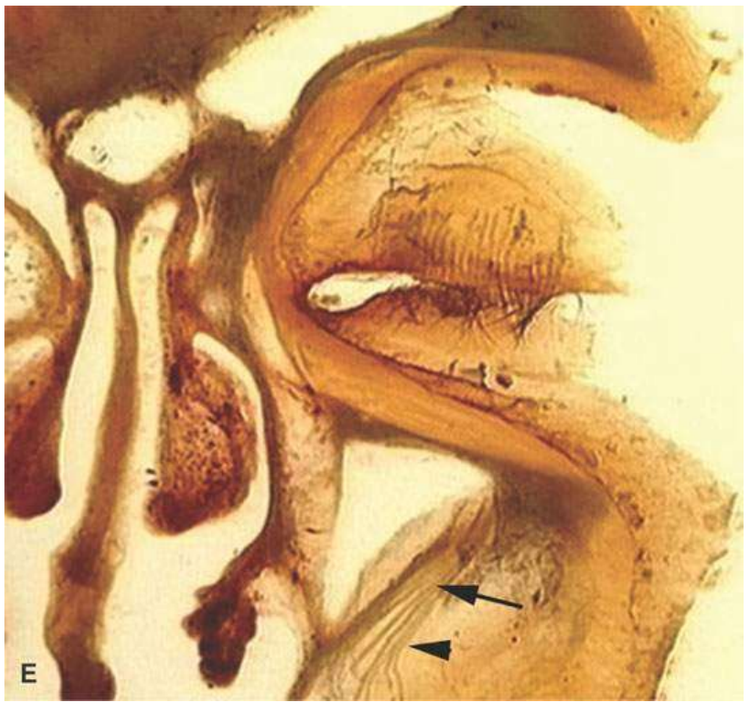

FIGURE 21.51. Anatomic diagrams of the distal fifth and seventh cranial nerves including their relationship to the superficial aponeurotic system (SMAS) of the face where appropriate**. A**: V1 deep to the SMAS (arrowhead) at the supraorbital notch**. B:** Supraorbital and supratrochlear divisions of V1 superior medially in the orbit *(white arrows)***.** Also note the infraorbital branch of V2 in the orbital floor/infraorbital canal *(black arrow)***. C**: Possibly the course of the zygomaticotemporal branch of V2**. D**: Distal branches of V2 *(black arrow)* deep to the SMAS *(arrowhead)***.** Likely distal branch of the facial nerve *(white arrow)* superficial to the SMAS**. E**: Distal infraorbital branch of V2 *(arrow)* and its even more distal ramifications *(arrowheads)* on the cheek in the fat anterior to the maxillary sinus wall.

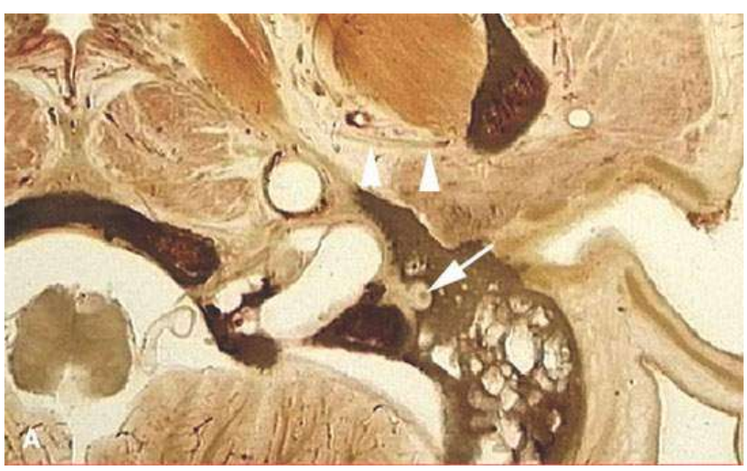

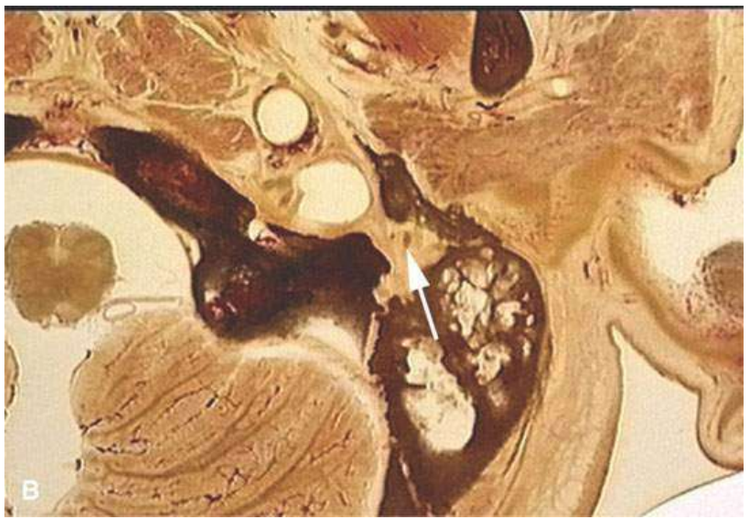

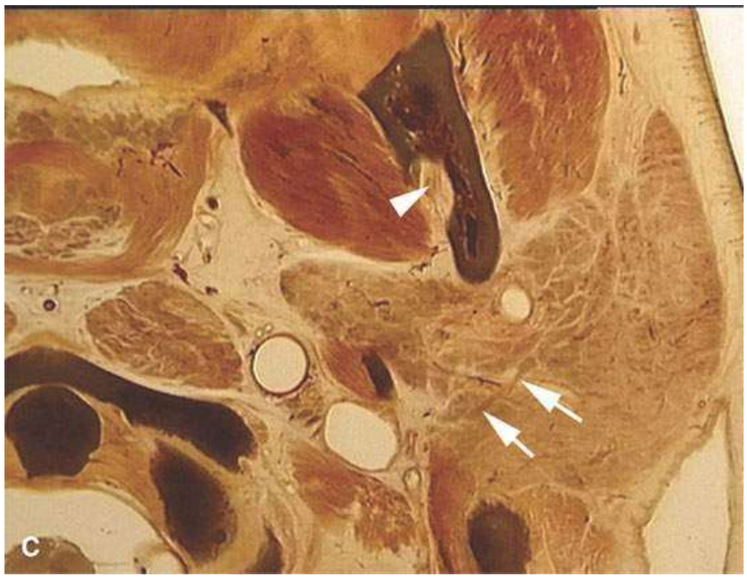

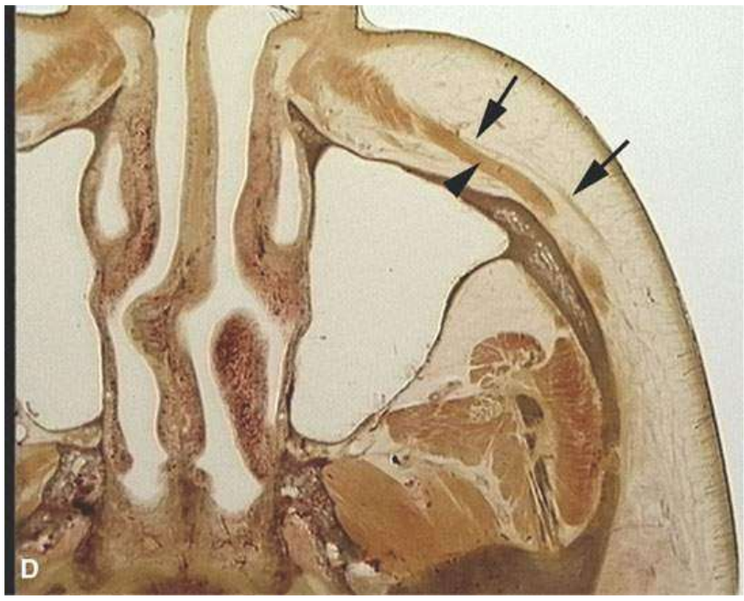

FIGURE 21.52. Anatomic diagrams of the seventh cranial nerve. **A**: The facial nerve *(arrow)* in the distal stylomastoid canal emerging into its fat pad just below the skull base. Also note the auriculotemporal nerve *(arrowheads)*. **B**: The facial nerve *(arrow)* in its fat pad just below the skull base. **C**: The main trunk of the facial nerve in the parotid gland *(arrows)*. Also note the inferior alveolar nerve in the mandibular foramen *(arrowhead)*. **D**: The distal facial nerve *(arrows)* superficial to the superficial musculoaponeurotic system (SMAS) and innervating the muscles of the SMAS layer *(arrowhead)*.

On CT and MR, perineural spread is often manifest by obliteration of the tissue planes around the neurovascular structures in question. Prime examples of a fat plane of interest more centrally are the stylomastoid (Fig. 21.53) and pterygomaxillary fossa fat pads (Fig. 21.54). More peripherally, loss of tissue planes around the distal infraorbital nerves deep to the superficial aponeurotic system (SMAS) of the face are reliable indicators of pathologic perineural spread of cancer (Fig. 21.55). The tendencies seen in perineural spread of skin cancer are discussed in more detail in Chapter 23. Enlargement and/or abnormal enhancement of the nerves (Figs. 21.9–21.11 and 21.54), erosion of the bone forming their exit foramen (Fig. 21.53), and abnormal meningeal enhancement (Fig. 21.56) are other important primary and secondary signs of perineural spread of a benign or malignant tumor. These findings may appear "subtle" unless anticipated based on knowledge of the natural history and tendency of these diseases as summarized here and noted by others long before the advent of modern imaging with CT and MRI (3). Careful comparison to the same structures on the uninvolved side is important for detecting subtle change. An awareness of the possibility of such spread in a particular tumor and given primary site as well as the patient's signs and symptoms combined with anatomic knowledge sufficient for a complete search are all factors important to accurate diagnosis (Appendix C).

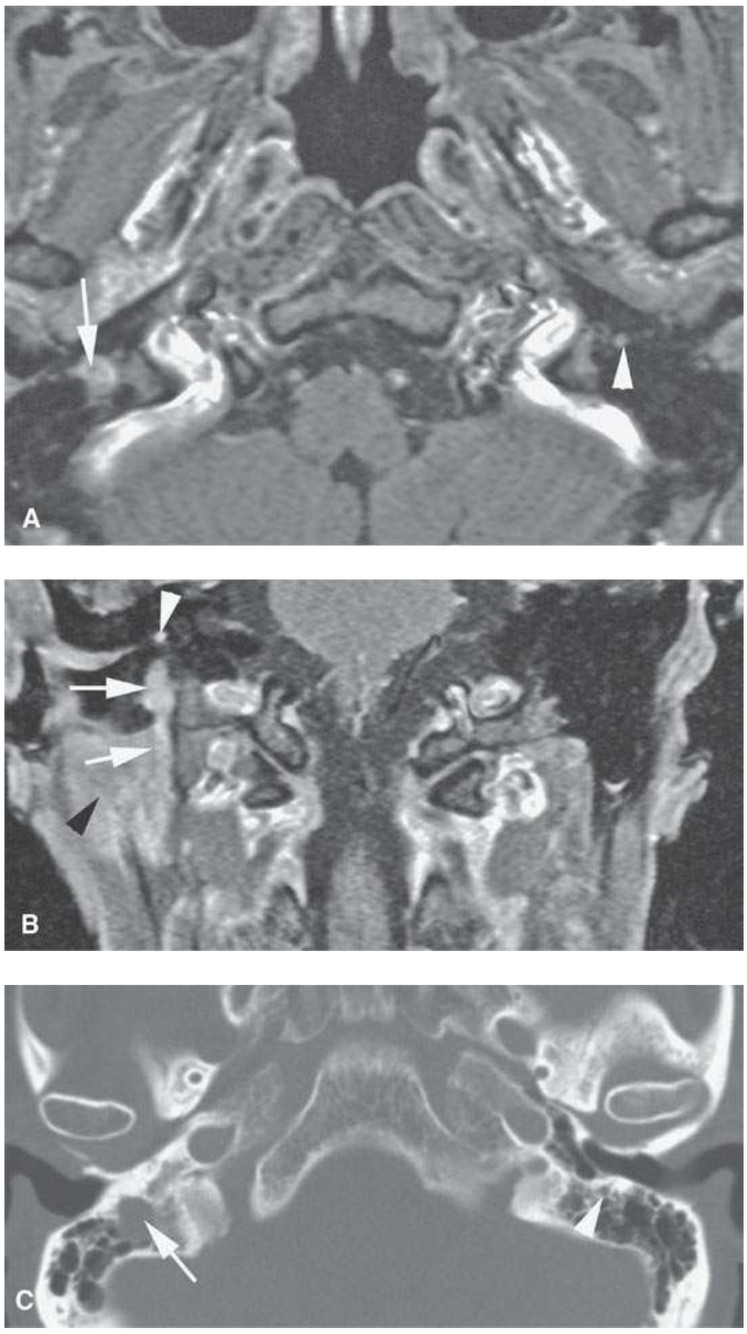

FIGURE 21.53. Computed tomography (CT) and magnetic resonance (MR) imaging of perineural spread along the facial nerve from parotid cancer**. A:** Contrast-enhanced axial MR showing an enlarged and enhancing facial nerve in the descending facial canal on the right *(white arrow)* compared to the normal nerve on the other side *(arrowhead)***. B:** Contrast-enhanced coronal MR showing perineural spread along the facial nerve including the extracranial and descending segments *(arrows)* and tympanic segment *(white arrowhead)* from the parotid cancer *(black arrowhead)***. C:** CT showing an enlarged and eroded descending canal on the right *(arrow)* compared to the normal *(arrowhead)* on the left**.**

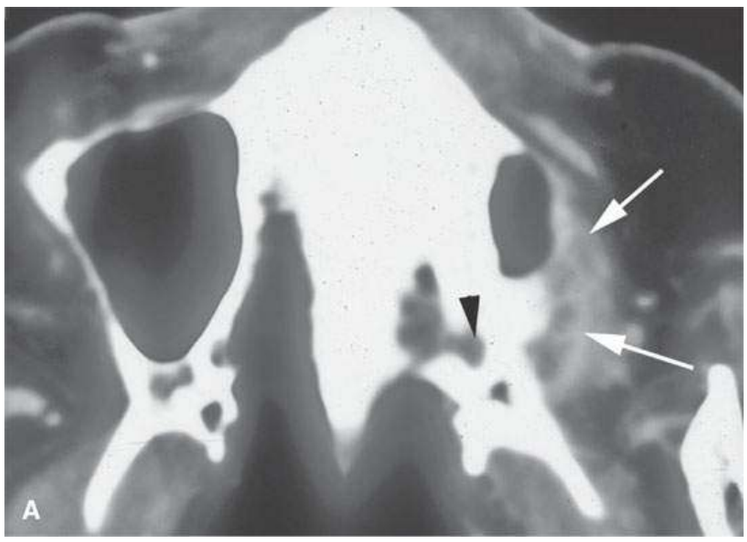

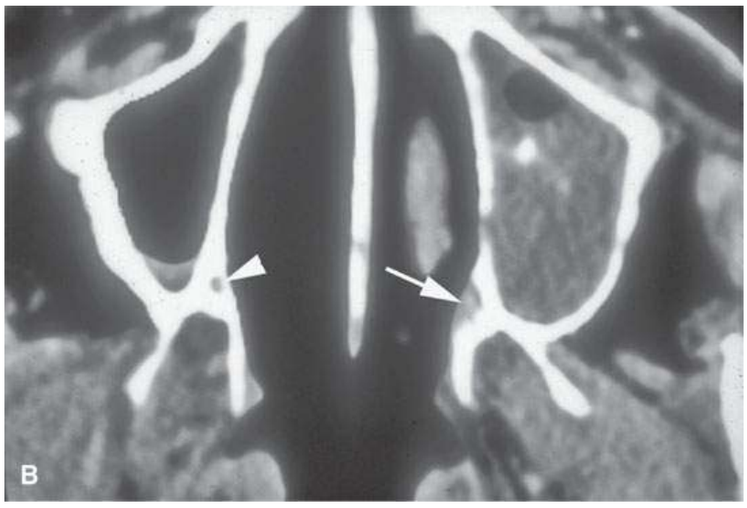
B

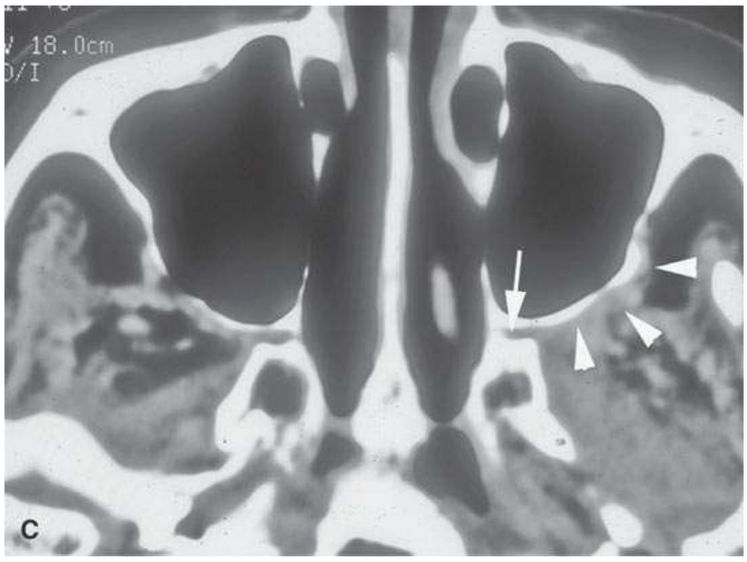
18.0cm
C

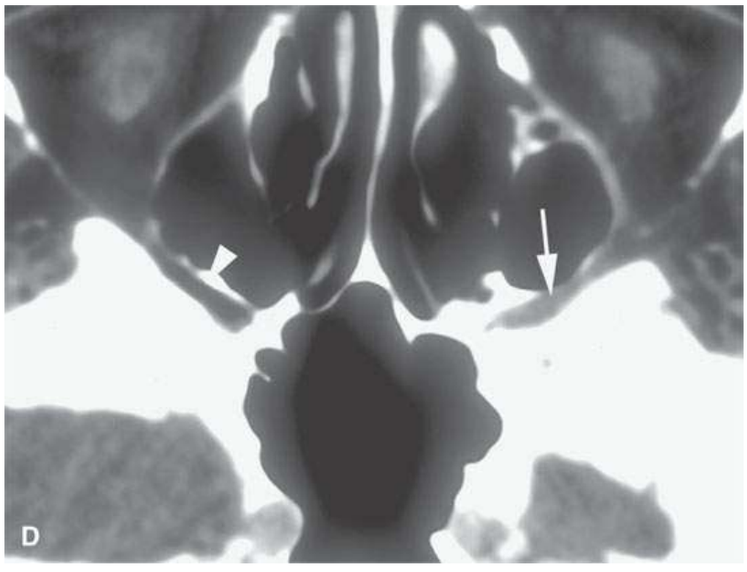
D

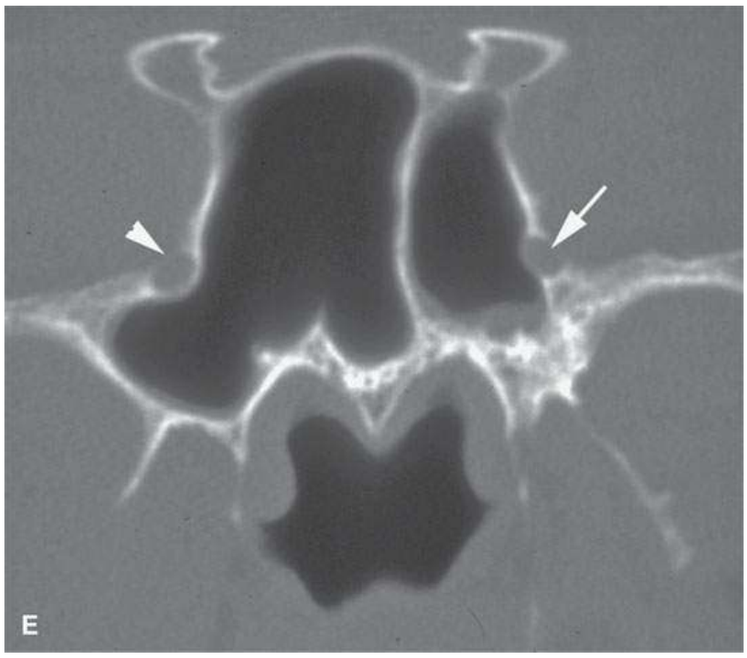

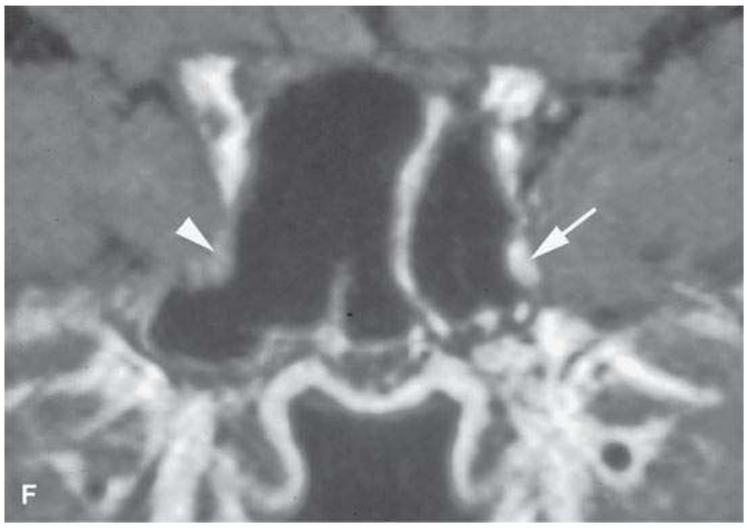

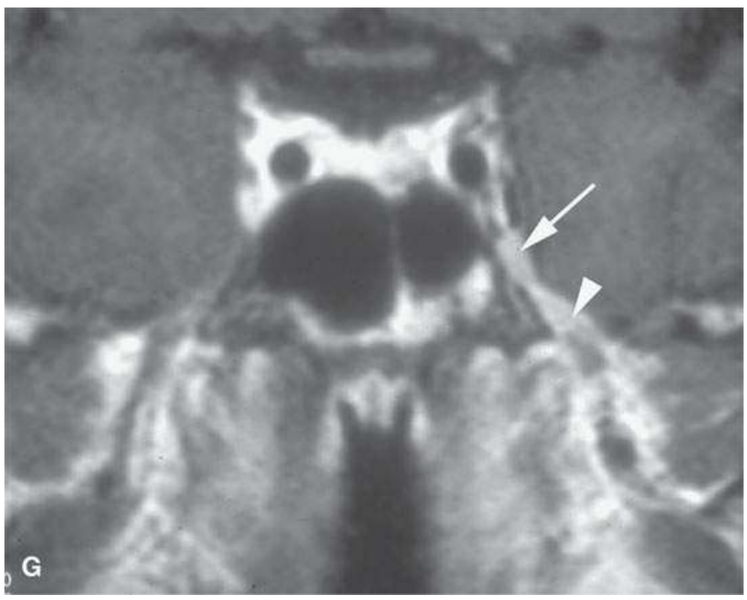

FIGURE 21.54. A patient with gingivobuccal sulcus cancer (*arrows* in **A**) with enlargement of the palatine foramina (arrowhead in **A**). **B**: Spread along the palatine foramina *(arrow)* compared to normal on the right *(arrowhead)*. **C**: Continued spread to the pterygopalatine fossa *(arrow)* and along the posterior superior alveolar vessels and nerves along the posterior maxillary sinus wall *(arrowheads)*. **D**: Continued spread to the inferior orbital fissure *(arrow)* obliterating its fat compared to the normal side *(arrowhead)*. **E**: No definite evidence of spread along V2 in the foramen rotundum *(arrow)* compared to normal *(arrowhead)*; however, compare to the magnetic resonance imaging in (fF). **F**: Contrast-enhanced T1-weighted (T1W) image shows definite enlargement and abnormal enhancement of V2 in the foramen rotundum *(arrow)* compared to normal side *(arrowhead)*. **G**: Contrast-enhanced T1W image showing tumor spreading anterograde from the V2 junction with trigeminal ganglion *(arrow)* to proximal V3 *(arrowhead)*.

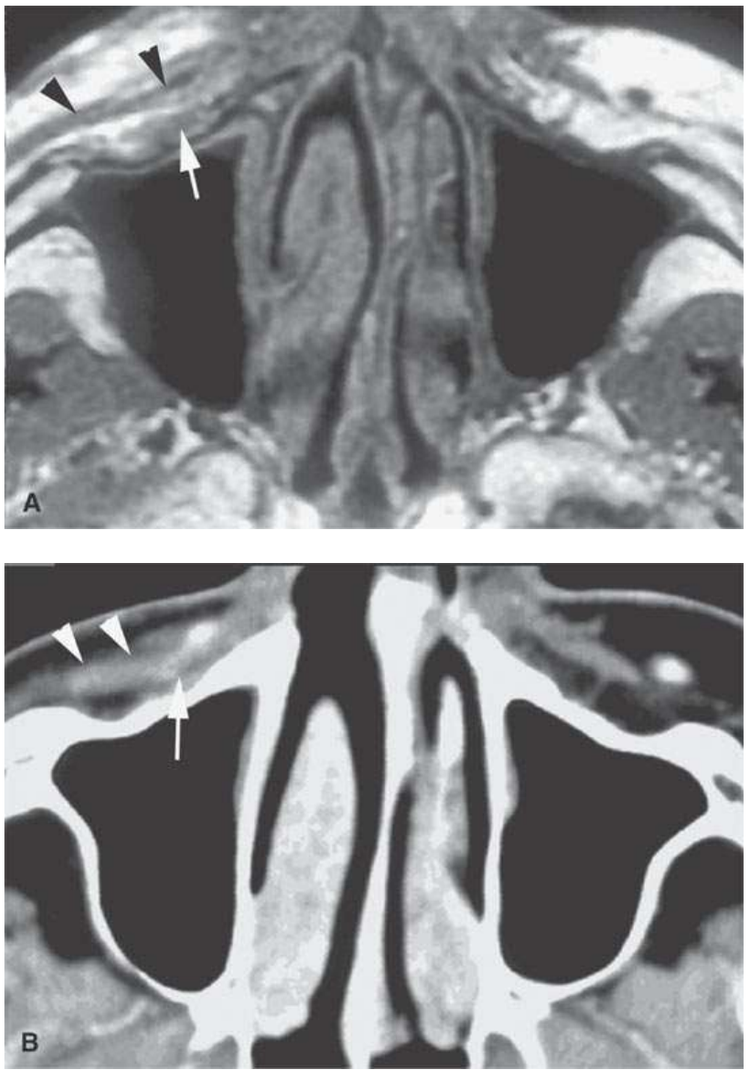

FIGURE 21.55. T1-weighted image **(A)** and contrast-enhanced computed tomography **(B)** in the same patient showing distal perineural spread of skin cancer along the distal branches of V2 *(arrows)* lying deep to the superficial musculoaponeurotic system *(arrowheads)*.

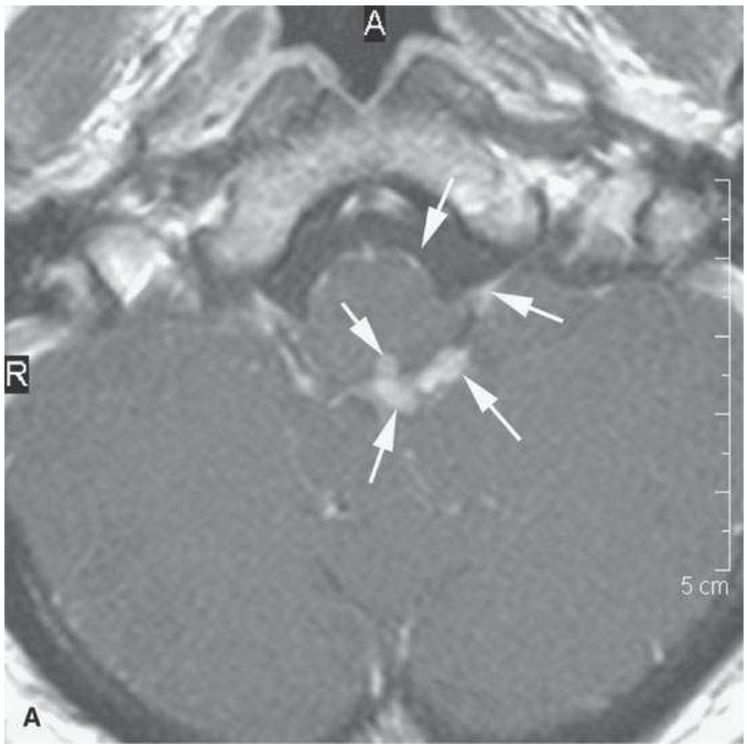

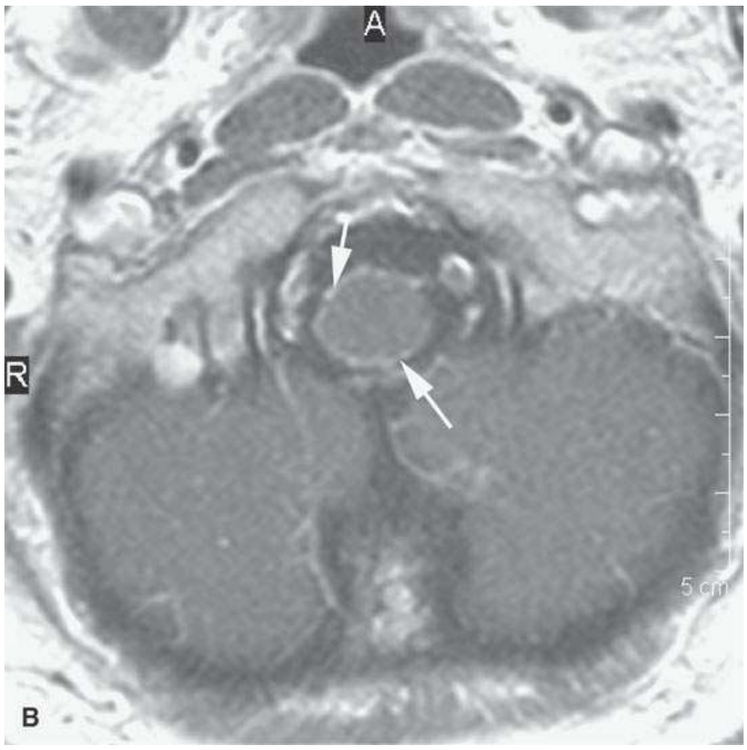

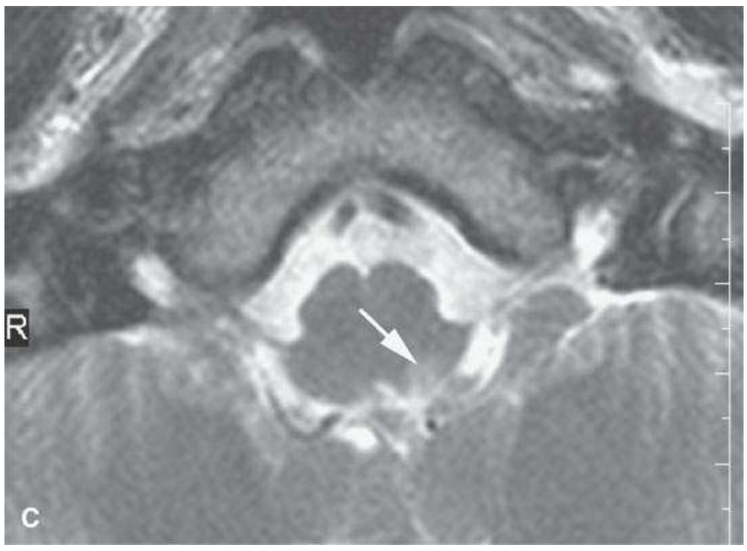

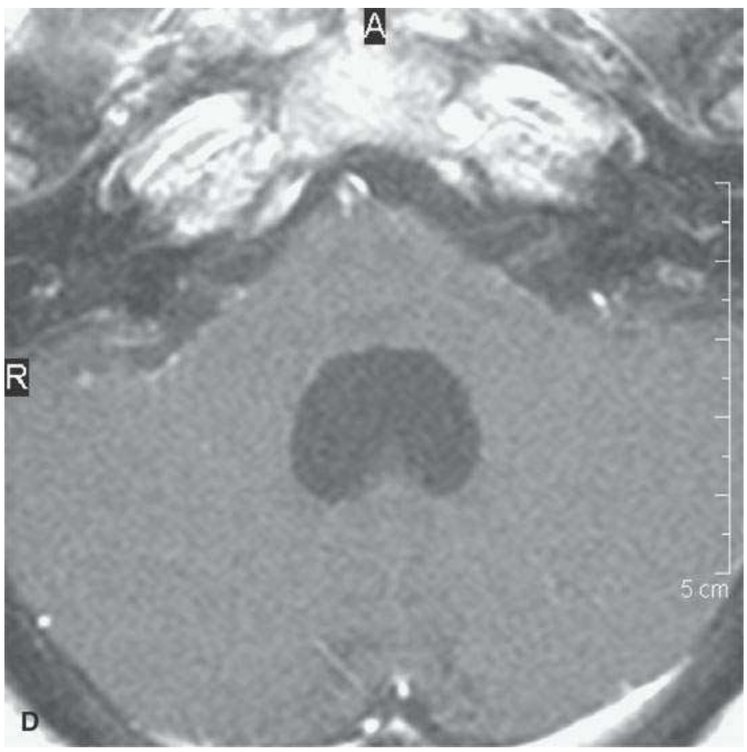

FIGURE 21.56. Meningeal carcinomatosis as seen on magnetic resonance imaging manifesting as nodular enhancement of the pia-arachnoid membrane (*arrowsheads* on the T1-weighted contrast-enhanced images in **A** and **B**)and edema along the surface of the brain stem (*arrow* in the T2-weighted image in **C**), and obstruction of the fourth ventricle (T1-weighted contrast-enhanced images in D)**.**

CEMR is capable of showing perineural spread better than CECT in most cases, especially near and within the skull base. It is critical to remember that most of the cranial nerves and their major divisions are surrounded by a plexus of vessels as they traverse their related bony canals and exit foramina**.** Perineural

enhancement that is often asymmetric is, therefore, a normal variation (Fig. 21.57). The diagnosis of perineural tumor spread on MR and/or CT may be by seeing the nerve itself enhance. Enhancement of a nerve can also be due to inflammation (Fig. 21.58).

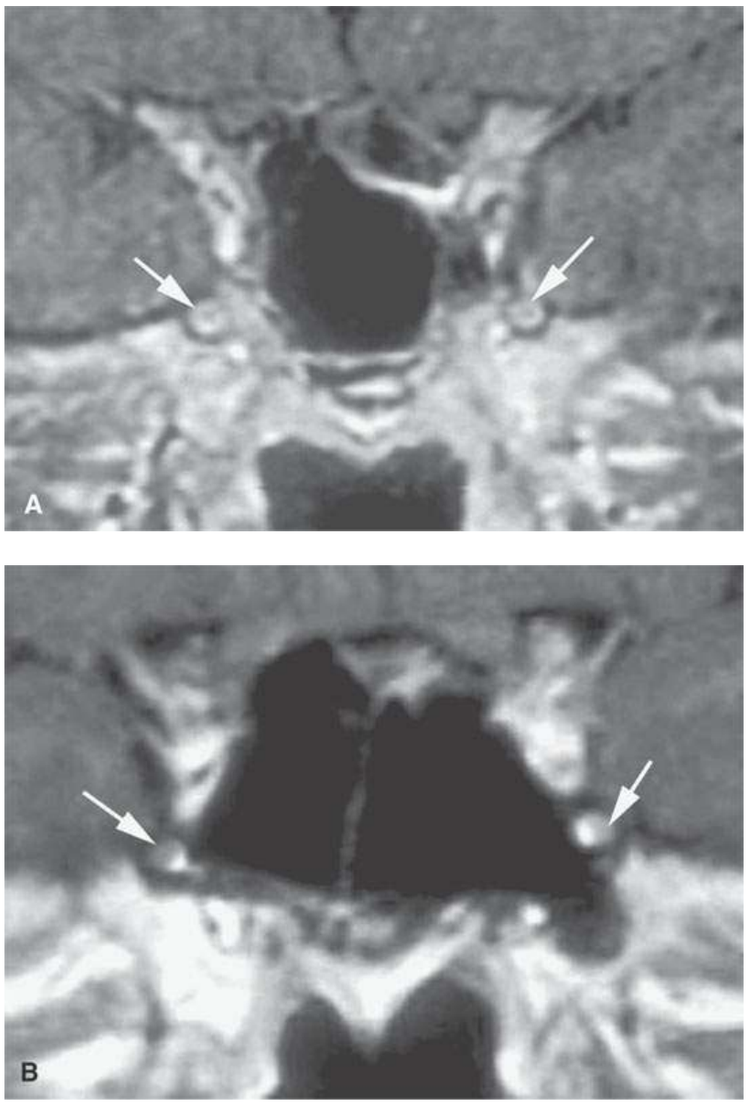

FIGURE 21.57. Contrast-enhanced magnetic resonance showing variations in normal perineural plexus enhancement around V2 within the foramen rotundum (*arrows* in the T1-weighted contrast-enhanced images in **A** and **B**).

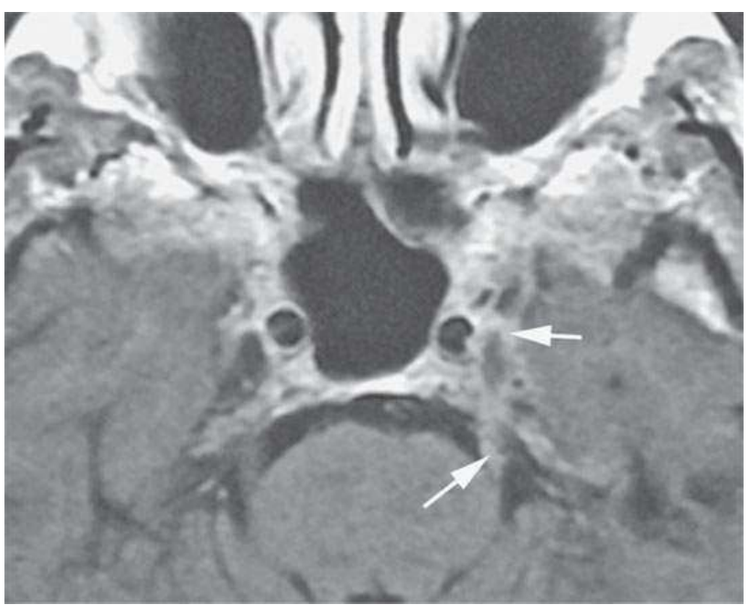

FIGURE 21.58. Contrast-enhanced magnetic resonance of a patient with herpes trigeminus producing abnormal enhancement of the trigeminal nerve rootlets and the nerve itself *(arrows)* demonstrating the lack of specificity of neural and perineural enhancement.

Spread of tumor along neurovascular bundles as just described can drastically affect treatment and prognosis. The same is true of true perineural spread, although this is harder to detect on imaging studies and is frequently only a microscopic finding. Spread of tumor within or around nerves is sometimes described as growth in "perineural lymphatics." In fact, experimental and autopsy studies demonstrate that the only lymphatic spaces related to peripheral nerves are in the epineurium. The epineurium is a layer of loose areolar tissue surrounding nerve fascicles that contains the vaso vasorum and lymphatics. The perineurium and endoneurium contain no lymphatics. Since tumor may be found in the epi-, peri- and endoneurium, the term *perineural spread* related to imaging studies should be used generically to describe spread along cranial and peripheral nerves, realizing that the tumor may bear varied microscopic relationships to the affected nerves. Some malignancies are more prone to manifest perineural extension at presentation. The most well-known is adenoidcystic carcinoma. Some sarcomas, especially neurogenic sarcomas, will also show this tendency (Fig. 21.9). Squamous cell and other carcinomas will often have gross perineural spread when they recur, and long-standing skin cancer not infrequently has perineural spread at initial presentation (Figs. 21.10 and 21.55). More aggressive carcinomas may also show microscopic perineural spread at presentation. Neurotropic lymphoma (Chapter 27) often spreads within the nerve, causing the involved nerve(s) to enlarge and enhance.

Nerve dysfunction does not necessarily imply invasion. Adjacent tumor can compress nerves while not directly invading them. An interesting example is compression of the lower cranial nerves by enlarged retropharyngeal nodes in nasopharyngeal carcinoma. Compressive nerve deficits may resolve following radiotherapy, whereas nerves invaded by tumor may not recover function so readily following radiotherapy; in fact, such disease is difficult to control with radiotherapy. Compression by benign tumors is probably more likely to resolve than that caused by a malignant tumor. Atrophy of the end organ and/or long-term paralysis will usually not recover. Control of perineural spread, especially in skin cancer, has improved in recent years.

Lymphatic Spread

Most cancers in the head and neck region may spread by capillary lymphatic channels to regional draining nodal groups.[10,11] Sometimes, a tumor that is almost always benign or mistakenly diagnosed histologically as benign will be revealed by imaging that shows nodal involvement (Fig. 21.59). The tendency for lymph node involvement is based on several factors. The major ones are (a) tissue of origin, (b) size, (c) location, (d) biologic aggressiveness, and (e) prior treatment.

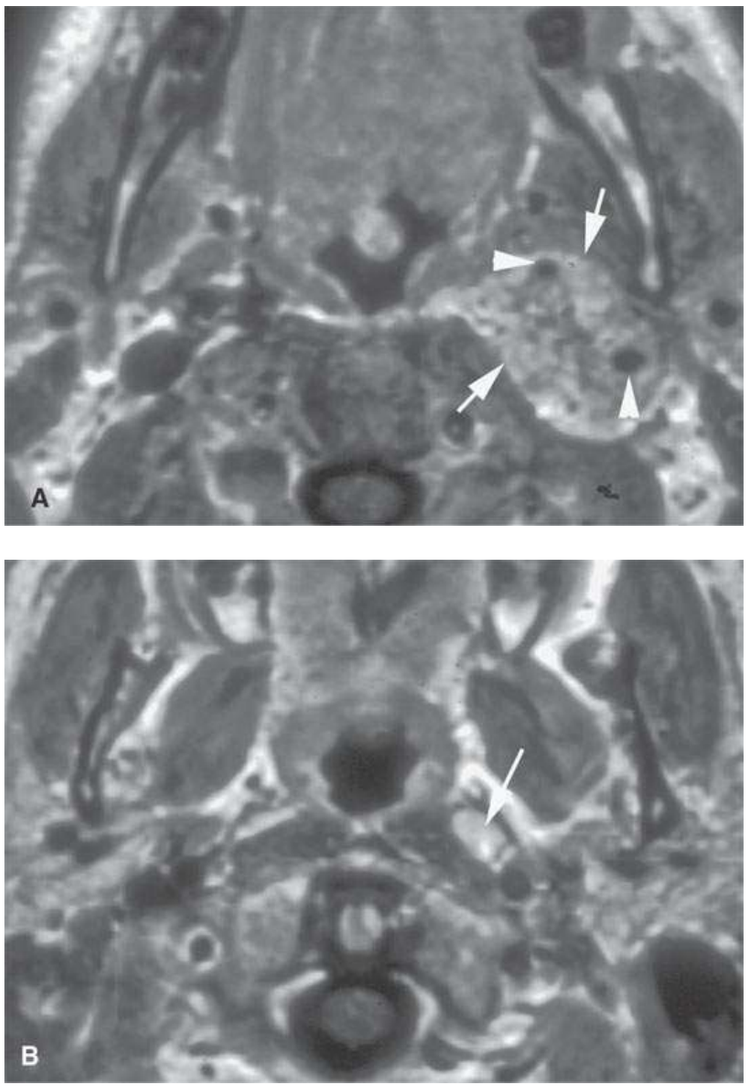

FIGURE 21.59. Contrast-enhanced magnetic resonance showing a paraganglioma somewhat atypical in appearance. **A**: The tumor tendency to encase rather than displace the carotid and jugular *(arrowheads)* and perhaps a little more irregular at it margins was considered worrisome for an unusual malignant variant. **B**: The enhancing retropharyngeal node *(arrow)*, however, was the most convincing sign of its malignant nature.

In carcinomas, the extent of cervical metastatic disease is often as important as that of the primary for planning management and estimating prognosis. In other malignancies, regional lymph node metastases are less frequent and often do not as critically impact therapeutic decision making. The impact of imaging on the assessment of nodes in squamous cell carcinoma of the upper aerodigestive tract is evolving and remains controversial with regard to evaluating risk in a clinically negative neck. Currently, properly done CT is better than MR for staging all head and neck nodal groups except the retropharyngeal nodes. MR and US are useful adjunctive studies at times. FDG-PET has a yet to be fully defined adjunctive role. It can detect involved nodes not detectible on CT, but it does not have a sufficient negative predictive value to alter treatment decisions. A significant outcome impact with regard to nodal staging is yet to be established. The natural history and morphology of nodal disease are reviewed in conjunction with cervical metastatic disease in Chapter 157. The trends and patterns of cervical metastases from various primary sites will be discussed along with the respective primary sites of those malignant tumors.

At this point, it is useful to understand that CT, MR, or other imaging studies are unlikely, in the foreseeable future, to reliably assess the risk of microscopic disease in cervical nodes. The trends of these risks, however, have been understood since the 1970s based on very reliable and reproducible clinical studies; thus, imaging risk assessment is really not paramount in clinical decision in the clinically negative neck. Also, size criteria alone, even if set in a useful range, are of essentially no usefulness in clinical decision making. The evaluation of the internal morphology and periphery of the node are more informative and useful than size for detecting clinically occult disease and assessing the possibility of capsular rupture and extent of extranodal disease. Perfusion data may add to overall accuracy of the principally anatomic CT and MRI studies. A more complete discussion of these and other factors related to the assessment of cervical and retropharyngeal lymph node metastases is presented in conjunction with cervical metastatic disease in Chapter 157.

POSTTREATMENT REACTION AND SCARRING VERSUS RECURRENT TUMOR

The manifestations of imaging findings after surgery and/or radiotherapy vary considerably with treatment modality, site of pathology, and the original extent and type of tumor treated. Several basic trends will be discussed here and then modified appropriately in the following site-specific chapters.

The Postoperative Inflammatory Response: Wound Healing and Scar

Soft Tissue Wound Healing Following Surgery

The concept of posttreatment “scarring” must be defined at the outset. The word *scar* usually refers to the end product of the inflammatory response, sometimes called *white scar*, that is a zone of relatively dehydrated, hypocellular and predominantly collagenous tissue. On T1W and T2W images, this end-stage, dehydrated scar will be isointense or hypointense to muscle and show minimal or no enhancement on CEMR. On CT, it is indistinguishable from muscle or tumor. The related imaging findings are described and illustrated in Chapter 13, and an additional example is shown in Figure 21.60.

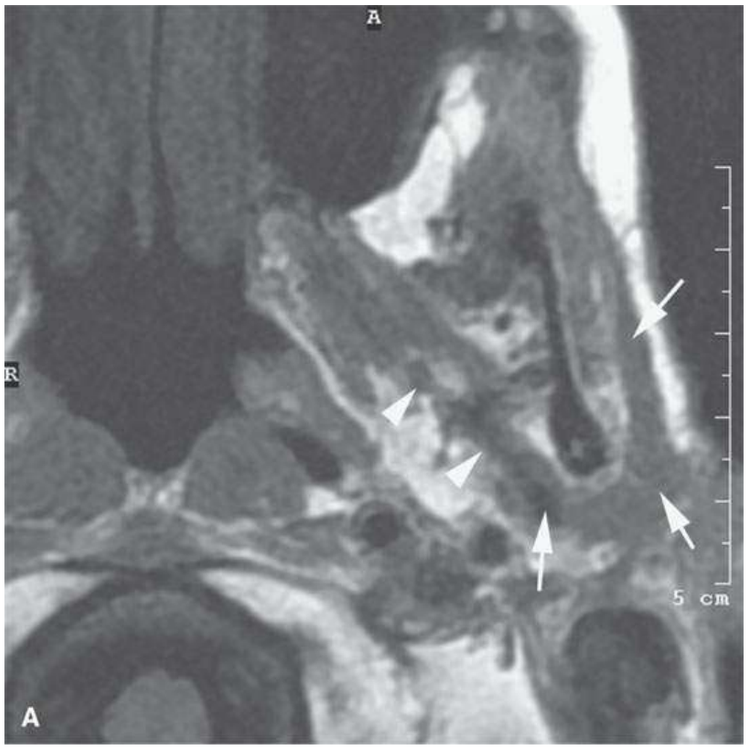

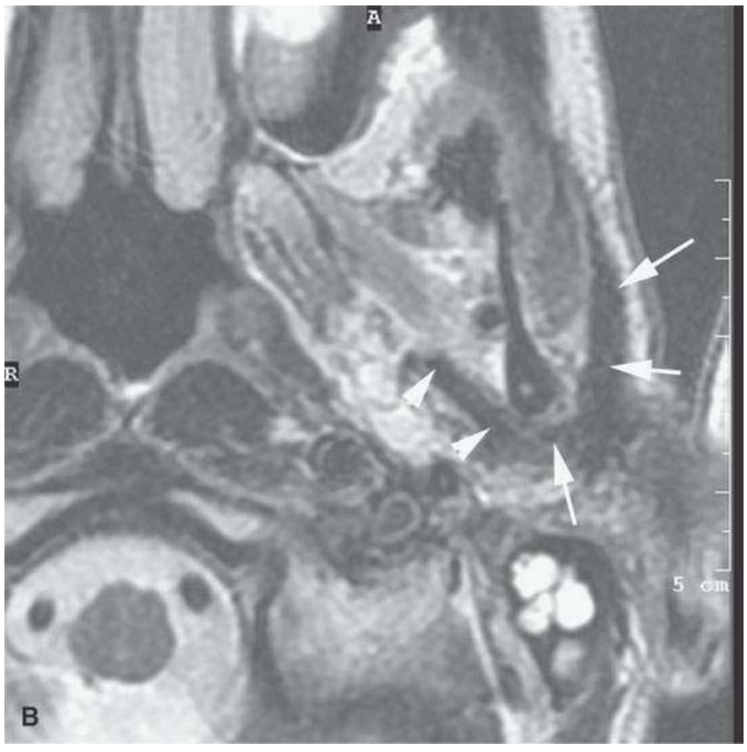

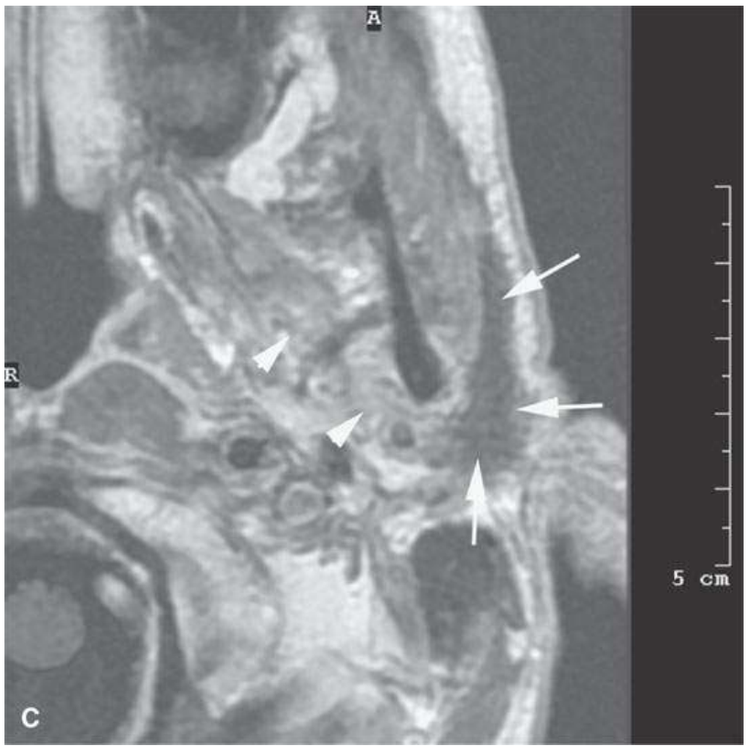

FIGURE 21.60. Contrast-enhanced magnetic resonance of a patient treated with surgery and radiotherapy for parotid cancer. **A:** Non–contrast-enhanced T1-weighted (T1W) image shows mainly a band of scar *(arrows)*, but notice how the more medial component *(arrowheads)* enhances markedly in (cC). **B:** T2-weighted image shows mainly a band of scar as less intense than muscle *(arrows)*, but notice how the more medial component *(arrowheads)* enhances markedly in (cC). **C:** Contrast-enhanced TIW images shows minimal if any enhancement of the scar seen as end-stage fibrosis in all images *(arrows)*; however, the medial component enhances *(arrow heads)* and was proven to be local and perineural recurrence spreading back to trigeminal ganglion (not pictured).

It is also reasonable to refer to the ongoing inflammatory response or granulation tissue as scar. This is essentially vascularized or "red" scar. This active inflammatory response to wound healing evolves to end stage or white scar just described. This granulation tissue will usually be isointense to hypointense to muscle on T1W images and slightly to markedly hyperintense to muscle on T2W images and will enhance so that it is indistinguishable from tumor. Fat suppression techniques, done with or without contrast, do not offer any benefit in distinguishing granulation tissue or active "scar" from tumor. In most areas of the head and neck, this subacute inflammatory response will resolve and progress to end-stage fibrosis within 3 to 12 months or sooner in surgically treated patients. A major exception to this is the dura that can manifest reactive enhancement on CEMR for years following surgery in the absence of persistent or recurrent tumor. The deep tissue changes outside the cranial vault will generally parallel the healing process in the skin. Postoperative seromas or hematomas and foreign material such sutures and wires may be responsible for foci of increased signal intensity and enhancement on MR images beyond that period. Such changes are less evident on CECT. These processes all may be hypermetabolic and lead to false-positive FDG-PET studies as well (Fig. 21.61). This accounts for a proportion of the false-positive rate of FDG-PET in upper aerodigestive tract carcinomas that occur before about 3 months after the completion of radiotherapy.

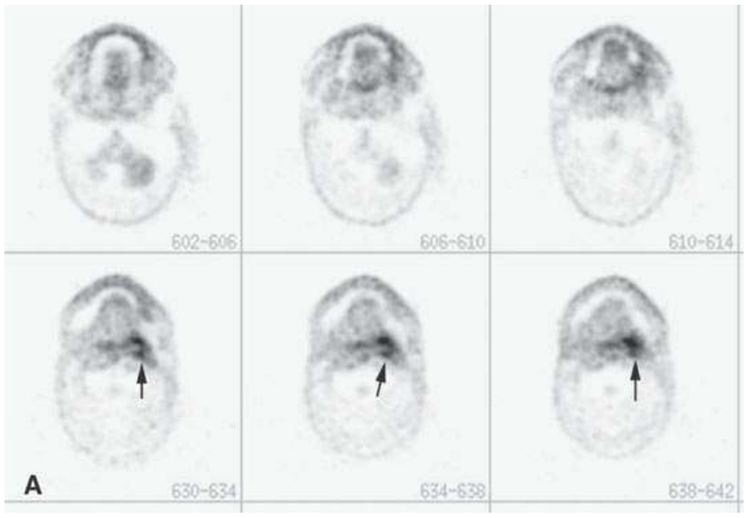

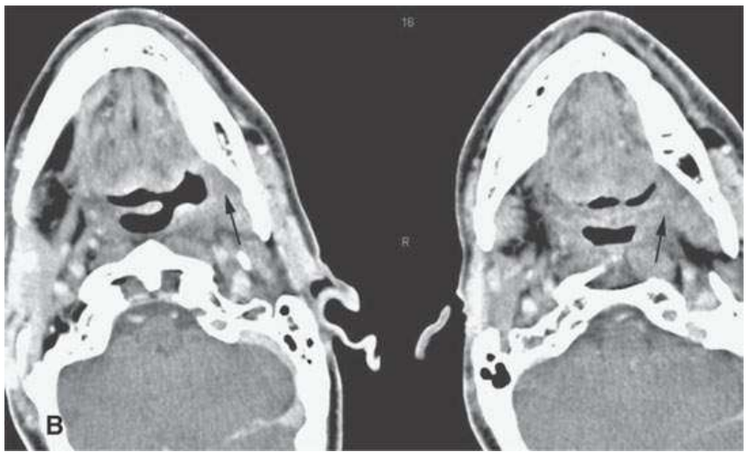

FIGURE 21.61. Patient with persistent pain following radiotherapy for tongue base cancer. **A**: Fluorine-18 2-fluoro-2-deoxy-D-glucose positron emission tomography (FDG-PET) on the same day shows the mass to be hypermetabolic 4 months after completion of all therapy. **B**: Diagnostic contrast-enhanced computed tomography shows persistent mass *(arrow)*. The patient has been followed for 5 years without evidence of recurrent tumor.

From this discussion, two things may be evident: (a) baseline scans intended for use in follow-up should be obtained no sooner than 12 weeks postoperatively, and (b) T2W and T1W CEMR are probably the most informative studies to use in follow-up. The second issue is true with the exceptions of detection of recurrent nodal disease and/or progressive, subtle bone erosion as signs of recurrent tumor, or at any site where motion artifact—for example, in the larynx—is likely to degrade MR image quality and CECT would be a better choice for the anatomic study used in posttreatment surveillance.

Bone Changes Following Surgery

Bony surgical margins will usually heal within months and result in a smooth cortical healed surface assuming that there is no tumor recurrence, bone necrosis, or infection. Screws placed in bone as part of screw-plate and screw-mesh constructs should be anchored well in bone without surrounding lucency (Fig. 21.62). Lucency between the bone and anchoring screws in the construct usually indicates loosening but can be due to inflammation caused by necrosis or infection and/or recurrent tumor threatening the integrity of the construct. Bone sclerosis between the bone and construct can be a sign of the same circumstances. This is also discussed and illustrated in Chapter 14.

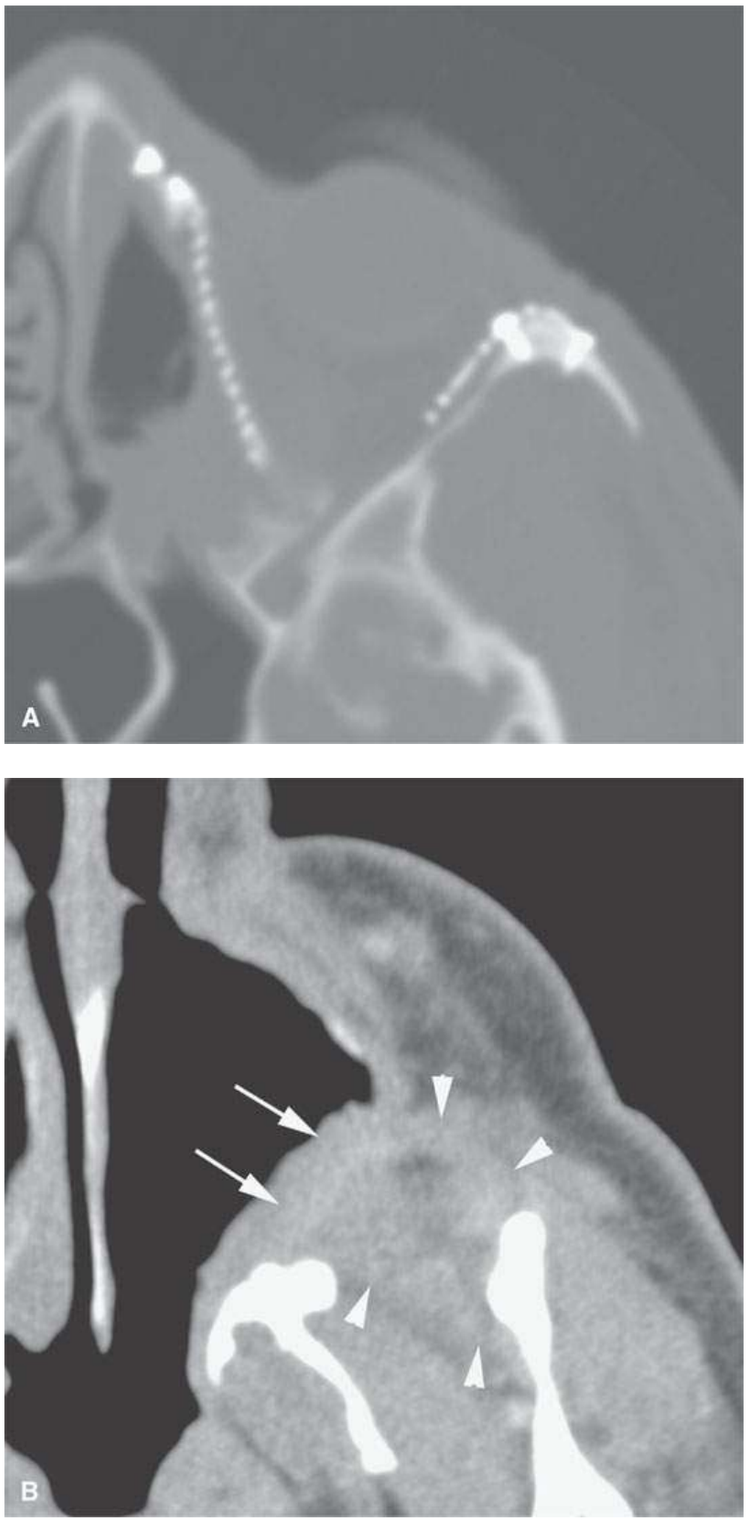

FIGURE 21.62. Computed tomography (CT) of a patient treated with surgery for sinus cancer. **A**: The construct of mesh and screws is normal. **B**: The thickness of the tissues along the closure *(arrows)* is suspicious for recurrence, and the deeper infiltrating masticator space mass *(arrowheads)* made recurrence very likely. Recurrence was confirmed by CT-directed biopsy.

Tissue Reaction and Healing Following Radiotherapy

The response to radiotherapy is similar to that just described for surgery with three important exceptions: (a) during therapy, there are significant intra- and peritumoral changes; (b) depending on the site radiated and dose, subclinical edema may persist for many months and evolve to permanent perilymphatic fibrosis; and (c) reactive mucosal changes are common and may persist for many months in the target tumor as well as irradiated normal mucosa.

Changes During Radiotherapy

During radiotherapy for cancers, the primary site and involved nodes usually show a progressive decrease in size on both CT and MRI and variable changes in signal on MRI. Enhancement changes will also be variable but in general perfusion will decrease as radiotherapy proceeds (Fig. 21.63). At some point, sites of tumor involvement may become frankly edematous and/or necrotic, and peritumoral edema will appear. The peritumoral changes usually peak toward the end of therapy. Changes due to necrosis and edema will be bright on T2W images. MR and CT imaging during radiotherapy is therefore potentially confusing if size is considered because the reactive edema and tumor bed may form an aggregate mass that seems larger than the original tumor. CEMR does not help, as the enhancement will be diffuse. Perfusion MRI or CT will likely show decreased perfusion of the primary and nodal disease, but this currently remains experimental and is not incorporated in routine medical decision making (Fig. 21.62).

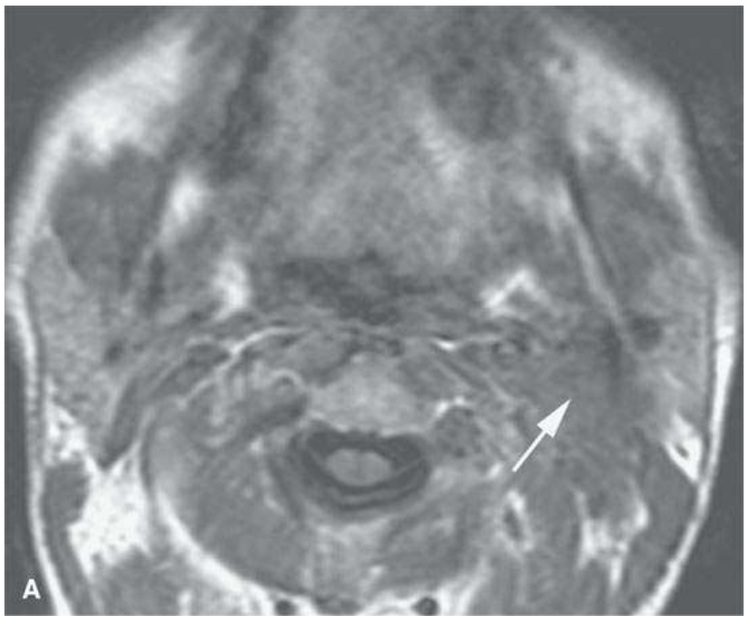

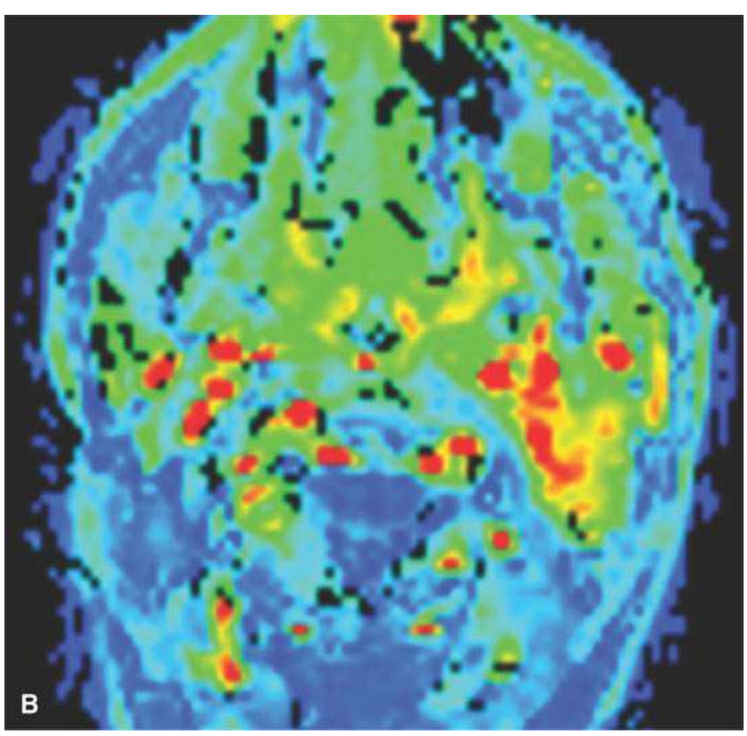

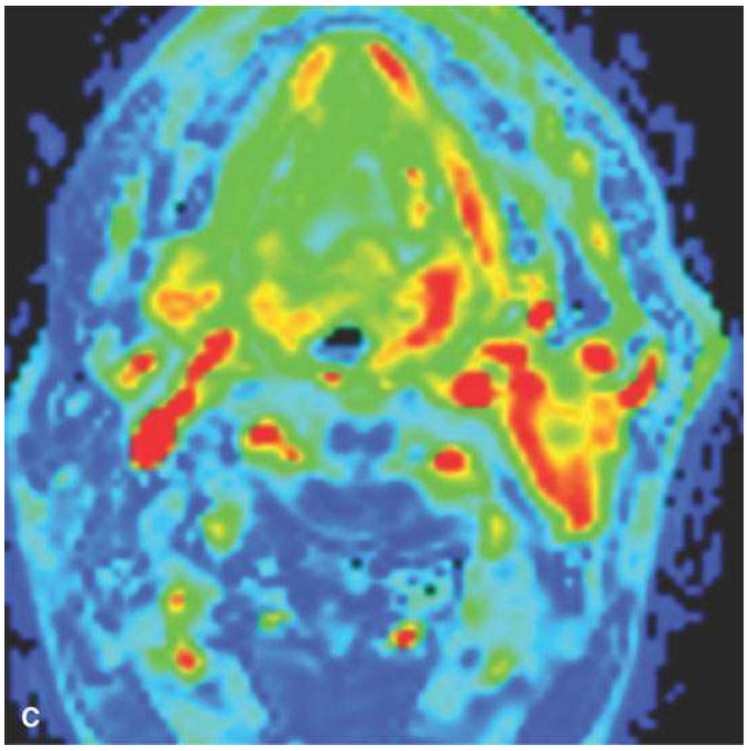

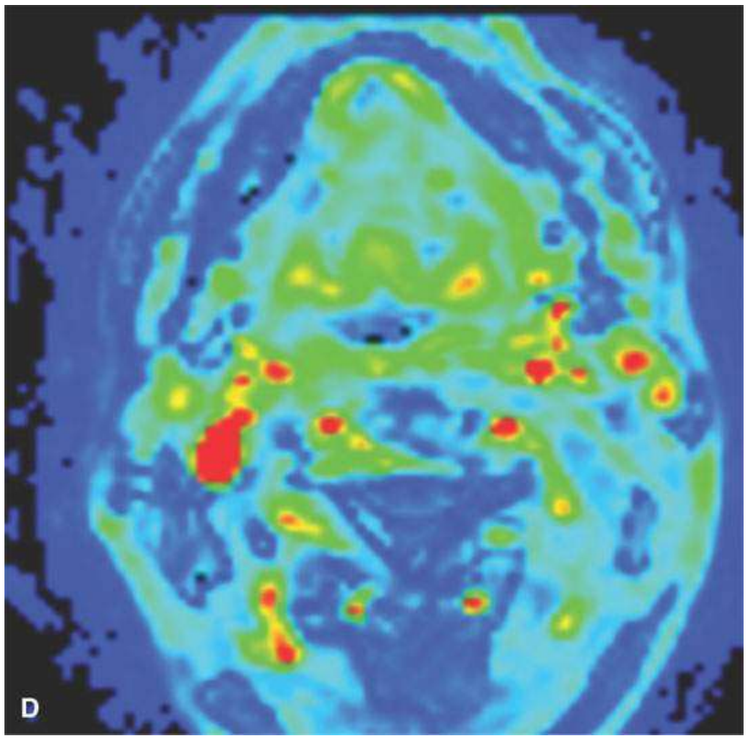

FIGURE 21.63. Contrast-enhanced magnetic resonance with perfusion maps showing decrease in perfusion of the nodal mass (*arrow* in **A** on the T1-weighted anatomic image)[SF2] during radiotherapy. The MRI perfusion map before treatment (B, C) at two different levels show the increased perfusion of the adenopathy compared to surrounding muscle and fat. One level perfusion map **(D)** shows the mass to have reduced in size and perfusion in response to therapy.

Changes in Malignant Tumors Following Completion of Radiotherapy

Obvious reduction in size or disappearance is the best sign of response to therapy. Most successfully treated cancers will shrink completely away, leaving no obvious mass or a relatively small zone (<1 to 2 cm) of end-stage change likely evolving fibrosis by 12 weeks post therapy (Fig. 21.64). Focal masses beyond 3 months that persist and/or enhance on CT or MRI and those that retain signal intensity greater than that of muscle on T2W images or contrast-enhanced T1W images may be considered suspicious for persistent disease, in which case the patient should be followed carefully (Figs. 21.64–21.66). Diffusion-weighted imaging may provide adjunctive information for differentiating tumor from a reactive or end-stage sterilized tumor bed, but its reliability in small areas of interest and adjacent to zones of susceptibility artifacts remain a significant barrier to its routine reliable use in clinical decision making (Fig. 21.67).

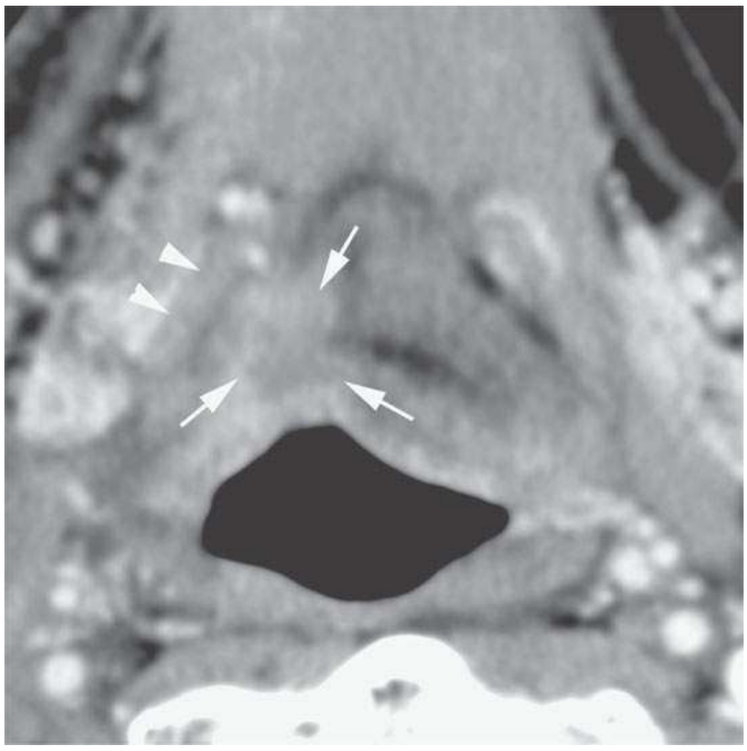

FIGURE 21.64. Contrast-enhanced computed tomography anatomic study at 6 weeks after the completion of radiotherapy to help determine the need for neck dissection following radiotherapy for tongue base squamous cell carcinoma showing a residual mass *(arrows)* and abnormality along the lingual neurovascular bundle *(arrowheads)*. Such a residual mass is common at 4 to 6 weeks post radiotherapy but is not consistent with control at that point. Most of such "suspicious" masses often stabilize or resolve. Fluorine-18 2-fluoro-2-deoxy-D-glucose positron emission tomography (FDG-PET) studies are not reliable until about 3 months following completion of all therapy to determine whether there has very likely been control.

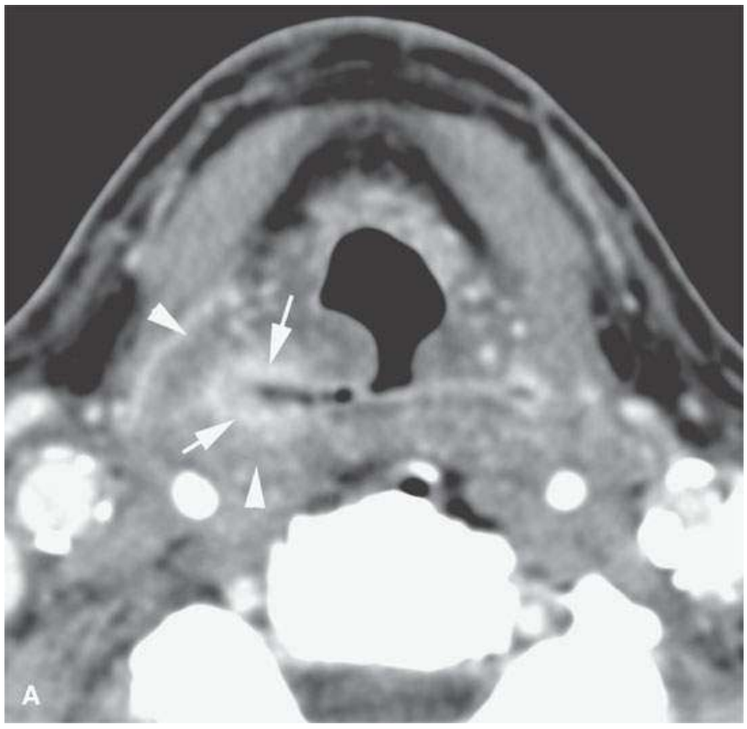

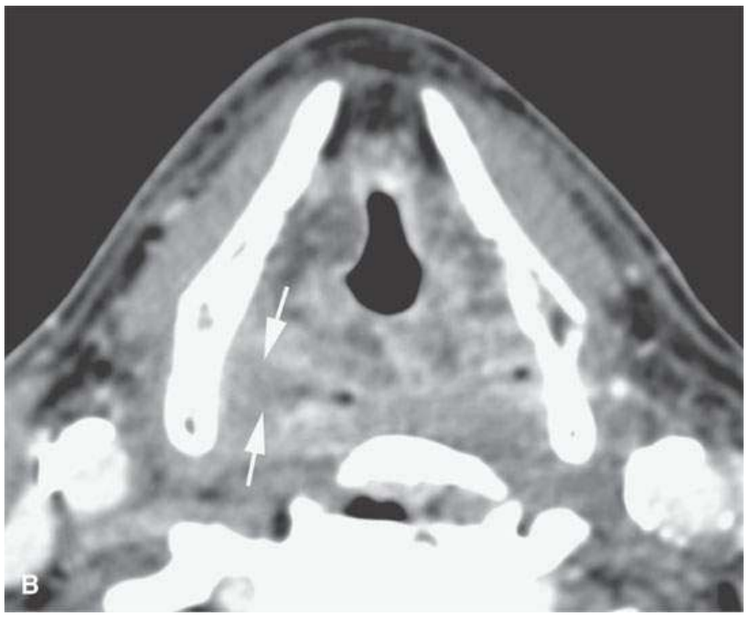

FIGURE 21.65. Contrast-enhanced computed tomography (A, B) shows a mucosal mass *(arrows)* and much surrounding swelling *(arrowheads)* as findings that are very suspicious for persistent at 3 months following completion of radiotherapy.[SF3] Recurrence was confirmed by biopsy.

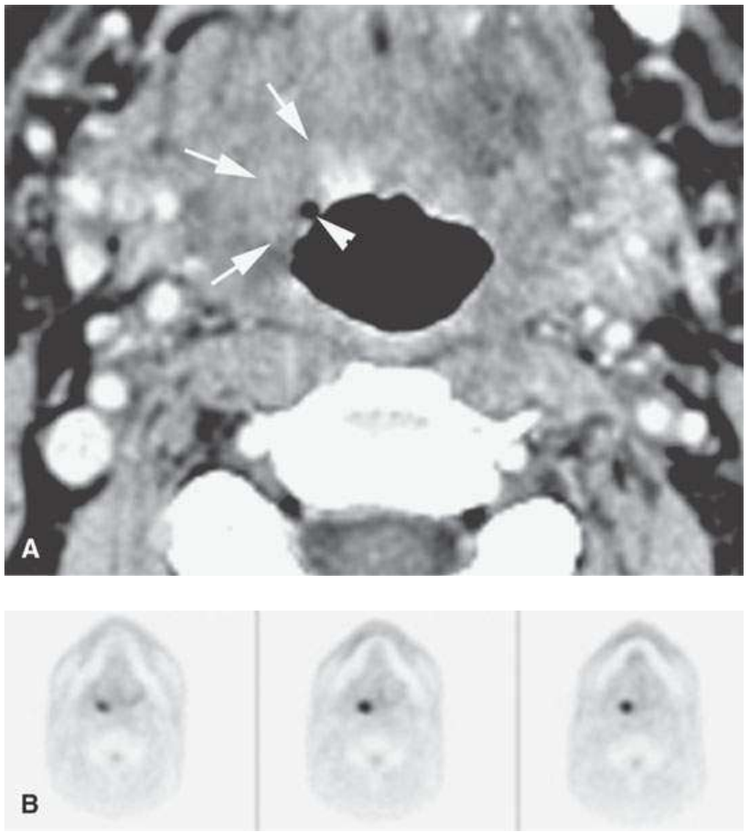

FIGURE 21.66. Contrast-enhanced computed tomography anatomic study showing a very subtle tongue mass *(arrows)* with a shallow ulcer *(arrowhead)* 6 months after the completion of radiotherapy for tongue base squamous cell carcinoma. The fluorine-18 2-fluoro-2-deoxy-D-glucose positron emission tomography (FDG-PET) study **(B)** showed a very hypermetabolic focus at the same site, and biopsy confirmed recurrence.

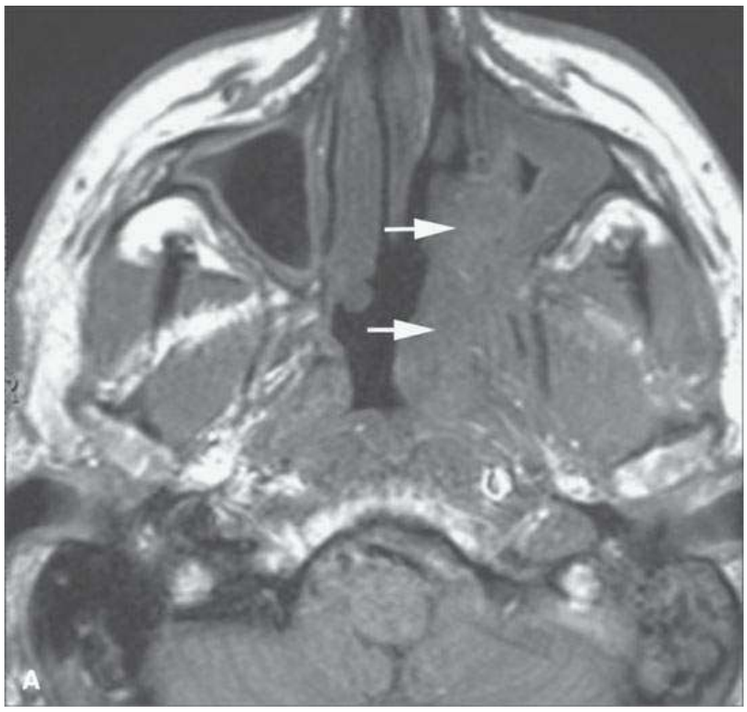
A

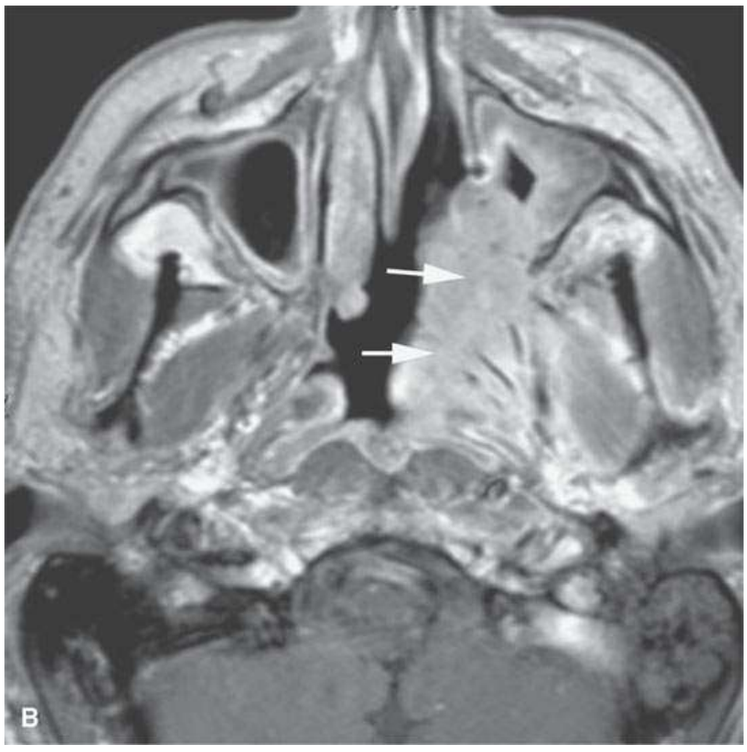
B

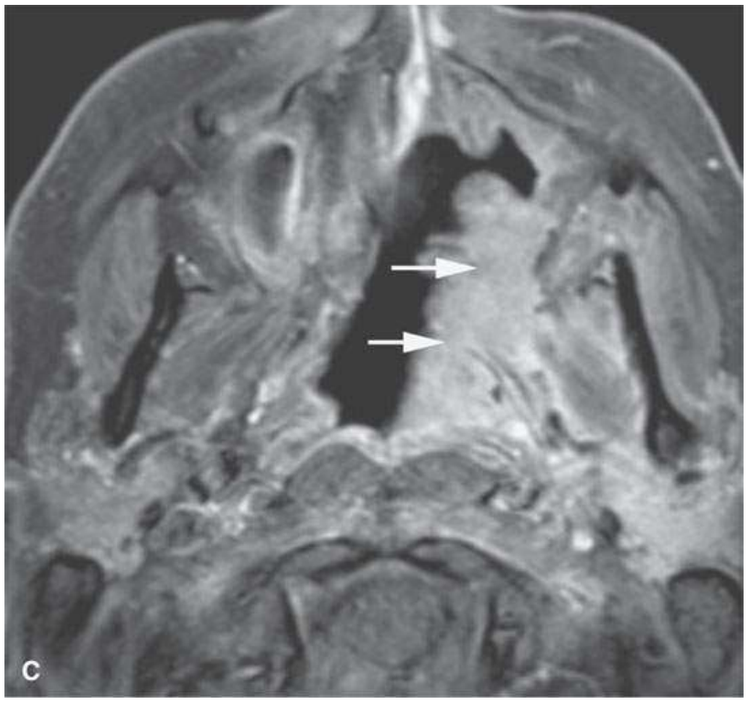
C

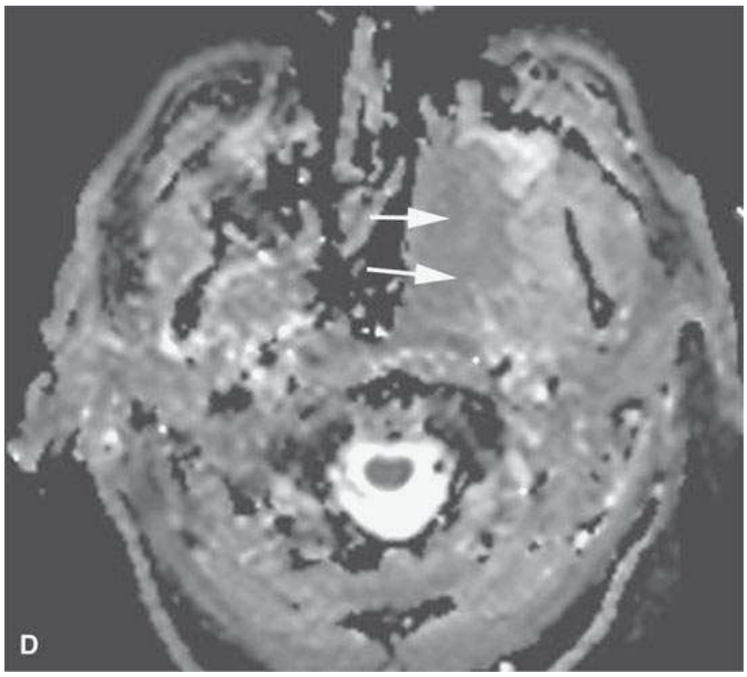

FIGURE 21.67. Contrast-enhanced magnetic resonance study and obvious infiltrating recurrent cancer (*arrows* in A–C) that shows restricted diffusion on the apparent diffusion coefficient map in (dD). Whether diffusion-weighted imaging adds consistently available and reliable data to decision making beyond anatomic imaging in tumor surveillance remains speculative.

The vast majority of these residual masses will stabilize or improve, and the primary site will be controlled. Some thought to imaging-guided biopsy of suspicious sites is appropriate if sites of concern are not amenable to clinical observation or traditional biopsy techniques. Biopsy in certain areas based on imaging findings alone must be pursued with great caution. This is especially true in the larynx, where deep biopsy can lead to chondronecrosis and loss of an otherwise salvageable larynx. Tissue necrosis or osteoradionecrosis cannot always be distinguished from tumor, and tumor coexistent with these conditions cannot be absolutely excluded by a single anatomic imaging study.

FDG-PET is not useful for resolving these issues of reactive changes versus necrosis versus tumor in the first 2 months following radiotherapy. After that period, false-positive rates still remain relatively high and should be interpreted in light of anatomic imaging findings on definitive diagnostic-quality studies and the particular clinical situation, such as whether any curative treatment can be offered if tumor has recurred. On the other hand, an FDG-PET study after 2 months has a negative predictive value likely over 95% for confirming control. A negative study may therefore be quite valuable to help avoid what may be a potentially damaging biopsy when there is a strong suspicion of recurrence based on anatomic imaging and clinical parameters.

More diffuse cellular malignancies such as lymphoma and plasmacytoma conditions that are radiated will usually disappear, leaving behind only reactive mucosal changes where they might have involved mucosal line spaces. When these lesions involve bone, the affected bone will heal often with long-term reactive sclerosis and such an end state will make the bone appear denser than it was originally.

General and Expected Changes in Nontumoral Tissues and Structures

Radiation therapy doses >6,500 cGy are often associated with permanent alterations in soft tissues. Thickening of the skin and platysma are common. Strands of tissue density in subcutaneous and deeper fat are probably due to perilymphatic fibrosis and/or thickening of pre-existing fibrous septae in these sites of areolar tissue (Figs 21.68 and 21.69). Subclinical, diffuse lymphedema may be present for years in susceptible sites such as the supraglottic larynx (Fig. 21.69). The pharyngeal wall frequently remains persistently thickened following high-dose radiotherapy for primary tumors of the oropharynx and hypopharynx. There may be profound atrophy and fatty replacement of radiosensitive structures such as lacrimal glands, salivary glands, and normal lymph nodes. In contrast, doses of 4,500 to 5,000 and up to 6,000 cGy usually produce virtually no visible MR or CT changes when imaged ≥6 weeks after therapy.

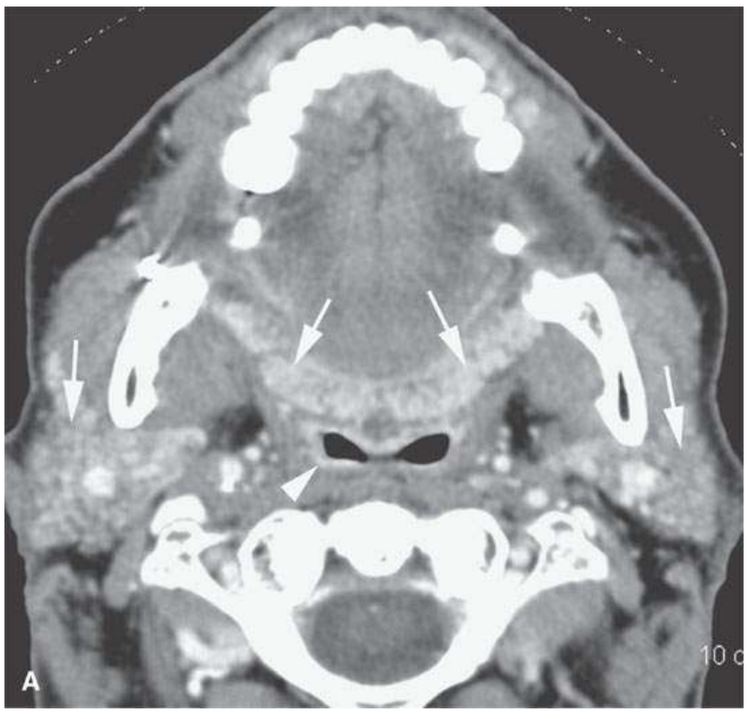

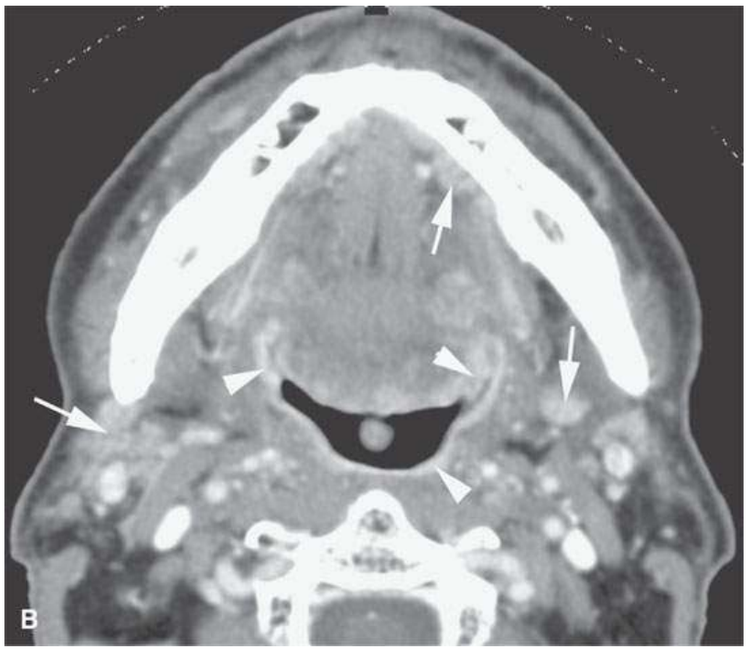

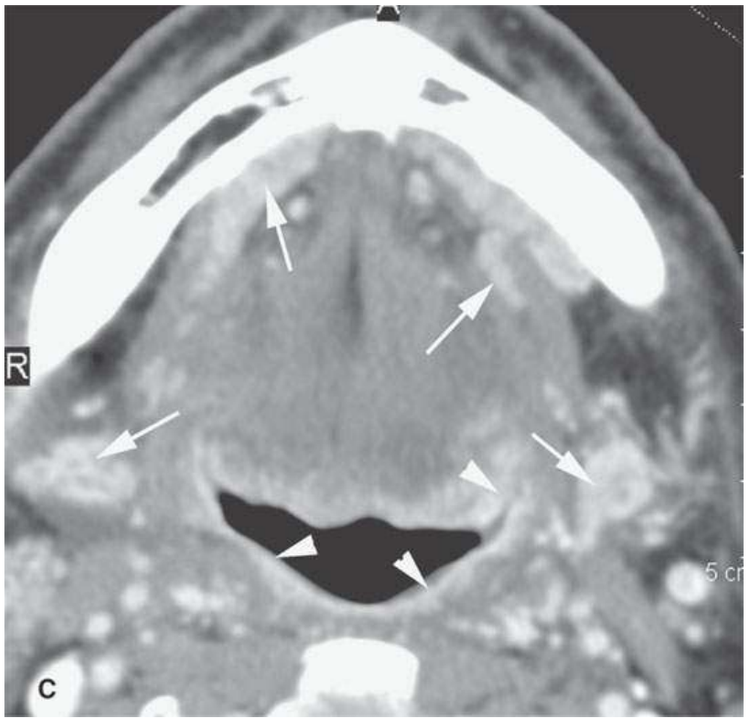

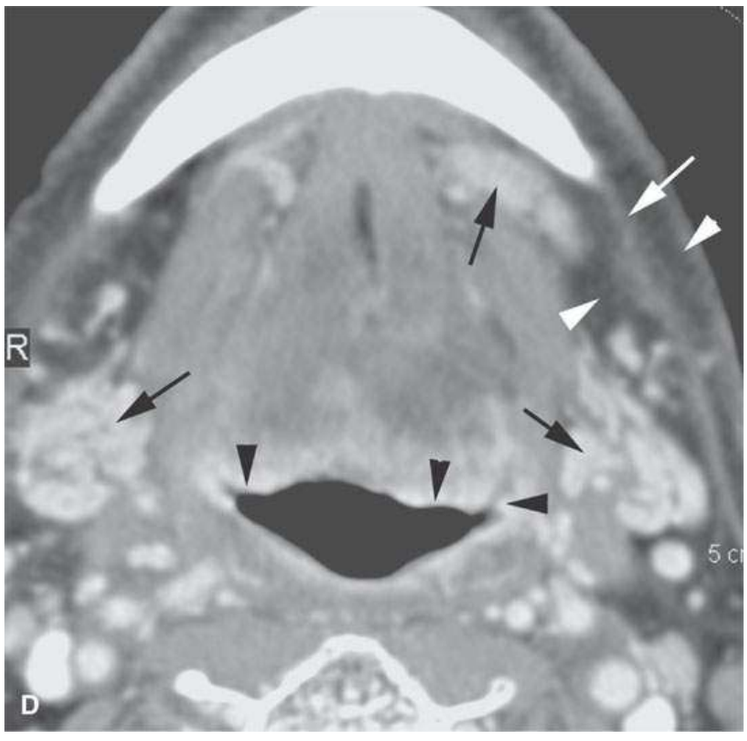

FIGURE 21.68. Contrast-enhanced computed tomography about 6 weeks after the completion of radiotherapy (RT) for squamous cell carcinoma of the tongue base. A–C: Enhancement of the salivary tissue, both major and minor, throughout the upper aerodigestive tract *(arrows)* and of radiation-induced mucositis *(arrowheads)* is a common finding up to about 3 months following the completion of RT. **D:** Salivary tissue *(black arrows)* and mucositis *(black arrowheads)* are

shown in addition to typical thickening of the superficial musculoaponeurotic system (SMAS) *(white arrow)* and the tissue planes superficial and deep to the SMAS and the superficial fascia *(white arrowheads)*.

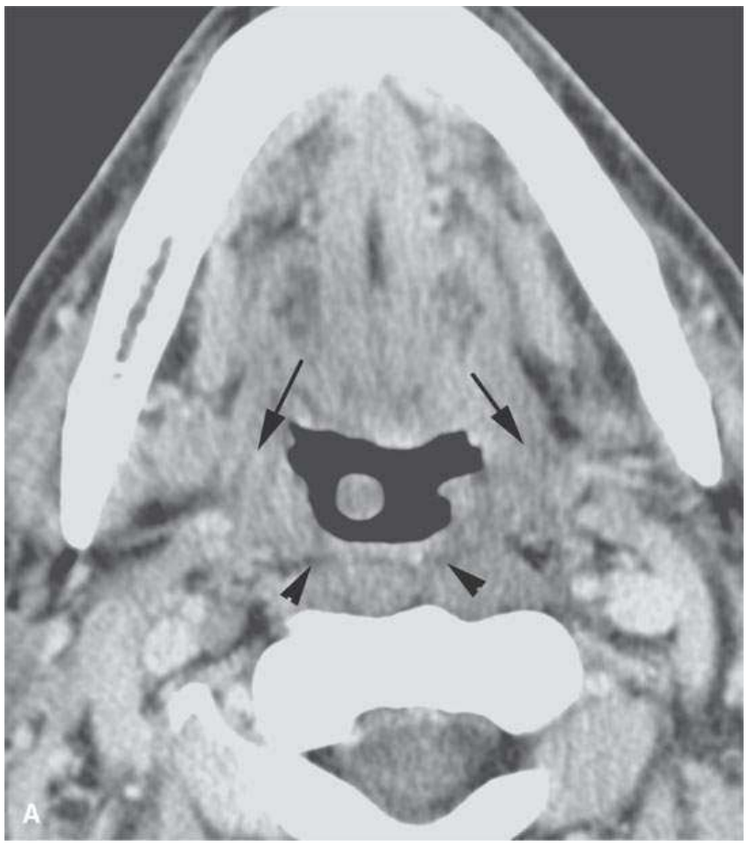

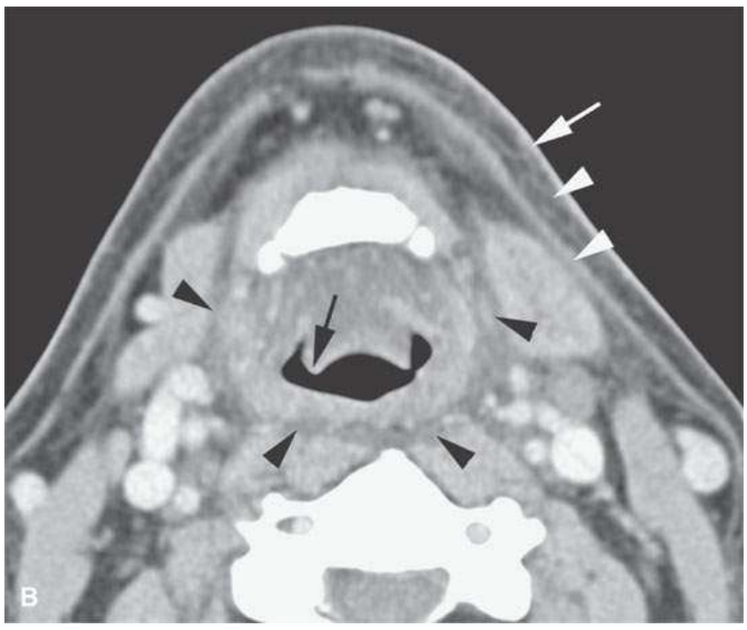

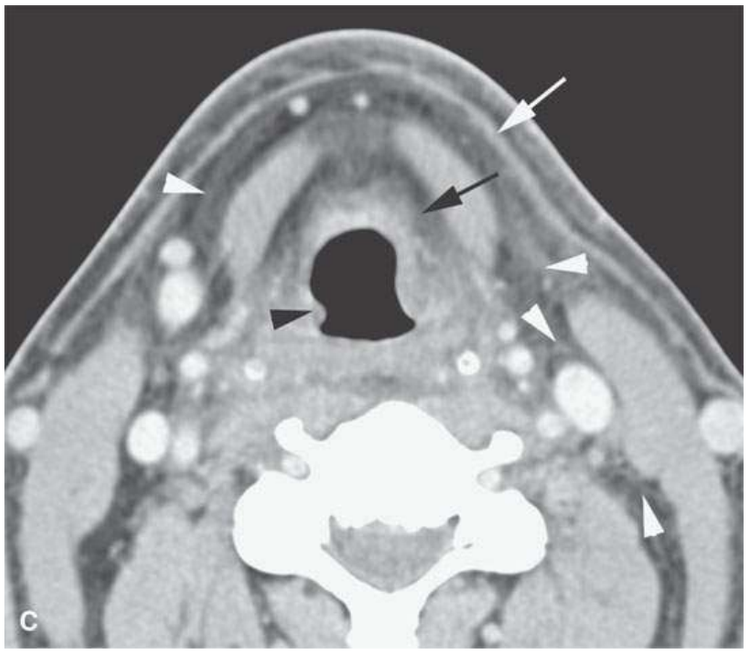

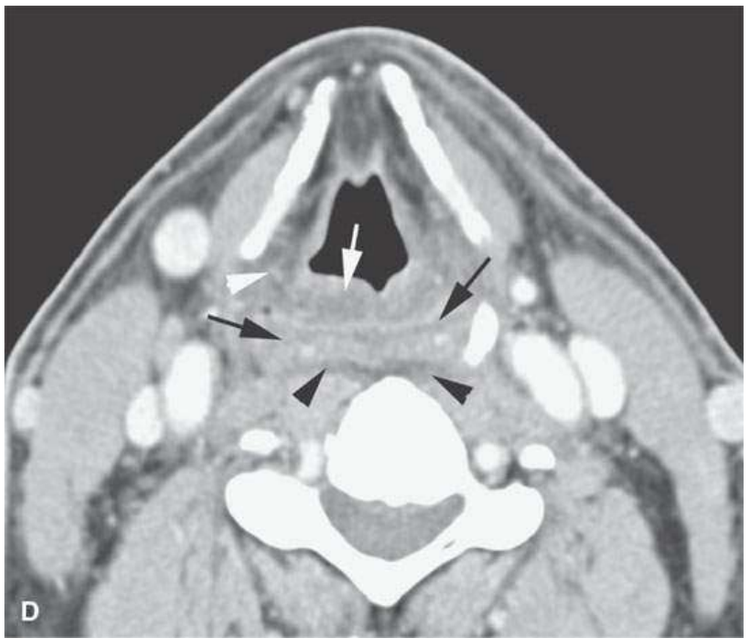
D

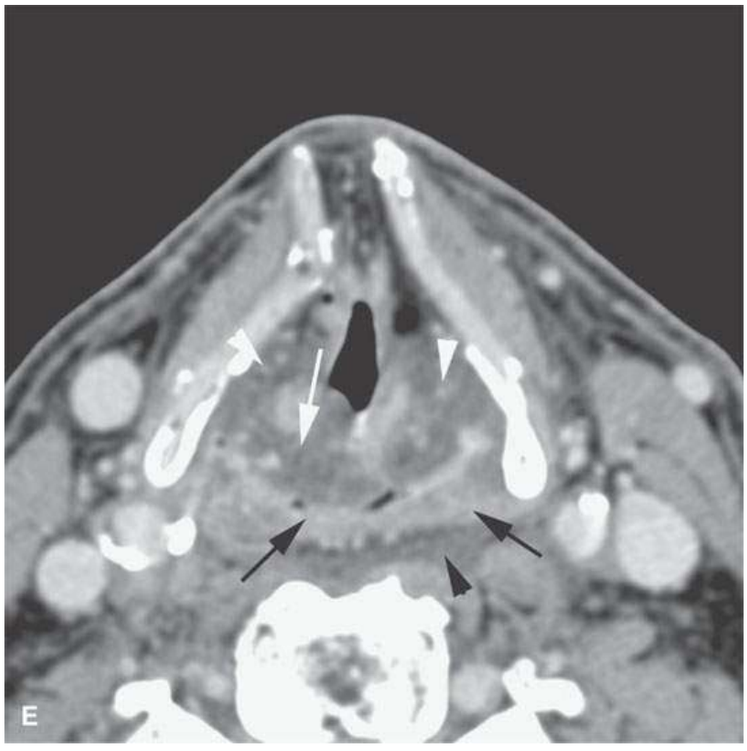
E

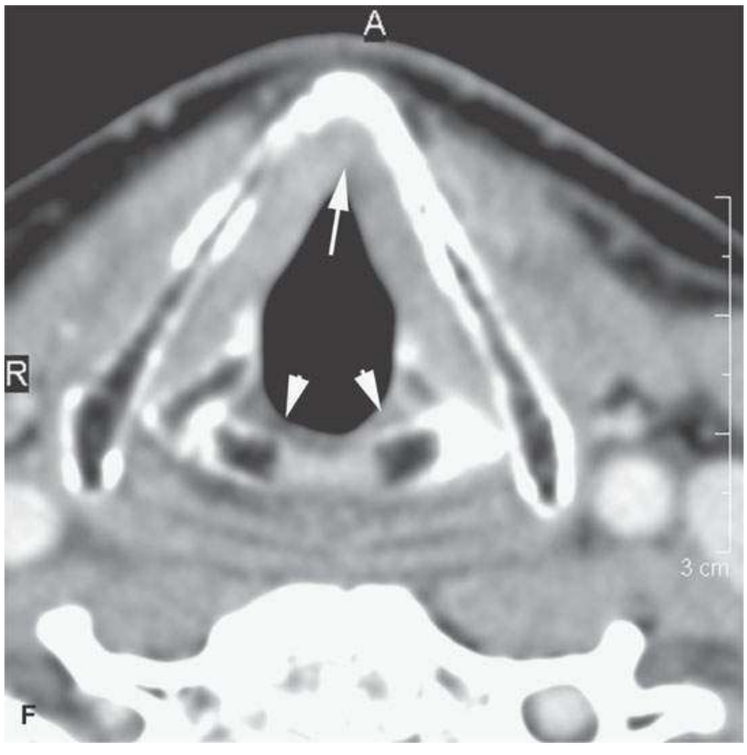
A
R
3 cm
F

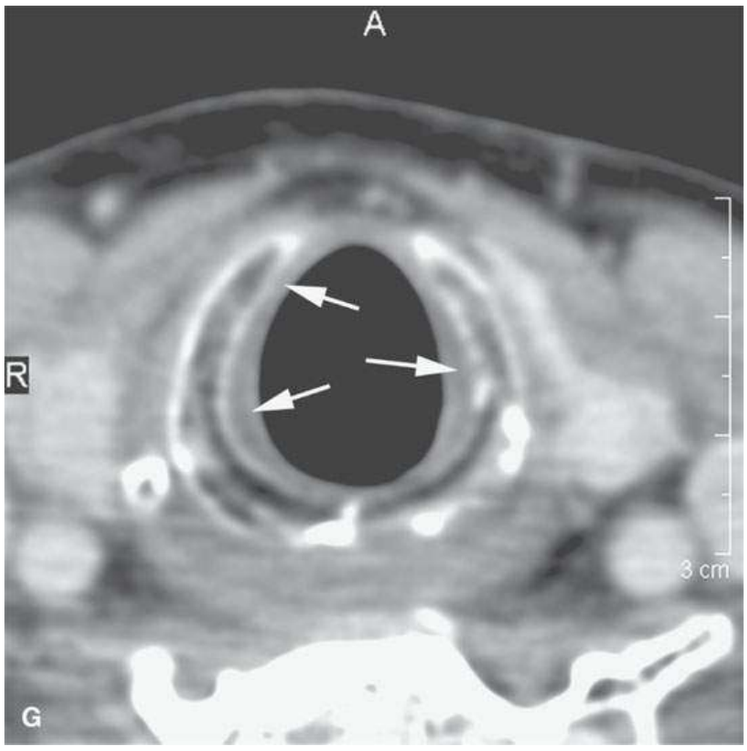

FIGURE 21.69. Contrast-enhanced computed tomography of patients done about 4 months after the completion of radiotherapy for hypopharyngeal cancer to demonstrate routine chronic changes, likely not to resolve with time following high-dose therapy. **A:** Modest thickening of lateral oropharyngeal walls *(arrows)* and minimal retropharyngeal edema *(arrowheads)* are present. **B:** Skin thickening *(white arrow)*, subcutaneous stranding, and thickening of the superficial fascia *(white arrowheads)* as well as thickening of the free margin of the epiglottis *(black arrow)* and edema *(black arrowheads)* in the peripharyngeal soft tissues. **C:** The superficial fascia is thick *(white arrow)*, and there is stranding in the deeper planes of the neck *(white arrowheads)*. Endolaryngeal changes include thickening of the aryepiglottic folds *(black arrowheads)* and increased density in the paraglottic space fat *(black arrow)*. **D:** Continued thickening of the aryepiglottic folds *(white arrow)* and increased density in the paraglottic space fat *(white arrowhead*) as well as thickening of the muscular posterior pharyngeal wall *(black arrows)* and retropharyngeal edema *(black arrowheads)*. **E:** In another patient, variation of changes seen in (dD) of continued thickening of the aryepiglottic folds *(white arrow)* and increased density in the paraglottic space fat *(white arrowheads)* as well as thickening of the muscular posterior pharyngeal wall *(black arrows)* and retropharyngeal edema *(black arrowhead*). F, G: In another patient, note the thickening of the tissues at the anterior commissure *(arrow)* and interarytenoid region *(arrowheads*) **(F)** and circumferential soft tissue thickening of the subglottic soft tissues (G).

Mucosal thickening and edema in the sinuses and mastoid and middle ear may persist indefinitely following radiotherapy. These changes will frequently not enhance after several months, indicating that they are more due to persistent edema rather than persistent high-grade inflammation.

Changes in Benign Tumors and Other Benign Conditions Following Radiotherapy

Some benign tumors are radiated to control their growth rate. Vascular tumors, such as juvenile angiofibroma and paragangliomas, are radiated to produce an endarteritis leading to ischemia of the tumor as well as to kill neoplastic cells. The overall goal of radiation is to stop or slow growth. Typically, between 3,000 and 4,500 cGy is given to such lesions. The tumors may rarely regress completely; however, only moderate (25%) or minimal shrinkage is the usual response. Since the goal is mainly to slow or stop growth, this is a perfectly acceptable response. Lack of complete shrinkage may also be seen in a benign or malignant mass that has a relatively inert stromal cell population. The tumor cells are killed, but the bulk of the tumor stromal elements such as a matrix or fibrous reactive tissue is left behind as a residual mass. Such residuals are usually hypointense to muscle on T1W and T2W images and show little or no change with CEMR and CECT. Foci of evolving hemorrhage or necrosis, thrombosed vessels, or persistent vascular channels within tumor masses may cause inhomogeneity in their MR appearance. The significance of a residual mass and its internal morphology can only be judged in light of the clinical findings of each case. Some will be removed, some followed with imaging, some biopsied, and some simply accepted as the appropriate end result of therapy.

Benign conditions that are radiated, such as Langerhans histiocytosis or Wegener granulomatosis, will usually disappear, leaving behind only reactive mucosal changes where they might have involved mucosal line spaces. When these lesions occur within bone, the previously affected bone will show healing with usually some long-term reactive sclerosis that end stage will make the bone appear denser than it was originally (Figs. 14.4 and 19.4).

Bone Changes Following Radiotherapy

Areas of bone destruction will heal following radiotherapy. This is most usually encountered in the central skull base following treatment of nasopharyngeal carcinoma invading the skull base. The bone healing is usually characterized by irregular sclerotic mineralization to the bony defect, suggesting that the mineralization is being applied to something other than a normal bony scaffold that originally was present (Fig. 21.70). This healing is reminiscent of the mineralization of fibrodysplastic bone.

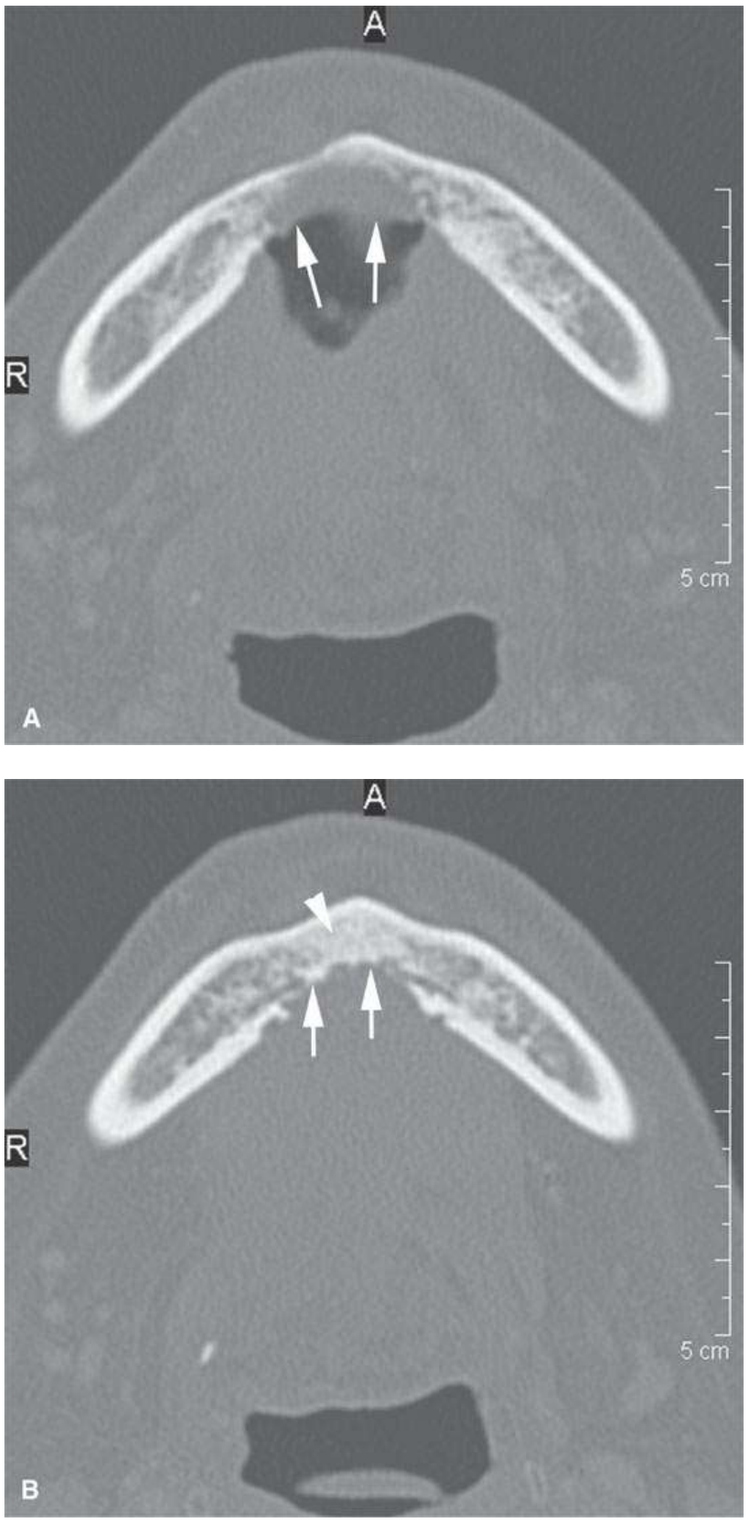

FIGURE 21.70. Computed tomography study showing mandible lingual plate destruction by squamous cell carcinoma (*arrows* in **A**) healing at the cortical margins *(arrow)* and within the marrow space *(arrowhead)* in (bB).

It is interesting that bone erosion due to malignancies will heal faster and more completely than bone loss due to benign lesions that have been radiated. This is especially true in the central skull base.

Osteoradionecrosis of bone is characterized by piecemeal sloughing of cortical bone, fragmentation, endosteal tunneling, and in general a pattern quite different than usually present when tumor recurs (Figs. 14.16–14.19). This is discussed in more detail in Chapter 14.

GUIDELINES FOR POSTTREATMENT SURVEILLANCE IMAGING

The use of imaging studies to monitor the results of therapy can be a highly effective adjunct to standard clinical follow-up. A few important limitations of imaging discussed here make it wise to follow these general guidelines:

(1) Imaging can never exclude the possibility that viable tumor cells remain in the treatment area even when no residual mass is seen.

(2) Studies intended to be the baseline for further follow-up should be obtained no sooner than 8 to 12 weeks after surgery or the completion of radiotherapy unless there is compelling clinical evidence or pretreatment risk of residual tumor that must be re-evaluated for further therapy.

(3) The preferred use of CT or MR as a follow-up study in malignant tumors depends on the tumor type, its site of origin, and whether lymphadenopathy or bone detail is an important consideration. If nodal detail is of prime interest, CT or FDG-PET is preferred. In benign tumors such as paragangliomas and juvenile angiofibromas, MR is almost always preferable.

(4) Imaging studies are expensive, and currently there is no data that suggest imaging is capable of routinely detecting recurrence before it is apparent clinically and that this leads to improved salvage rates. This point requires prospective analysis before specific recommendations about the use of imaging in follow-up can be made. There is a role for surveillance imaging in a group of patients identified as being at high-risk for recurrence; this is discussed more fully in conjunction with specific primary sites.

In reference to the last point (#4) made above, it is important for clinicians to triage cancer patients into groups at high- and low-risk for failure. This may be on the basis of pretherapy staging, tumor volume, and/or pathologic findings, such as operative specimen evaluation for close or positive margins or laboratory studies suggesting a biologically aggressive tumor. Optimal follow-up in selected patients might be at 3-month intervals for the first year and 6-month intervals for the next 2 years. Patients irradiated for aggressive benign lesions, such as juvenile angiofibromas and paragangliomas, are generally followed with imaging at 6-month intervals until the tumor size stabilizes. The follow-up interval is then lengthened to once per year for a year or two and then as clinically indicated or according to the patient's desires. More specific guidelines for use of imaging follow-up will be presented, when appropriate. The more profound effects that surgery and radiation have on lymphatic drainage and the effects that these changes have on the pattern and treatment of recurrent disease are discussed in conjunction with cervical metastatic disease in Chapter 157.

References

1. Mancuso AA, Hanafee WN. Elusive head and neck cancers beneath intact mucosa. *Laryngoscope*. 1983;93:133–139.

2. Muraki AS, Mancuso AA, Harnsberger HR. Metastatic cervical adenopathy from tumors of unknown origin: The role of CT. *Radiology*. 1984;152:749–753.

3. Dodd GD, Dolan PA, Ballantyne AJ, et al. The dissemination of tumors of the head and neck via the cranial nerves. *Radiol Clin North* Am. 1970;8:445–462.

4. Ballantyne AJ. Routes of spread. In: Fletcher GH, MacComb WS, eds. *Radiation therapy in the management of cancers of the oral cavity and oropharynx*. Springfield, Il: Charles C Thomas; 1962:91–115.

5. Ballantyne AJ. Significance of retropharyngeal nodes in cancer of the head and neck. *Am J Surg*. 1964;108:500.

6. Lederman M. *Cancer of the nasopharynx: Its natural history and treatment*. Springfield, Il: Charles C Thomas; 1961.

7. Lederman M. Cancer of the pharynx. *J Laryngol*. 1967;81:151.

8. Muraki AS, Mancuso AA, Harnsberger HR. CT of the oropharynx, tongue base and floor of the mouth: Normal anatomy and range of variations and applications in staging carcinoma. *Radiology*. 1983;148:725–731.

9. Mancuso AA, Bohman LG, Hanafee WN, et al. Computed tomography of the nasopharynx. Normal and variants of normal. *Radiology*. 1980;137:113–121.

10. Haagensen DC, Feind CR, Herter FP, et al. *The lymphatics in cancer*. Philadelphia, Pa: WB Saunders; 1972:60–208.

11. Fisch U. *Lymphography of the cervical lymphatic system*. Philadelphia, Pa: WB Saunders; 1968.

Related Posts:

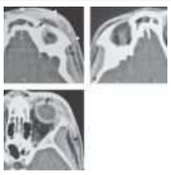
Preseptal Compartment:

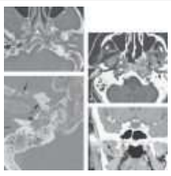
Necrotizing ("Malignant") Otitis

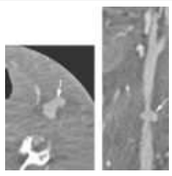
Cervicothoracic Junction: Brachial

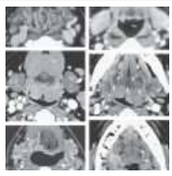
Oropharynx: Introduction

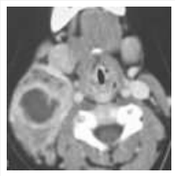
Branchial Apparatus


Mandible and Maxilla:

May 14, 2017 | Posted by admin in HEAD & NECK IMAGING | Comments Off